Design and Analysis of Multiple Input Non-Isolated DC-DC Converter for Fast Charging Station of Electric Vehicles

by

Abdalrahman Elshora

A thesis submitted to the
School of Graduate and Postdoctoral Studies in partial
fulfillment of the requirements for the degree of

Master of Applied Science in Electrical and Computer Engineering

Department of Electrical, Computer, and Software Engineering
Faculty of Engineering and Applied Science
University of Ontario Institute of Technology (Ontario Tech University)
Oshawa, Ontario, Canada

August 2022

THESIS EXAMINATION INFORMATION

Submitted by: **Abdalrahman Mohamed Elshora**

Master of Applied Science in Electrical and Computer Engineering

Thesis title: **Design and Analysis of Multiple Input Non-Isolated DC-DC Converter for Fast Charging Station of Electric Vehicles**

An oral defense of this thesis took place on the 2nd of August 2022 in front of the following examining committee:

Chair of Examining Committee	Assoc. Prof. Dr. Jing Ren
Research Supervisor	Prof. Dr. Hossam Gaber
Supervisory Committee Member	Prof. Dr. Sheldon Williamson
Thesis Examiner	Assoc. Prof. Dr. Mohamed Youssef

The above committee determined that the thesis is acceptable in form and content and that a satisfactory knowledge of the field covered by the thesis was demonstrated by the candidate during an oral examination. A signed copy of the Certificate of Approval is available from the School of Graduate and Postdoctoral Studies.

ABSTRACT

In the last decade, multi-input DC-DC converters have been studied in various research areas related to plug-in vehicles, hybrid electric vehicles, and renewable energy applications. They have several advantages over conventional converters, such as reducing the number of components and the power conversion stages and centralizing the control. This research discusses a multi-input non-isolated converter in different operation modes to enhance the energy management of the fast-charging station of electric vehicles. The converter has a modular design with effective control functions. The converter was integrated into the proposed fast-charging station and simulated using MATLAB/Simulink in different operation modes, and the different losses of the converter and its efficiency are analyzed. The simulation results were verified by testing the converter at an experimental setup with a low power rate of 100 W. The results show an excellent performance of the proposed converter and verified the topology and the switching sequence of the converter.

Keywords: Electric vehicles; Multi-input DC/DC converter; Energy storage devices; Efficiency; EV Fast charging

AUTHOR'S DECLARATION

I hereby declare that this thesis consists of original work of which I have authored. This is a true copy of the thesis, including any required final revisions, as accepted by my examiners.

I authorize the University of Ontario Institute of Technology (Ontario Tech University) to lend this thesis to other institutions or individuals for the purpose of scholarly research. I further authorize the University of Ontario Institute of Technology (Ontario Tech University) to reproduce this thesis by photocopying or by other means, in total or in part, at the request of other institutions or individuals for the purpose of scholarly research. I understand that my thesis will be made electronically available to the public.

_____ Abdalrahman Elshora

STATEMENT OF CONTRIBUTIONS

The main contribution of this thesis is to study and test a multi-input converter for the fast-charging station of electric vehicles and to analyze its efficiency and losses in different operation modes using MATLAB/Simulink. In addition, to make a prototype of the proposed converter to validate the simulation work. The contribution of the design of the proposed converter compared to other designs of multi-input converters is it has less weight, cost, and power elements. In addition, it has a modular design, so we can extend the power sources or energy storage devices for the fast-charging stations, therefore this will reduce the load on the grid, the cost of the charging, and extend the lifetime of the energy storage devices with using a bidirectional converter. I have used standard referencing practices to acknowledge ideas, research techniques, or other materials that belong to others.

• Part of the work described in Chapters 1,2,4,5& 6 has been published and submitted for publication as:

- A. Elshora and H. A. Gabbar, "Design and Analysis of Multi-Input, Single-Output, Nonisolated DC/DC Converter for Fast Charging of Electric Vehicles," *2021 International Conference on Electrical, Computer, Communications and Mechatronics Engineering (ICECCME)*, 2021, pp. 1-7, doi: 10.1109/ICECCME52200.2021.9591071.

- A. Elshora, Y. Elsayed and H. A. Gabbar, "Modular Bidirectional Converter with Multiple Power Sources for Fast Charging of Electric Vehicles," *2021 IEEE 9th International Conference on Smart Energy Grid Engineering (SEGE)*, 2021, pp. 141-146, doi: 10.1109/SEGE52446.2021.9535008.

- H. A. Gabbar, Y. Elsayed, A. B. Siddique, A. Elshora, and A. Adeleke, "Design of Fast Charging Station with Energy Management for eBuses," *Vehicles*, vol. 3, no. 4, pp. 807-820, 2021.

- GABBAR, HOSSAM A. Fast Charging and Resilient Transportation Infrastructures in Smart Cities. SPRINGER, 2022.

- Hossam A.Gabbar , Yasser Elsayed , Manir Isham, Abdalrahman Shora ,Abu Bakar Siddique , Otavio Lopes Alves Esteves " Demonstration of Resilient Microgrid with Real-Time Co-Simulation and Programmable Loads". *Energies*. (2022).

- Hossam A.Gabbar , Abdalrahman Shora Design "Analysis and control of Modular Multi-Input DC/DC Converter for Fast Charging of Electric Vehicles" *Electronics*. (2022). (*Under review*)

ACKNOWLEDGEMENTS

I would like to thank my supervisor, Prof. Hossam Gaber, for his support, knowledge, guidance, and leadership during my graduate studies. I would also like to express my gratitude to my family, who always encouraged and supported me during my studies while living far away from them. My colleagues at the Smart Energy Systems Lab (SESL) and the Advanced Plasma Engineering Lab (APEL) helped me during my research and publications. To my friends, especially Dr. Hassan Zayton and Eng. Abdalrahman Salem who never hesitated to help me during my research work and studies. I am also thankful to the UOIT staff for giving me an exceptional work environment as well as the facilities to finish my research work. Finally, to CUTRIC, and MITACS for their funding and support.

TABLE OF CONTENTS

LIST OF TABLES

LIST OF FIGURES

LIST OF ABBREVIATIONS AND SYMBOLS

In order of appearance

EV	Electric Vehicle
HEV	Hybrid Electric Vehicle
BEV	Battery Electric Vehicle
PHEV	Plug-in Hybrid Electric Vehicle
PFC	Power Factor Correction
WPT	Wireless Power Transfer
IEC	International Electrotechnical Commission
SAE	Society of Automotive Engineers
EVSE	Electric Vehicle Supply Equipment
EMF	Electric and Magnetic Fields
CCS	Combo Charging System
PLC	Power Line Communication
SAC	Standardization Administration of China
ZCS	Zero Current Switching
ZVS	Zero Voltage Switching
ESS	Energy Storage Systems
FCS	Fast Charging Station
NiMH	Nickel-Metal Hydride
Li-ion	Lithium-ion
OCV	Open-Circuit Voltage
SOC	State of Charge
UC	Ultracapacitors
TOU	Time of Use
PID	Proportional-Integral-Derivative
MOSFET	Metal-oxide semiconductor field-effect transistor
ZEV	Zero Emission Vehicle
MISO	Multi Input Single Output

LIST OF SYMBOLS

In order of alphabetic

A	Amperes
AC	Alternating Current
C_{bat}	Battery capacity
C	Capacitor
D	Duty Cycle
DC	Direct Current
D_1, D_2	Internal diode of MOSFET's S_1 and S_2
f_s	Switching Frequency
I	Current
kHz	Kilohertz
kW	Kilowatts
L	Inductance
mH	milli-Henry
P	Power
S	Controllable MOSFET switch
T	Period
t	Time
V	Voltage
W	Watts
Ω	Ohm
μF	Microfarads

Chapter 1. Introduction

1.1 History of the DC-DC Converters and the Futuristic Perspective

DC-DC converters appeared with the invention of semiconductors in 1920 [1]. The first converter was used as a simple voltage divider and was only able to reduce the input voltage with very low efficiency. To obtain an output voltage that is smaller equipment for this conversion. Before the Second World War, basic converters were utilized in many industrial applications. Due to the war, the research in converters stood, but the applications were recognized. After the war, a low-power DC supply was one of the technical developments, and many DC-DC conversion techniques were developed later [2].

The recent research on fast charging of electric vehicles (EVs) and hybrid electric vehicles (HEVs) focuses on reducing the weight, cost, and components numbers of DC-DC converters and enhancing the energy management of the fast-charging stations, and maximizing the lifetime of the energy storage devices with minimum cost. Typically, fast-charging stations (FCS) for EVs and HEVs utilize batteries and ultracapacitors as energy storage devices for their operation as they combine the high energy density of the former and the high power density of the latter. As multi-input converters can integrate at least two energy sources or power sources and supply at least one output, they show an excellent application in the fast-charging stations of EVs to employ the advantages of the batteries and the ultracapacitors as a hybrid energy system. Moreover, they can be utilized in applications that use many energy sources, such as portable electronics, aerospace, micro-energy grids, and automotive [3].

1.2 Background and Motivation

The sales of EVs are increasing rapidly in the automobile market over the world to face climate change. The transportation sector in Canada generated 186 Mt CO2 eq (25%) of emissions in 2018 [4]. Therefore, the Canadian government set a plan to increase the percentage of EVs from the light vehicles by 10% by 2025 and by 2030 to 30%, and finally, to 100% by 2040 [5]. Hence, increasing the fast-charging stations is essential to make this technology more convenient and popular. The charging power rate of EVs in fast-charging stations is an average of 50 kW, and the power consumption of one house is 5 kW; as a result, charging electric vehicles

during peak hours can put a significant load on the grid. In addition, the cost of generation, transmission, and distribution will increase obviously by aggravating the critical peak load [6]. Thus, the main challenge of designing the fast-charging stations is reducing the charging time, charging cost, and mitigating the load on the grid while charging the EVs during peak hours. The fast-charging stations use different energy storage devices such as batteries, ultracapacitors, and flywheels that have different energy and power density characteristics to achieve the previous objectives. These energy storage devices (ESD) are connected to bidirectional DC-DC power converters to control the power transfer rate between the storage devices and the vehicle. In addition, between EDS and the grid or any energy or power source like PVs or wind turbines. The DC-DC converters play an important role in increasing the lifetime of the energy storage devices. For example, to increase the battery's lifetime, it should be charged with SOC not less than 20% and not more than 80% [7]. Improving the efficiency of the converters is very important to decrease the power losses of the system and enhance the efficiency gain of the station. Several studies have been conducted in DC-DC converter topologies to utilize different energy sources for battery electric vehicles (BEVs) and Plug-in Hybrid Electric Vehicles (PHEVs) [8].

Moreover, multi-input converters are being used in many applications nowadays, such as hybrid and plug-in electric vehicles, due to their ability to combine different input voltages and supply the load with various output levels. These converters have many merits over the conventional ones, such as reducing the number of components, the power conversion stages, and increasing efficiency. Similar to the conventional converters, the multi-input converters have different topologies that can combine one or more features like the number of operation modes, power flow capability, and component numbers. In addition, they add modularity to the design to integrate more energy sources. However, obtaining all features and characteristics in one topology is impossible. The multi-input converters can be utilized in fast-charging to reduce the charging stations cost, the cost of the charging, reduce the load on the grid during the peak hours, and enhance the charging station maintenance with centralized control.

1.3 Scope of the Thesis

The scope of this thesis is employing multiple-input, single-output, non-isolated DC-DC converter to enhance the energy management of FCS of EVs with a hybrid energy storage system. The proposed design of FCS aims to minimize the cost of operation, charging time, impact on the grid, and enhance the lifetime of the energy storage devices. It uses a single converter for all energy storage devices with a simple control strategy in order to reduce the overall cost of the system and facilitate maintenance and troubleshooting. The converter will be simulated at the power rate of (0-500 V DC, 0-60 A, and 17 kW) and tested in an experimental setup of 100 W to validate the simulation work.

1.4 Problem Statement and Solution Methodology

This research aims to design a dual input DC-DC converter that has a simple and modular configuration, so we can easily add more energy storage devices and power sources to the converter. Additionally, implement a control algorithm to make the converter work in different operation modes effectively. In addition, study different ways to reduce the voltage and current ripples of the converter, extend the lifetime of the battery, and calculate the converter losses and efficiency in different operation modes. To solve this problem, we will use MATLAB/Simulink to design and control the converter and calculate its losses and efficiency in different operation modes. The components' power rating will be set according to the market rate and to match the specifications of the FCS components as much as possible.

We will utilize seminal research publications to find the design calculations and equations required to determine the control parameters that will get the desired transient response. MOSFETs are selected as power switches for the proposed converter as they have good efficiency, high switching frequency, and can work at a high-power rate. To validate the proposed topology and the switching sequence in the different operation modes, this DC/DC converter design will be implemented in an experimental setup at a power rate up to 100 W.

1.5 Research Objectives

The thesis aims to design and simulate a multi-input non-isolated DC/DC converter in five operation modes with a hybrid energy system and analyze its different operational losses and efficiency in those modes. In addition, the proposed

converter is tested with fast-charging station (FCS) to charge an electric vehicle's (EV) battery. This battery has the same voltage rates as the one used in the famous Nissan Leaf EV. The energy storage devices within the FCS will be able to charge the EV's battery individually or simultaneously. Furthermore, the simulation work is implemented in a hardware scale with a lower power rate for demonstration and validation purposes.

1.6 DC-DC Converters

DC-DC converters are used to convert input voltage to a voltage that is less than or higher than that voltage. They are divided according to power flow capability into unidirectional and bidirectional. In the unidirectional case, power is transferred in only one direction at a time. While in the bidirectional one, power is transferred between the source and the load in both directions. DC-DC converters do not only transfer power between a given source and load, but can also transfer it between two energy storage devices without changing their voltage.

They are also divided into two categories: isolated and non-isolated. For isolated converters, their input and output sides are magnetically coupled using transformers or inductors. Also, each side has its separate ground, which increases its safety. Conversely, the input and output sides of non-isolated converters are electrically connected and have a common ground. This reduces their cost and weight; however, non-isolated converters have a limited voltage gain which can be increased by adding inductors, but this is not often recommended as it increases their loss, weight, and cost [9]. Table 1.1 summarizes the different topologies of isolated and non-isolated converters.

Table 1.1. Different topologies of DC-DC converters.

Non-isolated	**Isolated**
Buck	Half-bridge
Boost	Full-bridge
Buck- Boost	Flyback
Cuk	Forward
Zeta	Push-pull
Sepic	Boost Half-Bridge

The DC-DC converters use passive and switching elements for power conversion. The converter uses inductors and capacitors to reduce the current and voltage ripples. The power is converted by storing energy as a magnetic or an electric field on the input side. Magnetic field components include inductors and transformers, and the electric field components are capacitors. The stored energy is released through switching elements such as power switches and diodes at different output voltage levels. The supplied power to the load is controlled by changing the duty cycle of the power switches. The main objectives of designing any DC-DC converter are to increase its efficiency, reduce output ripples, and operate with good stability. The switching frequency of the converter determines the size, losses, and thermal/electric characteristics of the converter. For example, increasing the switching frequency will reduce the size and weight of the elements such as the inductors, but it will increase the switching losses of the converter.

1.7 Multi-Input DC-DC Converters

Similar to conventional converters, multi-input converters have different topologies. They have many merits over the traditional converters, such as reducing the number of components and the number of power conversion stages. They also offer better efficiency and centralized control. Each topology can combine one or more of these merits and features and add modularity to the converter to integrate more energy sources. However, obtaining all features and characteristics in one topology is impossible. The multi-input converters can be utilized in fast-charging stations to reduce the number of DC-DC converters and their cost and increase the conversion efficiency with centralized control. The multi-input DC-DC converters have proposed several topologies with various features and characteristics. The features include the number of operation modes, the number of components, the power flow capability, the number of input sources, and design modularity. Similar to conventional DC-DC converters, there are isolated and non-isolated multi-input DC-DC converters. The non-isolated converters are smaller in size and weigh less than the isolated converters, but the isolated converters are inherently safer due to the galvanic isolation between the input and the output.

1.8 Thesis Outline

This thesis consists of six chapters to discuss the design and topology of the proposed multi-input single-output (MISO) DC-DC converter for a hybrid energy system

of a fast-charging station (FCS) for electric vehicles. It also shows the simulation results of the converter in different operation modes, as well as the simulation results of the FCS with the multi-input DC-DC converter implementation. The experimental work for validation is also discussed. This thesis is organized as follows: Chapter 2 presents a comprehensive overview of EV charging standards and technologies and recent topologies of the MISO non-isolated DC-DC converters. Chapter 3 presents different energy storage devices like batteries and supercapacitors. Chapter 4 discusses in detail the design, analysis, and modeling of the converter, its five operation modes, and its controller.

Moreover, it presents the design of the proposed FCS in detail, including the control system. Chapter 5 shows the simulation results of the five operating modes of the standalone converter and the simulation results of the converter while integrated into the proposed FCS. Chapter 6 shows the experimental results of the operational modes of the converter to validate the simulation work. Finally, chapter 7 summarizes this work and suggests future improvements.

Chapter 2. Literature Review

2.1 Fast Charging Last Technologies

The fast-charging technologies play an essential role in reducing the charging time of the electric vehicle (EV)'s battery and increasing its lifetime. The EV's charger should be reliable, and have good efficiency. To maintain the power quality at a high level with a high-power factor, the current drawn from the grid by the EV's charger should have low harmonics. Many standards like IEEE1547, IEC1000-3-2, and the US National Electric Code (NEC) 690 determine the levels of the harmonics and DC injection into the grid. Therefore, most EV chargers are designed according to these standards, as well as the boost converter is used for power factor correction (PFC) for this objective in the traditional EV chargers. The fast-charging technologies are divided mainly into conductive charging and inductive charging. In conductive charging, the EV is connected directly to the charging plugs, while in inductive charging, the power is transferred magnetically to the EV. The topology of the power converters of each technology determines whether the power transfer will be bidirectional or unidirectional. Minimizing the battery degradation and hardware requirements can be achieved by unidirectional power transfer. The bidirectional charging system allows power transfer between the EV and the gird or the energy storage devices [10]. Many power electronics converters are used in fast charging technologies, like AC/DC converters, DC/AC inverters, and DC/DC converters, based on the need for a particular application. Typically, an EV charger has a front-end AC/DC converter with a back-end DC/DC converter. Buck/boost converter topology is used to achieve the PFC; therefore, modern EV charging design has this topology [11].

2.1.1 Conductive Charging

Conductive charging has different standards that determine the charging power rate and the connector type. Each region and country uses its standard; for example, the USA uses SAE and IEEE, Europe uses IEC, Japan uses CHAdeMO, and China uses Guobiao (GB/T). The GB/T is similar to IEC standards for AC and DC charging, and the most common standards used globally are IEC and SAE. The conductive charging is mainly divided into off-board and onboard charging regarding where the power conversion takes place. In the onboard charging, the power electronics are placed inside the vehicle, increasing the vehicle's size and weight and using AC power at low power

rates. The power electronics are placed outside the vehicle in the off-board charging, allowing the EV to charge with DC power at high power rates. Most fast-charging stations use this technology due to their capability to reduce the charging time of the EV.

2.1.1.1 Onboard Charging

The power electronics components in onboard charging, as mentioned previously, are placed inside the vehicle, and this limits the charging power rate [10]. However, these components are located inside the vehicle, allowing the user to charge from anywhere using any outlet. This is one of the main advantages of the onboard charging technology compared to off-board charging, as it reduces the infrastructure cost and increases the charging spots for the users [12]. The manufacturers utilize these components for charging and traction of the vehicle to improve the functionality of the power electronics components. The vehicle drive train consists of a traction machine, inverter, and DC-DC converter that can charge the EV battery in case of charging from the AC grid, as shown in Figure 2.1 [13].

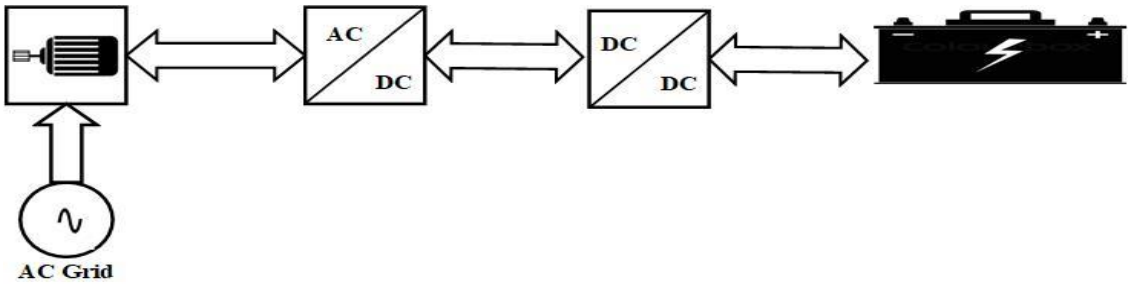

Figure 2.1 Utilization of the traction power electronics in the onboard charging.

As seen in Figure 2.1, the inductance of the traction machine is connected to the AC source, the inverter of the traction machine is used as a rectifier, and the battery is charged from the DC-DC converter. Using a DC microgrid instead of an AC grid means no need for the traction machine and traction inverter, as the DC microgrid will connect directly to the DC link. The vehicle will use only one built-in bidirectional DC-DC converter for voltage regulation of the DC link for EV's battery charging. To increase the safety of the vehicle, the onboard DC-DC converter should have galvanic isolation in case of the DC microgrid is connected directly to the DC link [13].

2.1.1.2 Off-board Charging

Nowadays**,** fast charging refers to off-board charging, and the size and weight of the EV can be reduced by using it, as the charging equipment will be located outside of the EV, as shown in Figure 2.2, compared to onboard charging.

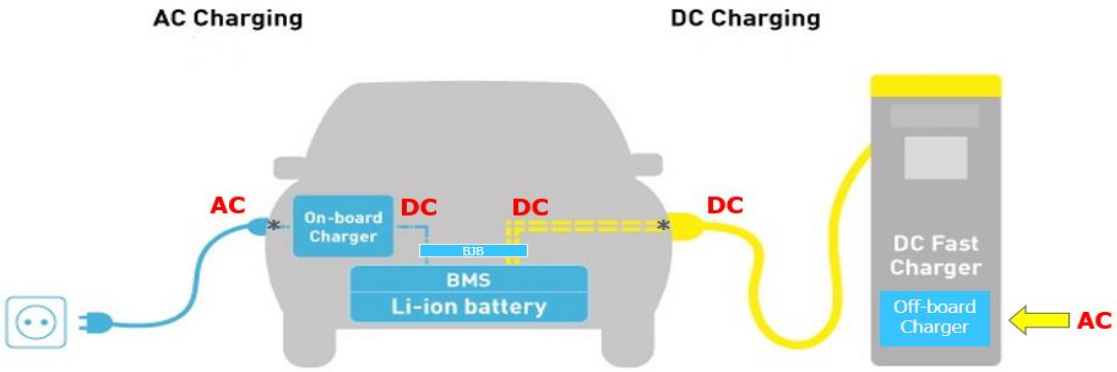

Figure 2.2. Onboard and off-board charging location in the vehicle [14].

The charging station's design should be capable of charging different vehicles with different connectors and communication standards. Therefore, the National Platform Electric Mobility recommends using the Combined Charging System to achieve the previous targets. The charger should also be able to charge the different types of EV battery configurations with different voltage levels. The fast-charging power rate is typically between 22 kW and 400 kW, and the three-phase AC circuit at 208, 240, 380, 480, or 575 V is used to achieve the previous charging power rate [15]. The power rate of charging determines the capability of bidirectional power flow in the fast charging station. As shown in Figure 2.3, the Off-board charging system generally consists of a rectifier with a filter to reduce the harmonics and DC-DC converter to charge the EV's battery from the DC link with its voltage rate.

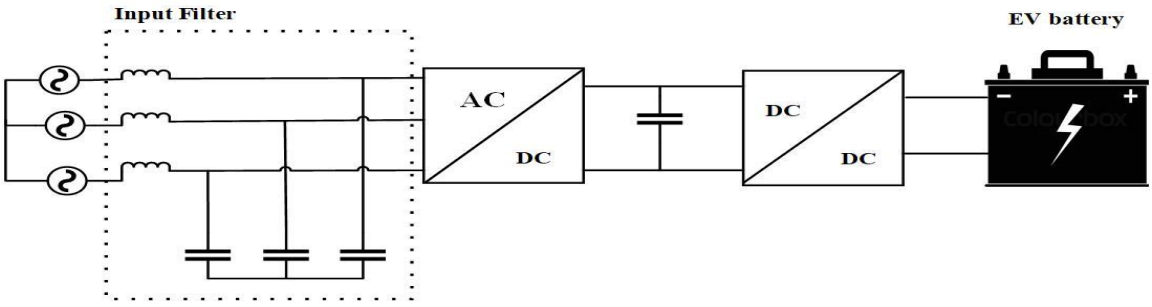

Figure 2.3 Off-board charger configuration.

Different rectifier and DC-DC converter topologies could use in this technology based on the application and charging power rate. The medium voltage grid connection could use additional transformers, increasing the space of the station. The cooling system is essential in fast-charging stations, and it is vital to use the water cooling in the high-power charging rates instead of the air cooling. In addition, as the charging occurs with high current rates, it is essential to cool the plugs with water [13]. Table 2.1 summarizes the power levels, power level types, typical use, and charging time of onboard and off-board charging [10].

Table 2.1. Onboard and off-board charging [10].

Power level types	Typical use	Power level	Charging time
Level-1/Single phase **120 Vac (US)** **230 Vac (EU)**	Charging at home	1.4 kW (12 A) 1.9 kW (20A)	4-11 hours 11-36 hours
Level-2/Single or three-phase **240 Vac (US)** **400 Vac (EU)**	Charging at private or public outlets	4 kW (17 A) 8 kW (32 A)	1-4 hours 2-6 hours
Level-3/ Three-phase (208-600 Vac or Vdc)	Commercial or public	50 kW 100 kW	0.2-0.5 hours

2.1.2 Inductive Charging

EV batteries can be charged without direct contact between the charging system and the EV by utilizing a varying electromagnetic field to transfer the power remotely across the air gap. Currently, a lot of research is being conducted to improve this technology as the inductive power transfer has several merits. For example, it can increase the convenience of the customer as he can charge his vehicle without leaving it. In addition, its weatherproof technology as the EVs can be charged in harsh weather such as heavy snow or rain without massive cables and thick duty plugs. Moreover, it increases the safety of the system as it is based on galvanic isolation and the availability of autonomous charging of EVs.

The efficiency of inductive charging is lower than conductive charging as the energy losses during the transmission are high. This will consume a lot of electricity to compensate for the energy losses of running an EV and is more expensive. One of the

main disadvantages of inductive charging is producing high magnetic fields that could harm the customer in the long term. The previous drawbacks make inductive charging availability in the market low.

As shown in Figure 2.4, the wireless charging system generally is based on converting the AC current drawn from the grid to high frequencies in the primary winding to induce AC currents in the secondary winding. The induced AC current is rectified to charge the EV [13]. The conversion of the AC currents into high frequencies and the primary winding are placed off-board, while on the vehicle, the secondary inductance, the AC-DC conversion, and battery charging take place.

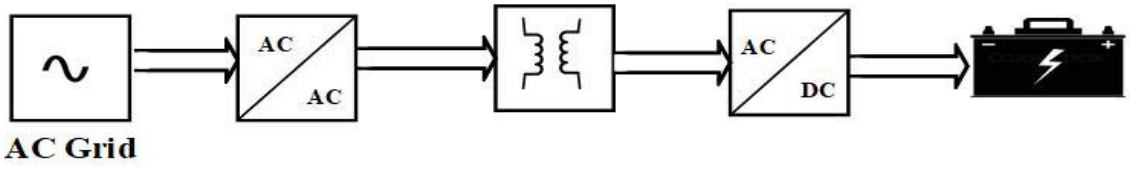

Figure 2.4 General inductive charging system.

Figure 2.5 shows an example of an inductive charging system in detail in [16]. Based on the electric isolation of the charging system, the system's components are divided into the components of the primary side and the secondary side. The primary side consists of the utility input, AC to DC Converter, DC to AC Converter, transformer, and matching circuit. The utility input supplies power in low frequency, either single-phase or three-phase. The utility's power is converted from AC to DC using the AC/DC converter with a power factor compensator to obtain a regulated DC voltage. Using an entirely switched bridge DC/AC converter can convert the power to high-frequency power. The system use transformer for isolation purposes to increase its safety, and the matching circuit uses low losses energy storage elements to inject high-frequency energy to the secondary side. The secondary side consists of a matching circuit similar to the primary side's matching circuit to inject the energy into the AC/DC converter. The converter has an LC filter on its output that supplies the battery of the vehicle with DC power.

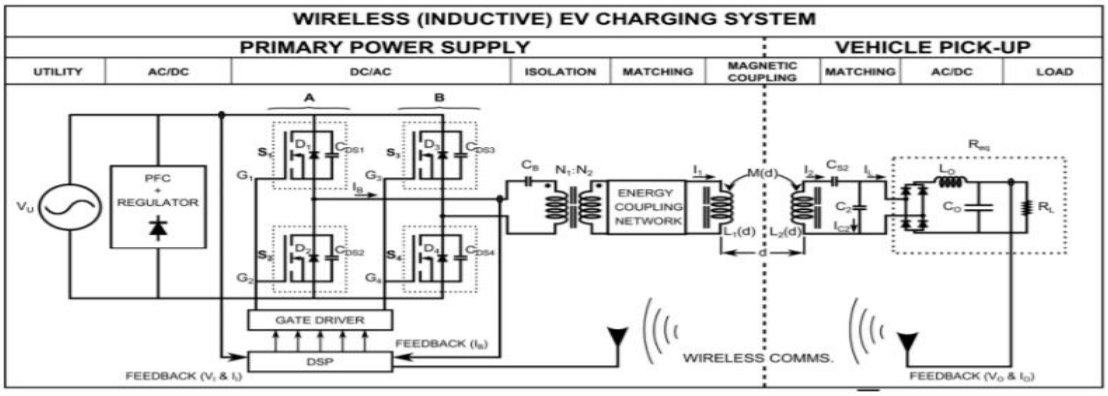

Figure 2.5 Detailed inductive EV Charging System [16].

The design of the coupled winding is the core of the inductive charging as the efficiency, power transfer level, the excepted levels of shielding and magnetic emissions, and overall performance-based on it [17]. The resonant converters are mainly used in inductive charging systems. The resonance frequency of the system depends on the alignment of the vehicle to the primary winding; if the alignment changes, the resonance frequency will change. The maximum power is achieved in the resonance frequency; thus, regulating the operating frequency to the resonance frequency is crucial to maximizing the power transfer. Using materials like silver-plated copper or aluminum for the secondary coil will reduce its size and resistance, and improve the charging system performance. Besides, increasing the transmission frequency will increase the power transfer efficiency by using the same power density. However, increasing the transmission frequency is not always possible, as the power electronics of the charging system could not be capable of working with these high frequencies [17].

Equation (2.1) shows the relation between the switching frequency, duty cycle, the input voltage of the inverter, and the amount of power transferred to the secondary coil.

$$U_1(t) = \frac{4\,U_{d0}}{\pi}\sin(d\,\frac{\pi}{2})\cos(\omega t) \qquad (2.1)$$

Where U_{d0} is the high-frequency power inverter rail voltage, d is pulse duty ratio, and ω is the angular frequency as by controlling these parameters, the power transferred can be regulated [8]. The SAE J2954™ team determines three classes of wireless power transfer (WPT) of EVs and PEVs. The first one is up to 3.7 kW, the second is 7.7 kW, and the third is 22 kW [17].

This technology is still under development as few companies offer wireless charging. Qualcomm Halo produced wireless charging at a power rate of 22 kW and was successfully used by the Formula E electric race series. BWM will sell a wireless charging pad capable of charging an EV in 3.5 hours [18]. The researchers are now working to optimize the cost and efficiency, increase misalignment tolerance, and reduce the size of the WPT chargers.

2.1.2.1 Stationary Charging

In stationary wireless charging, the EVs are charged by placing the vehicle in a specific charging spot where the primary coil of the site is coupled with the secondary coil placed in the vehicle, as shown in Figure 2.6.

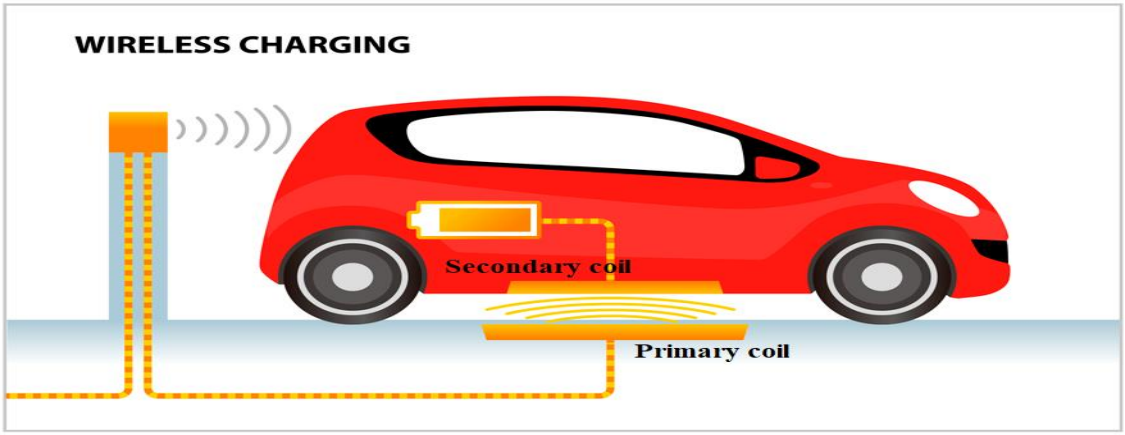

Figure 2.6 General configuration of stationary charging.

This technology could be suitable in some applications like embarking and disembarking the passengers while charging the bus. To prevent floods or any other hazardous situations in the primary coil, it is sealed in rubber or covered with plastic. The primary coil is located in a pad that contains ferromagnetic materials to shape the magnetic field, reduce the leakage of the magnetic field, and includes metal rings or plates. Installation of an automatic guidance system can increase the coupling between the primary and the secondary coils, as the driver can align directly above the primary pad using this system [19]. The efficiency of the charging increase by increasing the overlapping area between the primary and secondary coils. With air gaps of 1-150 mm between the primary coil and secondary coil, the stationary charging can transfer power up to 50 kW [20].

2.1.2.2 Road-Embedded Charging

The road-embedded charging is presented as an alternative to the fast-charging stations as the EV can be charged while it is moving, as illustrated in Figure 2.7, as the primary coil is located on the pavement, and the secondary coil is located inside the vehicle.

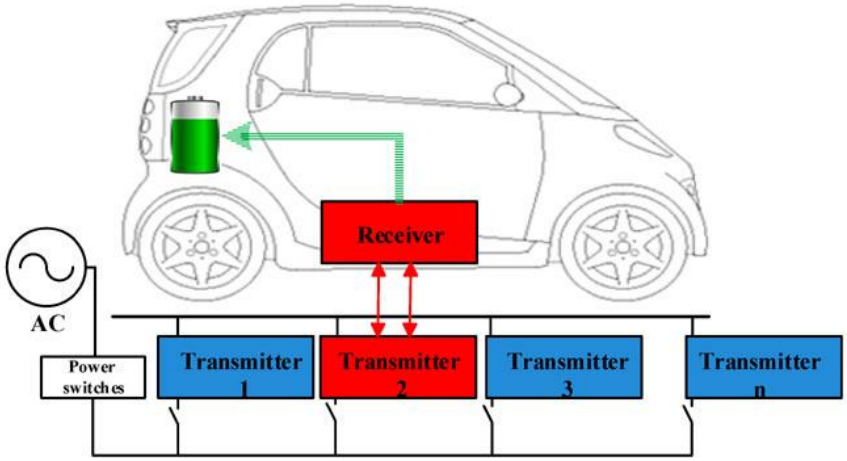

Figure 2.7 Road-embedded charging concept.

The battery in road-embedded charging is continuously charged, which will reduce the battery size and hence reduce the size and cost of the vehicle. Also, the battery is continuously charged, which will eliminate the range anxiety. As the primary transducers need to be installed on all the roadbeds, this will increase the installation and maintenance costs of this technology. One of the main drawbacks of this technology also is the coupling between the primary and secondary coils is low due to the high air gap between them. Many research has been conducted on-road embedded charging to study the relationship between highway driving cycle and inductive power transfer systems with power levels varying from 10–60 kW and coverage from 10–100%. The results as shown in Figure 2.8 shows that 50% of the road can be covered with a 20 kW power of the driving range or 20% with a power of 50 kW. For power transfer greater than 20 kW, a very high driving range can be obtained for coverage of more than 50% [21].

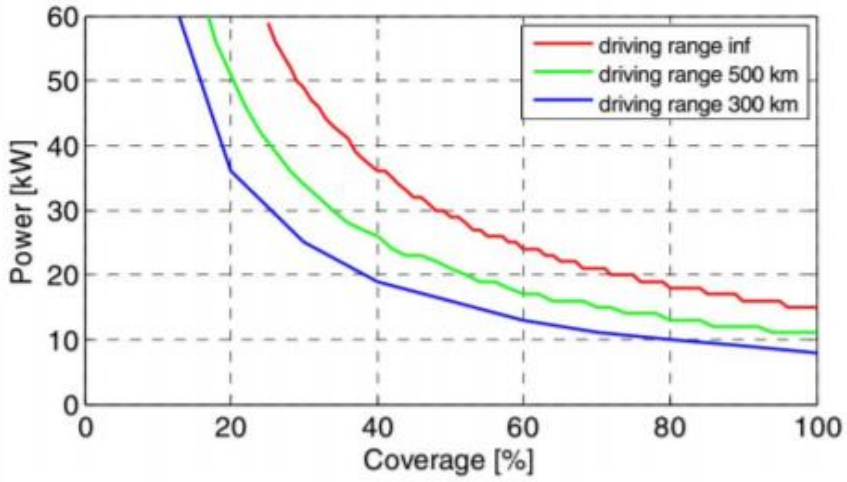

Figure 2.8 Power rate transferred for different coverage of road embedded charging and the driving range [21].

More development has also been applied to integrate renewable energy sources using several technologies like wind generators and solar roadways in road-embedded charging for charging EVs on the highways [22]. Generally, road-embedded charging has lower efficiency and high costs than stationary charging [13].

2.1.3 Battery Swapping

One of the suggested methods for fast charging is using the swapping battery technique as the discharged battery could be replaced by charged one, by opening the bottom of the vehicle manually or automatically and then changing the battery in the swapping charging station. The range anxiety of the EVs is one of the main challenges of EV adoption, and this technique could face this problem. The battery swapping could take 5-15 minutes for energy replenishment to minimize the charging time. Battery swapping can play an important role in reducing the price of the EV, as the total price of the EV will be reduced by reducing the cost of the battery.

However, this approach still has many limitations in being applicable, such as the batteries of the EVs should have the same type, dimensions, and size. In addition, the internal connections and shape of the battery should be standardized by all manufacturers. The manufacturers reject this method as it will reduce the OEM's freedom of design [13].

2.2 Fast Charging Standards and Protocols

Many standards have been established to deal with EV charging infrastructure worldwide. Each region and country use its standard; for example, the USA uses SAE and IEEE, Europe uses IEC Japan uses CHAdeMO, and China uses Guobiao (GB/T) as

well as similar to IEC standards for AC and DC charging. The most common standards used globally are the IEC and SAE standards.

2.2.1 IEC Standard

The International Electrotechnical Commission (IEC) is a British standardization organization that develops electrical, electronic, and related technologies standards. Several IEC standards for fast charging of EVs are applied depending on the equipment used and the operation condition [23].

2.2.1.1 IEC 61851

The IEC 61851 has been used for off-board and onboard charging of EVs at a voltage rate of 1500 V DC and 1000 V AC. Table 2.2 summarizes the different sections of the IEC 61851 standard and their definitions [24].

Table 2.2 Sections and definitions of the IEC61851 standard.

Section	Definitions	
IEC61851-1	The standard for cable connection and plug setups to charge EVs and it is divided into 3 cases A, B, and C	Type 1: The EV is attached permanently to the cable, but it is detachable at the charging station.
		Type 2: The cable is not attached permanently to the EV or the charging station.
		Type 3: The charging station permanently to the charging station.
IEC61851-21-1	The EMC requirements of the onboard charging for AC/DC supply of conductive charging.	
IEC61851-21-2	The EMC requirements of the off-board charging for conductive charging.	
IEC61851-23	The DC fast-charging station requirements.	
IEC61851-24	Addressing the digital communication to control the DC charging between the equipment of the EV supply and the charging controller of the EV.	

2.2.1.2 IEC 61980

The standard of IEC 61980 applies for wireless power transfer for EVs from supply networks in voltage rates up to 1500 V DC and 1000 V AC and from on-site storage systems such as buffer batteries [25].

2.2.1.3 IEC 62196

IEC62196 standard defines requirements and tests for different accessories and equipment used for conductive EVs charging. Table 2.3 summarizes the various sections of the IEC 62196 standard and their definitions [26].

Table 2.3 Sections and definitions of the IEC62196 standard.

Section	Definition
IEC62196-1	Identify the requirements for plugs, socket-outlets, connectors, inlets, and cable assemblies of conductive charging of EVs in voltage and the current rate of 690 V AC and 250 A, and voltage and the current rate of 500 V DC and 400 A.
IEC62196-2	Applies for different accessories and equipment of standardized configurations in voltage rate of 480 V AC and the current rate of 63 A for 3 phase and 70 A for 1 phase.
IEC62196-3	Applies to EVs couplers with pins and contact tubes in EV conductive charging in voltage rate of 500 V DC and the current rate of 250 A and voltage rate of 1000 V AC and the current rate of 250 A.

2.2.2 SAE standards

The Society of Automotive Engineers (SAE) is an American organization that develops standards for different industries, especially in the transportation sector like aerospace and automotive. Several SAE standards for fast charging of EVs are applied depending on the equipment used and the operation condition [27].

2.2.2.1 SAE J2293

This standard establishes requirements for transferring electric energy for EVs from the electric utility in North America. It also defines all the characteristics needed for the energy transfer system to ensure functional interoperability between electric vehicle supply equipment (EVSE) and the EV.

2.2.2.2 SAE J2293-1

This section addresses the physical requirements to transfer power during the operation condition of inductive charging, DC and AC conductive charging between EVSE and EV, and to send the information between them [28].

2.2.2.3 SAE J2293-1

This section identifies the communication requirements and the network architecture to communicate between the EVSE and the EV [29].

2.2.2.4 SAE J1772

This standard defines the connector's configuration for EV conductive charging couplers and the EV charging station communication protocol for DC and AC charging, including the three charging levels. The standard discusses the different types of equipment rating of EV charging, such as charging current, voltage, and circuit breaker

rating. All EVs sold in North America have SAE J1772 charging sockets except Tesla, as it uses an adaptor. Table 2.4 summarizes the voltage and current rates in IEC 62196, IEC 61851, and SAE J1772 standards [30, 31].

Table 2.4 Voltage and current rates in IEC62196, IEC61851, and SAEJ1772 standards.

Standard	Source	Mode/Level	Voltage (V)	Phase	Max Current (A)
IEC 62196	AC	Mode 1	120	Single	16
		Mode 2	240	Single	32
		Mode 3	250	Single	32-250
	DC	Mode 4	600	DC	400
IEC 61851	AC	Mode 1	120	Single	16
		Mode 2	240	Single	80
	DC	Mode 4	200-450	DC	80
SAE J1772	AC	Mode 1	120	Single	16
		Mode 2	240	Single	32-80
	DC	Mode 1	200-450	DC	80
		Mode 2	200-450	DC	200

2.2.2.5 SAE J1773

This standard establishes the minimum interface requirements for manual connected inductive charging of EVs in levels 1,2 and 3 in North America. This standard is not applicable for automatic connection or transferring power at frequencies significantly higher than power line frequencies [32].

2.2.2.6 SAE J2847 and SAE J2836.

Along with SAE J1772, these two standards define the communication needs between the charging infrastructure and an electric vehicle. SAE J2847 describes the communication requirements, while SAE J2836 specifies the use cases and testing infrastructure. Table 2.5 lists the various sections and names of the SAE J2847 and SAE J2836 standards and the application areas that can be inferred [32, 33].

Table 2.5 Sections of the SAEJ2847 and SAEJ2836 standards and their definitions.

Section	Definition
SAEJ2847/1-2	Communication between plug-in vehicles, off-board DC chargers, and between plug-in vehicles and the utility grid.
SAEJ2836/1-2	Use cases for communication between plug-in vehicles and the utility grid and between plug-in vehicles and an off-Board DC charger.
SAEJ2836/3	As a DER, use cases for plug-in vehicle communication
SAEJ2836/4- 6	There are use cases for diagnostic, customer, and wireless charging communication for plug-in automobiles.

2.2.2.7 SAE J2931

This standard specifies the requirements for digital communication between electric vehicle supply equipment, plug-in automobiles, service providers or utilities, advanced metering infrastructure, energy services interface, and the home area network. Table 2.6 summarizes the different sections of the SAE J2931 standard and their definitions [34].

Table 2.6 Sections and definitions of SAE J2931 standard.

Section	Definition
SAEJ2931-1	The architecture and general needs for digital communication are defined in this standard.
SAEJ2931-2	Using FSK and the SAE J1772TM Pilot wire, define a MAC and PHY layer implementation of digital communications.
SAEJ2931-3	Using NB OFDM and either the SAE J1772TM Pilot wire or mains, define a MAC and PHY layer implementation of digital communications.
SAEJ2931-4	Defines the digital communications MAC and PHY layer implementation using BB OFDM and either the SAE J1772TM Pilot wire or mains.

2.2.2.8 SAE J295

Wireless power transfer (WPT) of light-duty plug-in electric vehicles for acceptance criteria for interoperability, electromagnetic compatibility, electric and magnetic fields (EMFs) identified in this standard for an industry-wide. In addition, minimum performance, safety, and testing are determined in this standard. This standard is designed for stationary applications (charging while the vehicle is not in motion) [34].

2.2.3 Combo Charging System (CCS)

The Combo Charging System (CCS) is an international standard that SAE has approved. It has many advantages, like combining the AC charging of a single-phase or three-phase with DC charging in a single charging connector in a power rate of 50 kW-350 kW. Besides, it is easier to use the system and much lighter charging cord than CHAdeMO. The standard is used in the USA and Europe and uses the power line communication (PLC) for communication as part of control charging using smart grid protocol [35].

2.2.4 CHAdeMO Standard

CHAdeMO is a DC charging standard developed by the CHAdeMO Association for electric vehicles with power ratings ranging from 6 kW to 400 kW and voltage and current ratings up to 1000 V and 400 A with 900 kW. It uses the CAN protocol to ensure

smooth communication between the EV and the charger [36]. The standard is based on four principles:

1-Security: by creating chargers that are safe to use in any environment.

2- Future-proof: by including bi-directional charging and compatibility with any local or optional functions in addition to charging.

3- Ease of use: The protocol is compatible with CAN and onboard communication networks, making integration with the rest of the vehicle simple and reliable.

4-Uniformity: The CHAdeMO connector is the same worldwide and can be used with or without an AC adapter. It allows for cross-continental EV travel and saves EV manufacturers money.

2.2.5 Guobiao Standard

The Guobiao (GB/T) is a Chinese standard published by the Chinese National Committee of ISO and IEC and the Standardization Administration of China (SAC). The GB/T standard specifies the general criteria for electric vehicle conductive charging, the connection settings for both AC and DC charging couplers, communication protocols, and electric energy metering. Table 2.7 lists the various sections of the GB/T standard and their definitions [37].

Table 2.7 Sections and definitions of GB/T standard.

Section	Definition
GB/T20234.1	Defines the requirements, testing methodologies, and testing specifications for the conductive charging connection set for electric vehicles.
GB/T 20234.2	The characteristics and dimensions of an AC charging coupler for conductive charging of electric vehicles at maximum voltage and the current rate of 63 A AC and 440 V AC are specified.
GB/T 20234.3	The characteristics and dimensions of a DC charging coupler for conductive charging of electric vehicles at maximum current and voltage rate of 250 A and 1000 V DC are specified.
GB/T 27930	The CAN communication protocol between the EV battery management system and the off-board conductive charger is defined in this standard.
GB/T 28569	Specifies the technical requirements of electric energy metering for the EV AC charging spot.

2.3 Existing Topologies of the Multi-input Converters

Several research has been conducted on the multi-input DC-DC converters to employ them in many applications like integrating renewable energies in microgrids, hybrid generation systems, and HEV/FCV applications. Increasing the modularity of the

multi-input converters becomes one of the main research targets of this technology, so it can easily integrate more energy sources and enhance the energy management of some applications. Many studies have been conducted to lower the switching losses of multi-input DC-DC converters using zero current switching (ZCS) or zero voltage switching (ZVS). The characteristics of the multi-input DC-DC converters are also based on the control methods; therefore, many studies have been implemented to improve the control strategies to enhance and increase the energy management of different energy resources. The merits and limitations of each topology decide which applications it can be used for.

Several topologies have been proposed in the multi-input DC-DC converters. Each topology has its features and characteristics, such as the number of the operation modes, the number of components, the power flow capability, the number of input sources, and the modularity of the design. Similar to the conventional converters, the structure of the multi-input converter is divided into non-isolated and isolated converters. This section discusses different topologies of non-isolated structure, as the non-isolated converters have less size and weight than the isolated converters. The comparison between the different topologies will be in terms of the number of components, the operation modes, the power flow capability, and the modularity of the design.

2.2.6 Multi-input Buck/Buck-Boost Converter

This topology [38] works in four different operation modes. As shown in Figure 2.10 the two power sources supplying the load using two power switches and two diodes and one inductor. This converter has a unidirectional power flow since the two sources can deliver the power separately or together to the load, but the power can not be transferred from the output to the input.

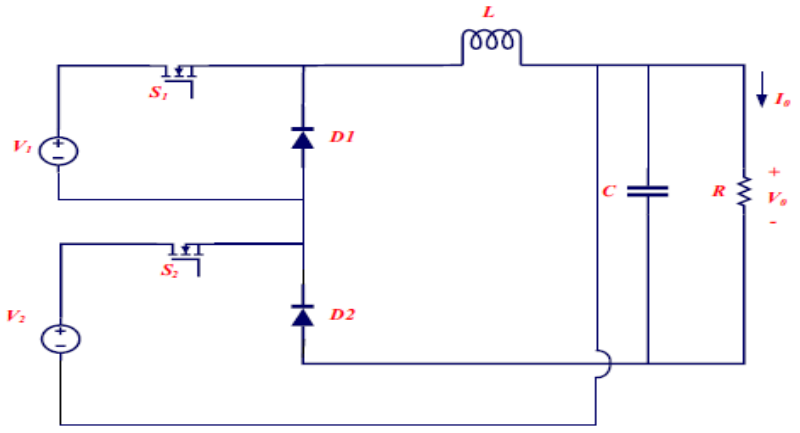

Figure 2.10 Multi-input buck/buck-boost converter.

The four operation modes of this topology are:

1. Switch S_1 is turned on, and switch S_2 is turned off in the first operation mode, so the load is supplied from the first source, V_1.
2. Switch S_1 is turned off, and switch S_2 is switched on in the second operation mode, so the load is supplied from the second source, V_2.
3. The switches S_1 and S_2 are turned off in the third operation mode, so the load is supplied by Capacitor C.
4. The switches S_1 and S_2 are turned on in fourth operation mode, so the load is supplied simultaneously from sources V_1 and V_2.

2.2.7 Multi-input DC-DC Boost Converter

The topology [39] is typically used in renewable energy applications to utilize the distributed generation sources in an integrated structure. It utilizes two power sources, PV arrays and fuel cells, and one energy storage like a battery. As seen in Figure 2.11, the load is supplied with continuous input and output current using two power switches with high efficiency. It depends on two switching periods introducing two duty ratios to control the power from the power sources and the energy storage.

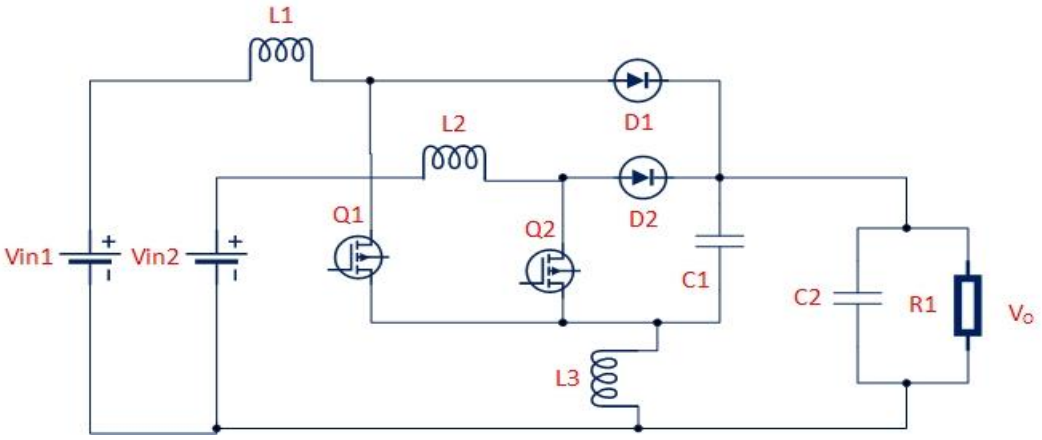

Figure 2.11 Multi-input DC-DC boost converter.

The three operation modes of this topology are:

1. Charging L_1 from the input source Vin_1 when the switch S_1 is turned on, and S_2 is turned off.
2. Supplying the load from both inductors L_1 and L_2 when the switches S_1 and S_2 are turned off.

3. Charging L_2 from the input source Vin_2 when the switch S_1 is turned off, and S_2 is turned on.

This topology works in the unidirectional power flow so that the input power sources can supply the load only.

2.2.8 Hybrid Buck/Buck DC-DC Converter

The topology [40] is suitable for applications whose output voltage needs a high voltage range, such as telecom power systems, renewable energy, and electric vehicles. This topology delivers power to the load from two power sources, either separately or simultaneously. From Figure 2.12, the main drawback of this topology is that it has high parts numbers. The converter works in four operation modes in unidirectional power flow and continuous conduction mode.

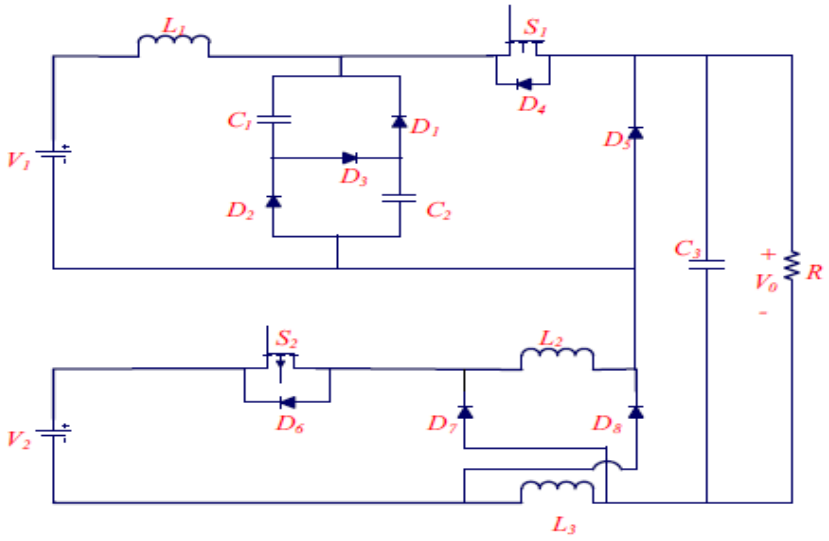

Figure 2.12 Hybrid buck/buck DC-DC converter.

The four operation modes of this topology are:

1. S_1 is switched on, and S_2 is turned off in the first mode, so the source V_1 charges inductor L_1 and supplies power to the load.
2. The switch S_1 is turned off, and S_2 is turned on in the second mode, so source V_1 charges capacitors C_1 and C_2, while source V_2 supplies power to the load and charges inductors L_2 and L_3.
3. The switches S_1 and S_2 are turned on in the third mode, so the sources V_1 and V_2 supply the power to the load.

4. The switches S_1 and S_4 are turned off in the fourth mode, so the inductors L_2 and L_3 and capacitor C_3 discharge in the load.

2.2.9 Bridge-type Dual-input DC-DC Converter

This topology [41] is used in DC microgrid applications to integrate two different sources that have different V-I characteristics. The load can be supplied from the two sources individually or simultaneously, and as seen in Figure 2.13, this topology utilizes three power switches to work in three different operation modes in unidirectional power flow. The structure of this topology has the advantage of connecting the two sources in series connection with fewer conduction losses [42].

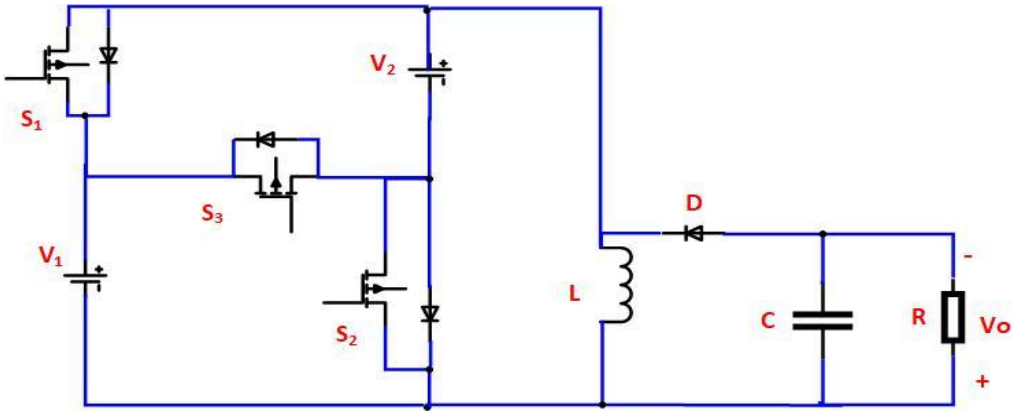

Figure 2.13 Bridge-type multiple-input DC-DC converter.

The three operation modes of this topology are:

1. The switch S_1 is switched on, and the switches S_2 and S_3 are turned off in this mode, so the source V_1 supplies the power to the load.
2. The switch S_2 is switched on, and the switches S_1 and S_3 are turned off in this mode, so the source V_2 delivers the power to the load.
3. The sources V_1 and V_2 supply the power simultaneously to the load when the switch S_3 is turned on, and S_1 and S_2 are turned off.

2.2.10 Multi-input Converter Based on Switched Capacitor

Many switched capacitor cells make up this topology [43], as seen in Figure 2.14. Each cell uses two diodes, one capacitor, and one power switch. The number of input sources equals the number of power switches and capacitors. This topology does not employ any magnetic components; it is based only on the active switches and capacitors; therefore, it has less weight and size than the many multi-input converters. It also has the advantage of modularity, as it can integrate many power

sources by adding more switched-capacitor cells and work in high frequencies with low losses. This topology suitable for the applications has many power sources like microgrids, as the output power is the summation of the input sources.

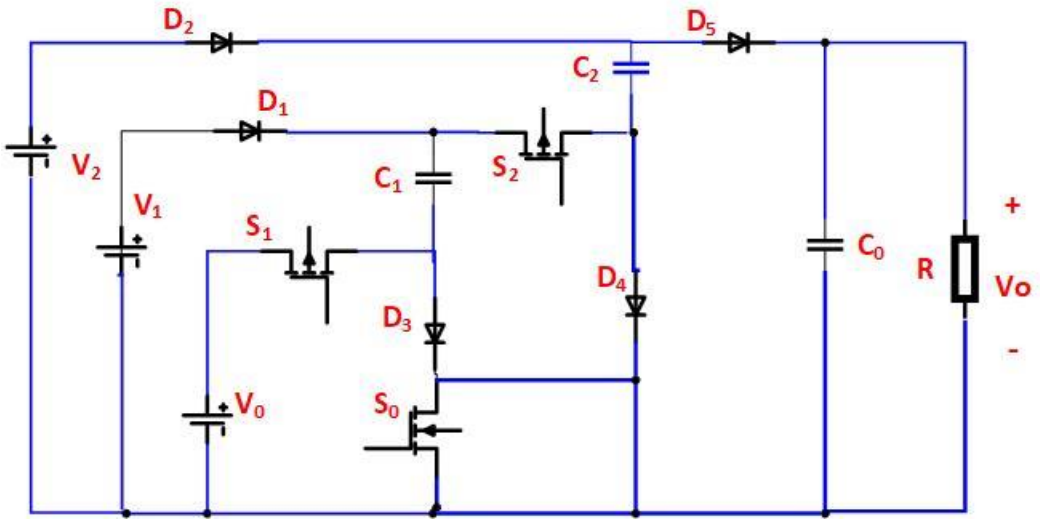

Figure 2.14 Multi-input converter based on switched capacitor.

This topology works in two different operation modes to supply the load:

1. The sources V_1 and V_2 are charging the capacitors C_1 and C_2 through the forward diodes bias D_1, D_2, D_3, and D_4 when the S_0 is turned on, and S_1 and S_2 are turned off and the output capacitor C_o is discharging in the load.
2. The capacitors C_1 and C_2 discharge through D_5 with source V_0 to charge the output capacitor C_0 when the S_0 is turned off and S_1 and S_2 are turned on.

2.3.6 Multi-Input Non-isolated DC-DC Converter with Vehicle to Grid Feature

This topology [44] is used in electric vehicle (EV) applications to charge the EV from the PV while parked and execute vehicle to grid or vehicle to vehicle operations. The proposed converter can work in six operation modes based on the EV's battery status, the power availability of the PV, and the bank of the battery. The proposed converter in Figure 2.15 consists of three IGBTs with antiparallel diode (S_2, S_m, and S_{Bi}), one IGBT without antiparallel diode (S_1), a diode (D_1), an inductor (L), an output capacitor (C) and four relays (R_1, R_2, R_3, and R_A).

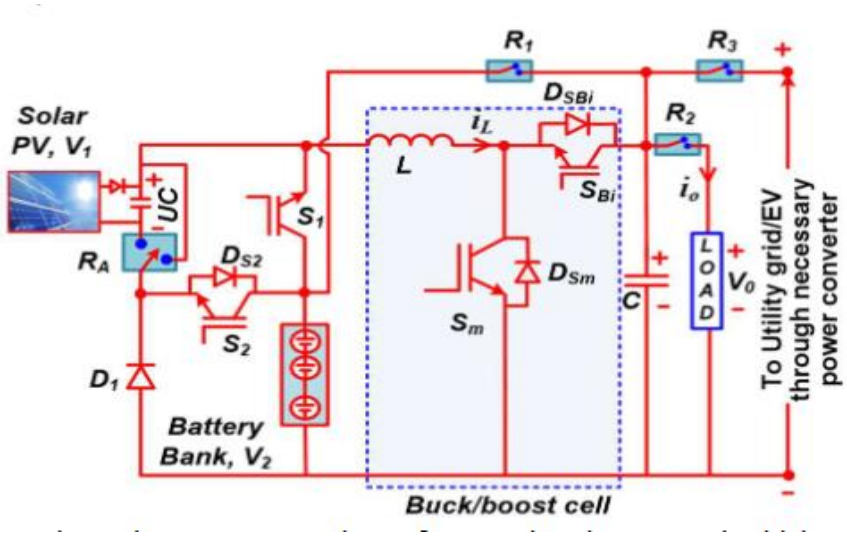

Figure 2.15 The converter topology of MISO with vehicle to grid feature.

The six operation modes of the proposed topology:

1. **Boost operation:** The R_2 and R_A relays are turned on in this mode, while the rest of the relays are turned off.
2. **Solar PV-powered operation:** The load is powered only by input source V_1. The relays R_2 and R_A are in the active state throughout this mode, whereas the other relays R_1 and R_3 are turned off.
3. **Battery-powered operation:** The load receives power only from the input source V_2. The relay R_2 is continually turned on, whereas the remaining relays are kept off.
4. **Battery charging from solar PV:** The relays R_1 and R_A are maintained on to charge the battery from solar PV, while the remainder of the relays are kept off.
5. **V2G in parking mode:** The relays R_3 and R_A are kept in the on position to export power from solar PV into the utility grid, while the rest are held off.
6. **Bidirectional rear-buck operation:** R_2 and R_A are enabled, while the remaining relays are disabled.

2.3.7 Expandable Non-Isolated Multi-Input Single-Output DC-DC Converter with High Voltage Gain

The proposed converter in [45] has several advantages, it has a simple switching sequence, the input sources have low current ripples, the low voltage stress on the switches, and the feature of extendibility to extend more PVs to the DC bus of the

system. However, it is a unidirectional converter, so the power can not be transferred to the input sources.

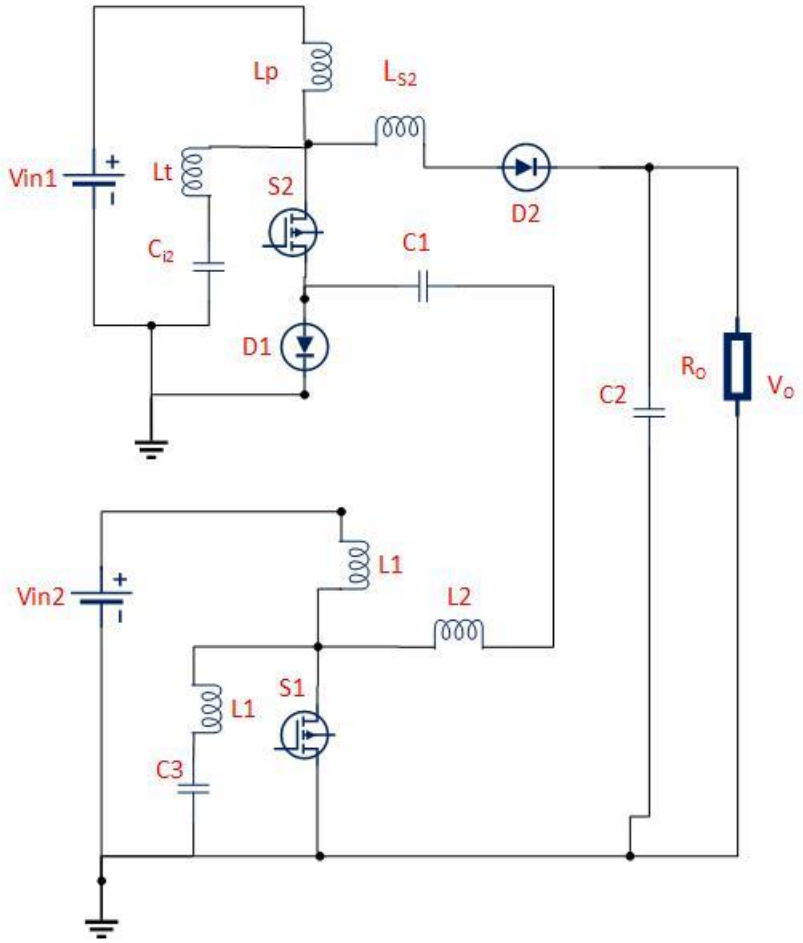

Figure 2.0:16 Multi-input converter with high voltage gain

Mode 1: In the first mode V_{i1} and V_{i2} charge inductors except for inductor L_{s2} through switches S_1 and S_2.

Mode 2: In the second mode**,** all the inductors including L_{s2} discharge in the load.

2.3.8 Single Inductor Bidirectional Multi-Input Converter with Continuous Battery Current Based on Integration of Buck and Three Port Boost Topologies

The proposed converter in [46] has the advantage of it can work in different operation modes with minimum components, as well the power can be transferred between the output and the input sources in bidirectional power flow capability. However, this topology lacks the modularity to extend the power sources or energy storage devices. This converter can work in five operation modes as follows:

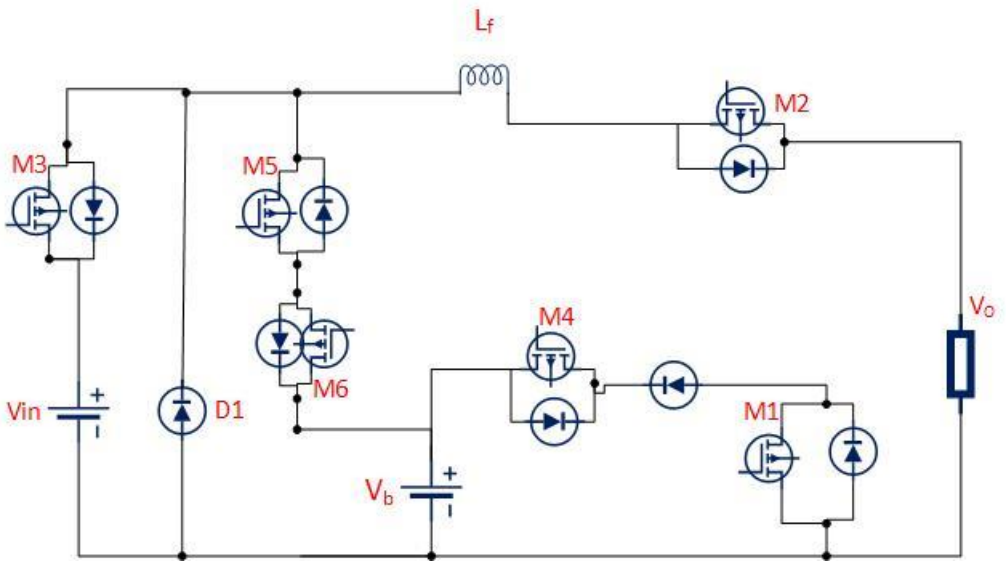

Figure 2.17 Multi-input converter with single inductor.

Single input single output mode (SISO) - P2O: In this mode switch M_3 is turned on to transfer the power from V_i to V_o in a boost topology**.** This mode can be utilized to charge the output load from the PV only.

Single input single output mode (SISO) - B2O: In this mode switch M_6 is turned on to transfer the power from V_i to V_o in a boost topology through the diode of M_5**.** This mode can be utilized to charge the output load from the battery only.

Single input single output mode (SISO) - P2B: In this mode switches M_4 and M_3 are turned on to transfer the power from V_i to V_b in a buck topology through the diodes D_2 and D_1**.** This mode can be utilized to charge the battery from the PV.

Single input single output mode (SISO) - O2B: In this mode switch M_5 is turned on to transfer the power from V_o to V_b in a buck topology**.**

Double input single output mode (DISO) - P&B2O: In this mode, the power is transferred from the battery and the PV simultaneously in 4 intervals to the output during peak hours**.**

Double input single output mode (DISO) - P&O2B: In this mode, the power is transferred from the output and the PV simultaneously to the battery when the PV can produce the power.

Single input double output mode (SIDO) - P2O&B: In this mode, PV produces power more than the output load, hence the extra power stored in the battery.

2.4 Reliability and Fault Analysis of the Power Converters

Reliability is defined as the probability that an item (component, subsystem, or system) performs required functions for an intended period of time under given environmental and operational conditions [47]. For power electronic systems, reliability research at the component level has been mainly focused on failure rate models for the key components in power circuits, such as power semiconductors, capacitors, and magnetic devices. The statistical reports on fragile components report that are more prone to fault parts are capacitors and semiconductor switching devices [48].

Chapter 3. Energy Storage Devices in Charging Stations

3.1 General

One of the main challenges the stakeholders face in increasing the number of fast-charging stations is the massive load caused by EVs on the utility during peak hours. The level 1 charging of EV load is equivalent to ½ of an entire home load, and a level 2 charging of EV load is equal to almost two entire homes. One of the suggested solutions to solve this problem is to use energy storage systems (ESS) to store the energy from renewable energy sources like solar PVs and wind turbines. Another solution is to charge EES from the utility grid during the off peak-hours using the low energy price hours and use it on the peak hours to charge the EVs. In addition, integrating an ESS into a fast-charging station (FCS) can mitigate the influence of the large-pulsating load of the FCS during peak hours. By integrating ESS, the high pulsating load demand is supplied through the ESS, while the medium voltage (MV) distribution grid supplies the relatively smaller and continuous load demand via the service transformer and cable. Thus, the investment in the transformer and cable can be considerably reduced. Moreover, it will also save the cost of EV charging from the customer's perspective.

3.2 Batteries

3.2.1 Batteries Technologies

The battery is an electrochemical device that uses electrochemical cells to transform chemical energy into electrical energy. Non-rechargeable batteries (which cannot be recharged due to irreversible chemical reactions) and rechargeable batteries (such as lead-acid, nickel-metal hydride (NiMH), and lithium-ion (Li-ion) batteries) are the main two types of the batteries. The cost and range anxiety of the battery of the EV is one of the main concerns for preventing EV penetration. Therefore, a lot of research has been conducted to develop and test new battery technologies to solve these issues. For example, graphene-based technologies charge in 15 seconds and supplement traditional EV batteries. Eliminating cobalt will significantly reduce the battery price [49], as it represents 25 … 50 % of the price of the electric vehicle, depending on the technology. It is expected by 2025, the price of the EV’s battery will reduce, and this can be observed by decreasing the cost of the production of the Li-Ion batteries by over 50 % from 2007 until 2014 [50]. Most EVs nowadays use 400 V battery systems, and the buses and trucks use 800 V battery systems. There is a trend toward increasing the personal EV’s battery

system to 800 V [13], as expanding the voltage battery will reduce the load current and the weight and size of the cables and connectors.

3.2.2 Equivalent Circuit

Figure 3.1 (a) shows the open-circuit voltage V_{oc} ,and the internal resistance rd in a basic equivalent circuit model for the battery. When the battery is fully charged, both can be estimated using open-circuit measurement [40]. The first-order equivalent circuit is shown in Figure 3.1 (b), where, V_o. and, V_{ocv} are the terminal voltage and open-circuit voltage (OCV), respectively, and the relationship between them can be expressed as (3.1) to (3.2). The ohmic voltage and polarisation voltage, respectively, are denoted by, V_R and, V_P.

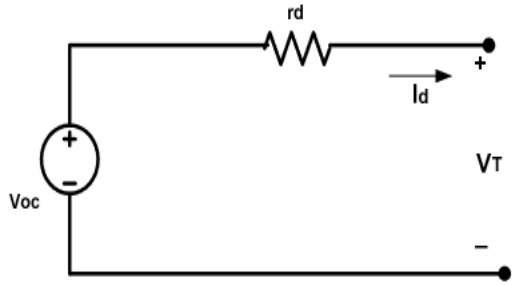

Figure 3.1 Open circuit voltage for battery model (a)

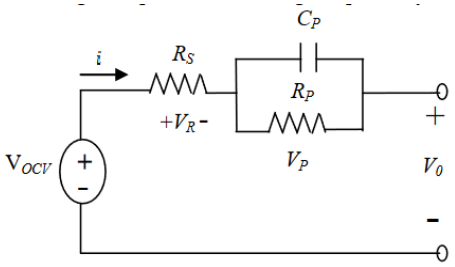

Figure 3.1 first order equivalent circuit for battery model (b)

$$V_o = V_{ocv} - (V_R + V_P) \qquad (3.1)$$

$$V_R = iR_S \qquad (3.2)$$

Temperature, operational current, and state of charge all affect ohmic resistance, and the variances in charge and discharge resistance are also labeled [40]. The following equation can be used to compute the state of charge (SOC) of the battery:

$$SOC = SOC(t-1) + \int_o^t \frac{I}{C_{bat}} . dt \qquad (3.3)$$

Where:

I	Charge/discharge current [A]
T	Time [h]
C_{bat}	Battery capacity [Ah]

SOC Battery state of charge at time t [%]

$SOC(t-1)$ Battery initial state of charge [%]

3.2.2 Types of Batteries

Several batteries today are accepted by the EV manufacturers to be used in the EV or for FCS as an energy storage device. Each type has its advantages, disadvantages, and chrematistics.

Lead-acid (Pb-acid)

The specific energy of this technology is low and typically between 20 and 40 Wh/kg. This technology has a short cycle and calendar life compared to Nickel Metal Hydride. Lead-acid batteries have less consideration to be used in future EVs due to their low maturity, and the work improvement on them is low. It has many advantages, like cheap manufacturing technology (about USD 100/kWh), which makes it suitable for small-range applications [8]; it also has a high electric power/weight ratio. The main disadvantages of lead-acid batteries include the handling of corrosive chemicals, the inclusion of lead in their manufacture, a poor stored energy/weight ratio, and a low stored energy/volume ratio [51]. Due to its low specific energy and high weight, the Lead-acid battery is not used for traction in EVs. The 12 V Lead-acid battery is used to supply the 12V board-net and electronic components besides the traction battery [52].

Nickel-Cadmium (NiCd)

The main advantage of Nickel-Cadmium it has the highest lifetime compared to other technologies as it has about 1500 charging and discharging cycles; therefore, it could be a good selection as ESD in the FCS. Using Cadmium metal harms the environment, humans, animals, and health. Therefore, this battery is limited in use from EU directives [51]. Before 2008, it was used as a spare part for EVs and its no longer used in vehicles currently [52].

3.2.2.1 Ni-MH batteries

Ni-MH batteries offer a better energy density and power density than Ni-Cd and Lead-Acid batteries, allowing for autonomous driving over 300 kilometers while using batteries with a specific energy of 70 Wh/kg. Its cheap technology compared to Li-Ion technology as it costs around USD 700–800/kWh. The energy density of the Ni-MH battery is between 60 and 80 Wh/kg, which does not match the needs of the EVs [8]. In

addition, it shows good performance in propulsion systems equipped with electric engines of 320 V AC, or 180 V DC, as the life cycle increases. The Ni-MH batteries have several merits, like the capability of recovering the regenerative energy, being manufactured from recyclable materials, and high range of operating temperature (starting from – 30 °C up until + 70 °C), and safe charging and discharging operations. The main disadvantages of Ni-MH batteries are their poor energy storage capacity, greater weight, and high self-discharge coefficient [19, 51]. Due to the previous drawbacks, the Ni-MH batteries can not compete with the Li-Ion batteries; hence, they will not use them in the future in EVs or FCS.

Li-Ion battery

Recently, Li-Ion batteries have been the most common technology in EVs and FCS. They have several merits like high energy density, increased power density, and excellent calendar life and life cycle. The main drawbacks of the Li-Ion batteries are their high cost (more than USD 700/kWh), out-of-use batteries can not be recyclable, and they have safety issues (overcharging can cause fires). However, the development is ongoing on the Li-Ion batteries to enhance their performance, solve safety issues, and reduce their cost. To control and monitor the temperature of the internal cells, it is important to have a Li-Ion battery management cell in this technology [19]. It is also recommended not to recharge the Li-Ion batteries at low temperatures to avoid early degradation [52]. The lithium-ion battery has different chemistries, with other characteristics and degrees of maturity. Table 3.1 summarizes the different chemistries of the Lithium-ion battery and their advantages and disadvantages.

Table 3.1 Different Lithium-ion battery technologies [42].

Technology	**Advantages**	**Disadvantages**
Lithium Cobalt Oxide (LiCoO2)	Power and energy density	Safety, cost
Lithium Polymer (LiMnO4)	Power density	Calendar life
Lithium-ion phosphate (LiFePO4)	Safety	Energy density, calendar life
Nickel Manganese Cobalt (NMC)	Power and energy density, calendar and cycle life	Safety
Nickel-Cobalt and Aluminium (NCA)	Power and energy density, calendar and cycle life	Safety

Lithium-ion Polymer

Although Lithium-ion Polymer batteries have a longer life cycle than standard Li-ion batteries, but they are functionally unstable when overloaded or discharged below a certain level [40].

NaNiCl

The Na-NiCl2 batteries, also known as ZEBRA batteries (Zeolite Battery Research Africa) have several advantages like high energy density (90 … 120 Wh/kg), high life cycle due to low resistance. In addition, they are cheaper compared to other batteries, fully recyclable, and can work in a significant temperature range from -40°C to +60°C as they have thermal insulation. The safe operation and the storage for longer periods are the main disadvantages of Na-NiCl2 [52, 53]. Batteries with a high coefficient of stored energy density are desired to power electric motors in EVs, as raising this coefficient increases the EVs' autonomy [51]. Therefore, the researchers are working on improving the energy density of the batteries to increase the auto market with electric vehicles. This type will be recommended as an energy storage device in the FCS due to its high energy density. The main characteristics of batteries currently developed and most used to equip electric vehicles and FCS are presented in Table 3.2.

Table 3.2 The main characteristics of different battery technologies [42,43].

Battery technology (type)	Specific energy (Wh/kg)	Energy/ Volume coefficient (Wh/L)	Power/ Weight coefficient (W/kg)	Self-discharge coefficient (% per 24 h)	Number of recharging cycles	Cost (Cdn$/kWh)
Pb-acid	40	70	180	1	500	144-180
Ni–Cd	60	100	150	5	1350	300-420
NiMH	70	250	1000	2	1350	240-420
Li-ion	125	270	1800	1	1000	240
Li-ion polymer	200	300	3500	1	1000	200
Na–NiCl	125	300	1500	0	1000	N/A

3.3 Supercapacitors

Supercapacitors are also known as ultracapacitors (UC) and are used as energy storage devices nowadays in many applications like microgrids and EVs. They have many good features like high power density and suitable energy density. Furthermore,

because there are no chemical fluctuations on the electrodes, they have a long-life cycle; therefore, they can charge and discharge for many cycles without losing their efficiency. Typically, they are used in hybrid energy systems to combine the high-power density of the supercapacitors and the high energy density of the batteries.

3.3.1 Configurations and Theory of Operation

The materials of the supercapacitor like electrode, electrolyte, separator, and current collector determine the performance of the supercapacitor. The internal resistance is reduced by choosing the suitable electrolyte and increasing efficiency. Figure 3.2 below [43] shows that the supercapacitor consists of two charged electrodes, a current collector, and a separator that allows for ion transfer while preventing direct electrical contact.

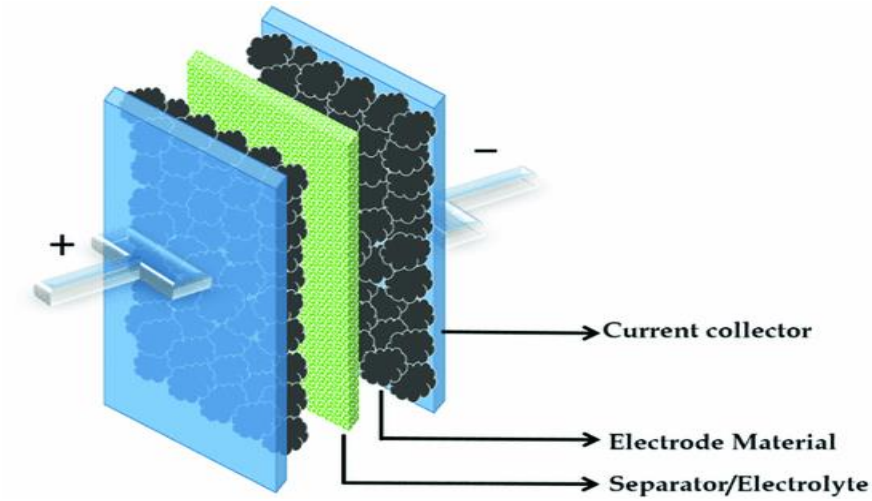

Figure 3.2 Supercapacitor configuration.

It stores energy as an electric field, as each electrode accumulates charges in opposite polarity. By applying potential difference, the negative ions in the electrolyte are attracted to the positive electrode. In contrast, the positive ions are attracted to the negative electrode, and the electrodes are separated at a very small distance to form two charging layers. Therefore, by increasing the surface area A of electrodes, the energy stored increased according to the law:

$$Q = CV = \frac{A\varepsilon}{d}V \qquad (3.4)$$

Where Q is the charge on the plates, C is the capacitance of the capacitor, V is the potential difference V across the two plates, A is the area of two plates, ε dielectric material constant, and d the distance between the two plates. Moreover, increasing the

permittivity of the dielectric ε will increase the energy stored, and increasing the distance d between the electrodes will reduce the energy storage [54].

3.3.2 Equivalent Circuit

The equivalent circuit of the supercapacitor can be shown in Figure 3.3, Where C_{DL} the capacitance of double layer, R_P the charge-transfer resistance, Z_{DIFF} the Warburg diffusion impedance, and R_S is the resistance of electrolytes.

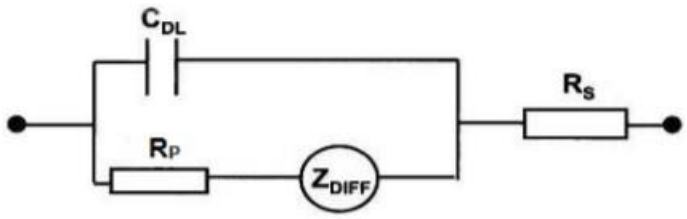

Figure 3.3 Equivalent circuit of the supercapacitor.

The overall capacitance in EDLC supercapacitor, C_{DL}, was considered as a series of capacitance, C_H and C_{DIFF} .

$$\frac{1}{C_{DL}} = \frac{1}{C_H} + \frac{1}{C_{\mathrm{DIFF}}} \qquad (3.5)$$

Where C_H is the capacitance of the Helmholtz layer that includes the inner capacitance of the plane and the outer capacitance of the plane, CDIFF is the diffuse layer's capacitance [55]. Supercapacitors are classified into three types: electric double-layer capacitors (EDLC), hybrid asymmetric capacitors, and pseudo capacitors based on the cell configuration, and their characteristics are summarized in Table 3.3 [56].

Table 3.3 The main characteristics of different supercapacitors.

Chemistry	**Power Density [Kw/kg]**	**Energy Density [Wh/kg]**	**Life Cycle**	**Operating temperature [°C]**	**Overall Efficiency [%]**
EDLC	1.5-6.0	5-20	1000 000	-40 to 70°C	82-98
Pseudo	Up to 6.0	10-25	100 000	-40 to 65°C	82-98
Hybrid Asymm.	0.01- 1.0	20-30	500 000	-40 to 65°C	< 90

The ultracapacitors have five technologies under development: foamed (aerogel) carbon, carbon/metal fiber composites, doped conducting polymer films on carbon cloth, carbon particulate with a binder, and mixed metal oxide coatings on metal foil. Carbon

composite electrodes using an organic electrolyte can achieve high energy density according to the high trends compared to carbon/metal fiber composite electrode devices with an aqueous electrolyte [54].

The material used in supercapacitors determines their electric properties. For example, the capacity of the EDLC type is affected directly by the electrode's surface material. Carbon is commonly used to make electrodes because it has several advantages such as low cost, availability, and long-term use. To obtain optimal performance, the electrode should have [44]:

- Chemical stability
- Low electrical resistance (milli ohm domain)
- Good mechanical stability
- Good accessibility and wetting for the electrolyte
- Stable interface and low contact resistance with the charge collector
- A convenient form for chosen capsule
- High capacitance density (F/m^3)

The breakdown voltage of the electrolyte determines the highest allowed voltage on a supercapacitor; therefore, choosing the electrolyte material is crucial since it affects the energy density of the supercapacitor. In addition, the type of the electrolyte: organic or aqueous, also affects the equivalent series resistance and hence the power density. The commercial supercapacitors use organic electrolytes as they have large dissociation voltage and a standard voltage of 2 V up to 2.5 V. However, the power density of organic electrolytes is low due to their high resistivity. Aqueous electrolytes have higher conductivity than organic electrolytes and break down voltages around the value of 1 V.

3.3.3 Characteristics of Supercapacitors

3.3.3.1 Charging Time

Charge and discharge times of supercapacitors are equivalent to those of conventional capacitors. Because of their low internal resistance, they can obtain significant charge and discharge currents. Batteries can take many hours to fully charge – a cell phone battery is a good example – whereas supercapacitors can reach the same charge state in less than two minutes.

3.3.3.2 Specific Power

The specific power of the battery or the supercapacitor is a statistic for comparing different technologies based on their maximum power output divided by the total mass. Supercapacitors have a particular power of 5 to 10 times that of batteries. A typical supercapacitor has a specific power of around 10 kW/kg, whereas Li-ion batteries have a particular power of 1 to 3 kW/kg. This property is significant in applications where the storage device must release energy quickly.

3.3.3.3 Cycle Life and Safety

Compared to traditional batteries, supercapacitors are safer; for example, short-circuiting batteries have been known to cause explosions due to excessive heating. However, supercapacitors do not heat much due to their low internal resistance. Shorting a fully charged supercapacitor causes a quick release of stored energy, which can cause electrical arcing and device damage; however, unlike batteries, the heat generated is not an issue. Supercapacitors, on the other hand, have a practically limitless cycle life and may be charged and discharged millions of times, whereas batteries have a cycle life of 500 times or less. This makes supercapacitors ideal for applications that require a lot of energy storage and release, like FCS [57].

Chapter 4. Proposed Topology of Multiple-input DC-DC Converter

4.1 Design and the Topology of the Converter

The proposed converter in Figure 4.1 is utilized to charge and discharge the energy storage devices in the FCS in Figure 4.2 simultaneously or individually. In addition, to exchanging power between the storage devices using a buck-boost bidirectional structure. The converter consists of six MOSFETs, two inductors, and one capacitor, as shown in Figure 4.1. Due to the modularity of the design, adding additional input sources can be achieved by adding a switching leg composed of a pair of switches and one inductor, for example, adding S_5, S_6, and L_2, as shown in Figure 4.1. The minimum values of inductors L_1 and L_2 are calculated using the equations listed in Table 4.1, and the capacitor C is designed to minimize the output voltage ripples. The parameters of the converter are listed in Table 4.2. As previously mentioned, the non-isolated converter is less safe than the isolated converter, because the input and output voltages are connected with the same common ground. This can be overcome by adding protection elements like circuit breakers in the DC link to protect against any faults in the FCS like short circuit currents. The proposed converter can work in five operation modes, and the output voltage of each operation mode can be changed by changing the value of the duty cycle, as we will discuss later. The switching sequence of the MOSFETs determines which operation mode the converter will work on, optimizing the energy management of the FCS and increasing the lifetime of the energy-storage devices.

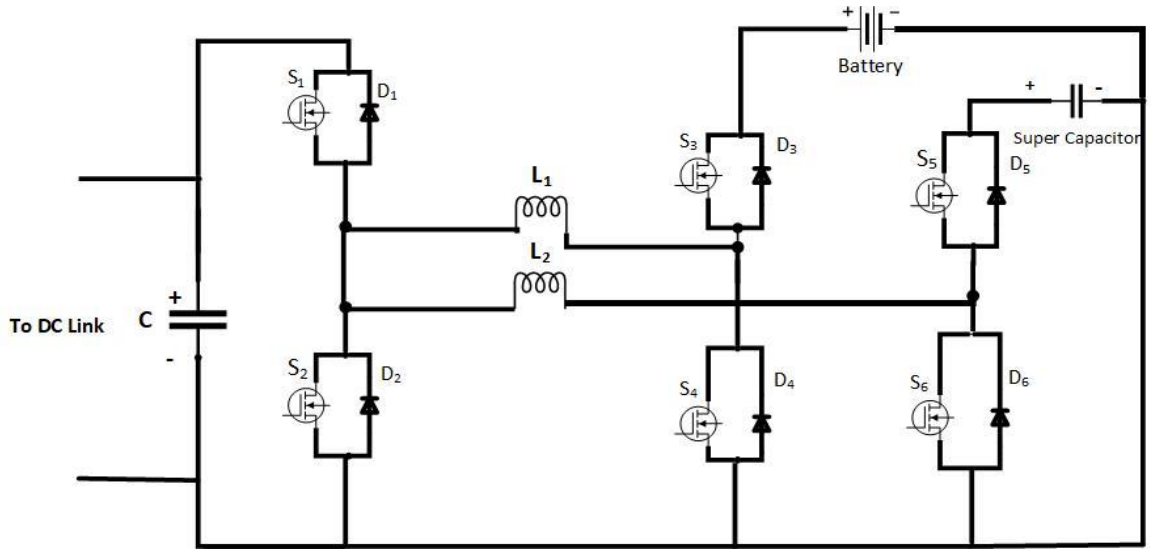

Figure 4.1 The proposed converter.

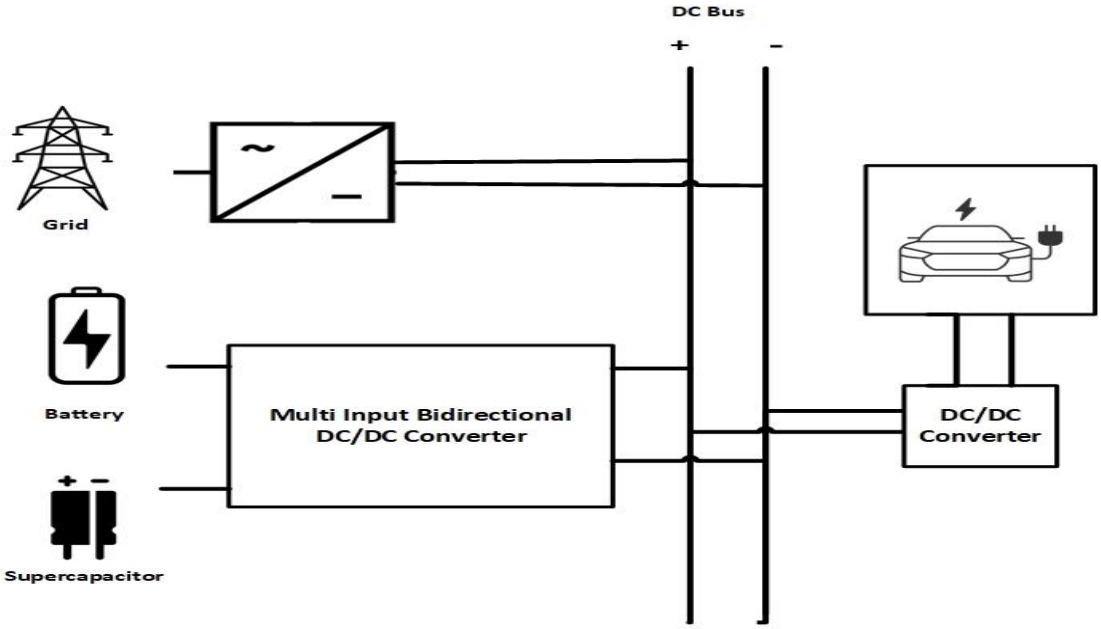

Figure 4.2 Proposed fast charging station.

Table 4.1 Inductance equations for different operation modes.

Mode	**1**	**2**	**3**	**4**	**5**
L_1, min	$\frac{(1-D).T_s}{\Delta I_{L1}}.V_{DC}$	-	$\frac{D.T_s}{2\Delta I_L}.V_{Bt}$	$\frac{V_{DC}.(1-d_2).T_s}{\Delta I_L}$	$\frac{(V_{DC}-V_{Bt})d_1.T_s}{\Delta I_{L1}}$
L_2, min	-	$\frac{(1-D).T_s}{\Delta I_{L2}}.V_{DC}$	$\frac{D.T_s}{2\Delta I_L}.V_{Bt}$	$\frac{V_{DC}.(1-d_2).T_s}{\Delta I_L}$	$\frac{(V_{DC}-V_{SC})d_1.T_s}{\Delta I_{L2}}$

Table 4.2 Design specifications of the proposed converter.

Specification	**Battery voltage (V_{BT}) and capacity**	**Supercapacitor voltage (V_{SC}) and capacitance**	**DC link voltage (V_{DC})**	**Switching frequency (f_s)**	**Inductors (L_1 and L_2)**	**Capacitor (C)**	**Power**
Values	200V/ 5 Ah	160 V/100 F	500 V	30 kHz	2mH and 2mH	500 µF	17 kW

As mentioned before in chapter 1, this study aims to reduce the cost, weight, and number of the components of the proposed multi-input converter compared to previous works mentioned in Chapter 2: a literature review. As the proposed converter is applied for EV charging, we will compare it to the proposed converter in Chapter 2, section 2.3.3, as it works in the same application, assuming they will work at the same power rate.

Using the Mouser Electronics Inc. website [58], the weight and cost of both converters can be approximately calculated.

The weight of the proposed converter is:

- 2 x 2.6 kg inductors = 5.2 kg
- 6 x 0.01 kg MOSFETs = 0.060 kg
- Capacitor = 0.04 kg
- 6 x 0.038 g heat sinks = 0.228 kg
- The total = 5.5 kg

By adding other components like controllers, wires, and ICs it is expected to weigh approximately 7 kg.

The price of the proposed converter is:

- 2 x $116 inductors = $232
- 6 x $12.94 MOSFETs = $78
- 1 x $12 capacitor = $12
- 1 controller x $40 = $40
- 3 x $30 Gate drivers= $90
- 6 heat sink x $7.5 = $45
- Total = $500

The weight of the proposed converter in section 2.3.3:

- 3 x 2.6 kg inductors = 7.8 kg
- 2 x 0.01 kg MOSFETs = 0.020 kg
- Output Capacitor = 0.04 kg
- 2 x 0.04 kg switching capacitor = 0.08 kg
- 6 x 0.01 kg diodes = 0.06 kg
- 2 x 0.038 kg heat sinks = 0.076 kg
- The total = 9 kg

By adding other components like controllers, wires, and ICs it is expected to weigh approximately 10.5 kg.

- 3 x $116 inductors = $348
- 2 x $12.94 MOSFETs = $26

- 1 x $12 output capacitor = $12
- 2 x $2 switching capacitors = $4
- 1 controller x $40 = $40
- 2 x $30 Gate drivers= $60
- 2 heat sink x $7.5 = $15
- 6 x $1 diodes = $6
- Total = $570

This price is expected to increase as other components will be considered, like PCB, wires, passive or active components, and ICs. The table below summarizes the difference between the proposed converter and the Hybrid buck/buck DC-DC converter in section 2.3.3, considering the aspects of cost, weight, power flow capability, and the number of components.

Table 4.3 Comparison between the Hybrid buck/buck DC-DC converter and the proposed converter.

Converter	**Hybrid buck/buck DC-DC converter**	**Proposed converter**
Weight	10.5 kg	7 kg
Cost	$570	$500
Number of components	14	9
Power flow	Unidirectional	Bidirectional
Number of inputs	Multi-input	Multi-input

4.2 Modeling, Analysis, and Operation Modes of the Proposed Converter

The converter can work in five operation modes as mentioned before utilizing the buck-boost topology by charging and discharging the inductors using different switching sequences to transfer the power from input sources to the output or vice versa. To achieve this, the converter must have a bidirectional power flow topology to discharge from the energy devices to the DC link, charge the energy storage devices from the DC link or exchange the power between the storage devices. The following sections present in detail the analysis and modeling of each operation mode of the converter, as well as the benefits of each mode to the FCS. The different operation modes help reduce the charging time, the charging cost, and the load on the grid. They also help increase the lifetime of the battery by charging it from a supercapacitor.

4.2.1 Mode 1: Exchanging Power between the Battery and the DC link

The DC link is supplied from the battery to charge the EV in this operating mode. This mode consists of three time-intervals T_1, T_2, and T_3, the switches S_2 and S_3 are turned on the first interval T_1 to charge the L_1 as shown in Figure 4.3 (a) and hence the inductor voltage V_{L1} is described by the following equation:

$$V_{L1} = L\frac{di_{L1}}{dt} = V_{Bt} \qquad (4.1)$$

In T_2, L_1 discharges its energy to the DC link through diodes $D_1$and D_4 while switches $S_2$and S_3 are turned off, as shown in Figure 4.3 (b). The switches $S_1$and S_4 are turned on in the last interval T_3 for continuous discharging of energy from L_1 to the DC link as opposed to using the diodes as in T_2 as shown in Figure 4.3 (c). The voltage across L_1 in T_2, and T_3 is described by the following equation:

$$V_{L1} = L\frac{di_{L1}}{dt} = -V_{DC} \qquad (4.2)$$

To reduce the voltage drop to a level of about 0.2 V, the switches S_1 and S_4 are used as synchronous rectifiers, and thus the system efficiency is improved. By applying the principle of volt-second balance for inductor L_1 using equations (4.1) and (4.2), the following equation can be deduced:

$$V_{L1} = D.V_{Bt} + (1-D)(-V_{DC}) = 0 \qquad (4.3)$$

By simplifying equation (4.3) under the steady-state condition, the relation between the DC-link voltage as an output and the battery voltage as an input can be obtained, resulting in the following equation:

$$V_{DC} = \frac{T_1}{T_2+T_3}.V_{BT} = \frac{D}{1-D}.V_{BT} \qquad (4.4)$$

Where D is the duty cycle ratio defined by $\frac{T_1}{T_S}$ where T_S is the total period of the switching cycle, and T_1 can be expressed as:

$$T_1 = L\frac{\Delta I_{L1}}{V_{BT}} \qquad (4.5)$$

And T_S can be expressed as:

$$T_s = \frac{1}{f_s} \qquad (4.6)$$

The battery discharges its energy to the DC link, so if its voltage becomes less than the DC link, the battery voltage is boosted by driving the duty cycle to run at $D > 0.5$.

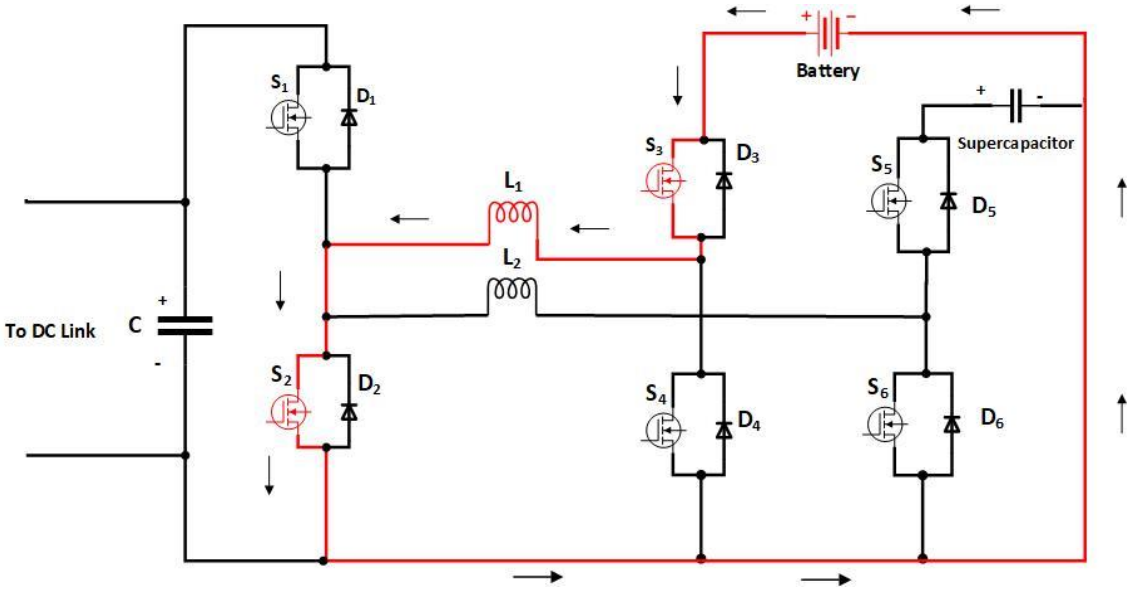

Figure 4.3 (a) Mode 1(a): T_1 Charging L_1 from battery.

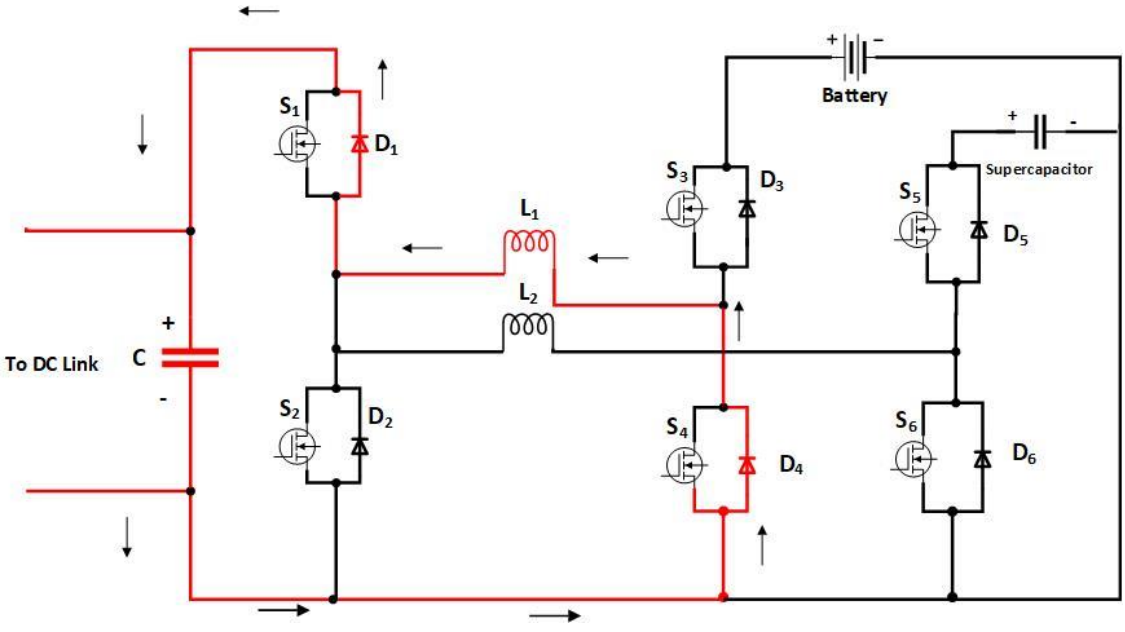

Figure 4.3 (b) Discharging from L_1 in DC link through the diodes.

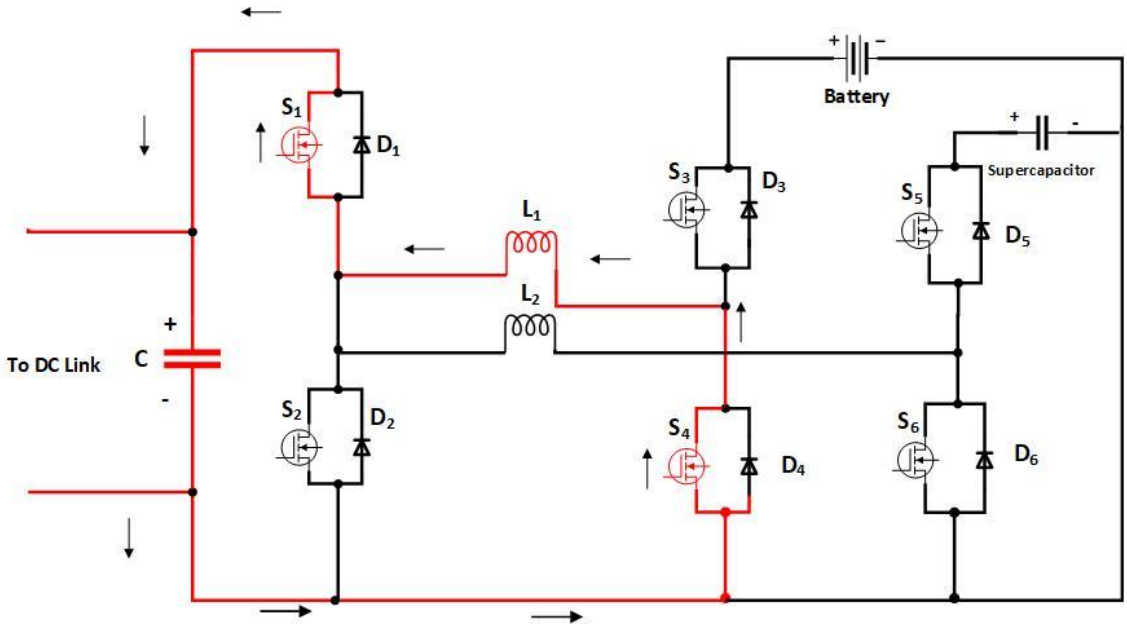

Figure 4.3 (c) Discharging from L_1 in DC link through the switches.

In the charging mode, the inductor L_1 is charged from the DC link in the time interval T_1 through the switches S_1 and S_4 as shown in Figure 4.4 (a). The inductor voltage V_{L1} can be described by the following equation:

$$V_{L1} = L\frac{di_{L1}}{dt} = V_{DC} \qquad (4.7)$$

In T_2 the L_1 discharges its energy to the battery through diodes D_3 and D_2 while switches S_2 and S_3 are turned off, as shown in Figure 4.4 (b). The switches S_3 and S_2 are turned on in the last interval T_3 for continuous discharging of energy from L_1 to the battery as opposed to the diodes in T_2 as shown in Figure 4.4 (c). They work as synchronous rectifiers, and the voltage across L_1 in T_2 and T_3 can be described by the following equation:

$$V_{L1} = L\frac{di_{L1}}{dt} = -V_{BT} \qquad (4.8)$$

By applying the principle of volt-second balance for inductor L_1 using equations (4.7) and (4.8), the following equation can be deduced:

$$V_{L1} = D.V_{DC} + (1-D)(-V_{BT}) = 0 \qquad (4.9)$$

By simplifying equation (4.9) under the steady-state condition, the relation between DC-link voltage as an input and battery voltage as an output can be described by the following equation:

$$V_{BT} = \frac{T_1}{T_2+T_3} . V_{DC} = \frac{D}{1-D} . V_{DC} \qquad (4.10)$$

Where D is the duty cycle ratio defined by $\frac{T_1}{T_S}$ where T_S is the total period of the switching cycle, and T_1 can be expressed as:

$$T_1 = L \frac{\Delta I_{L1}}{V_{DC}} \qquad (4.11)$$

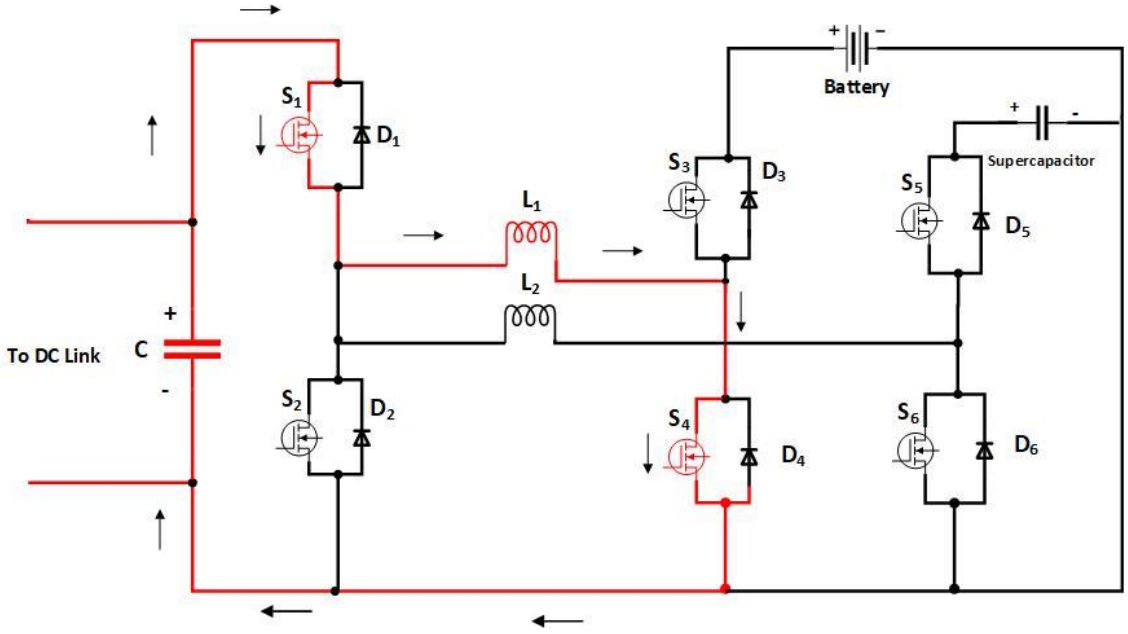

Figure 4.4 (a) Mode 1(b) T1 Charging L1 from DC link.

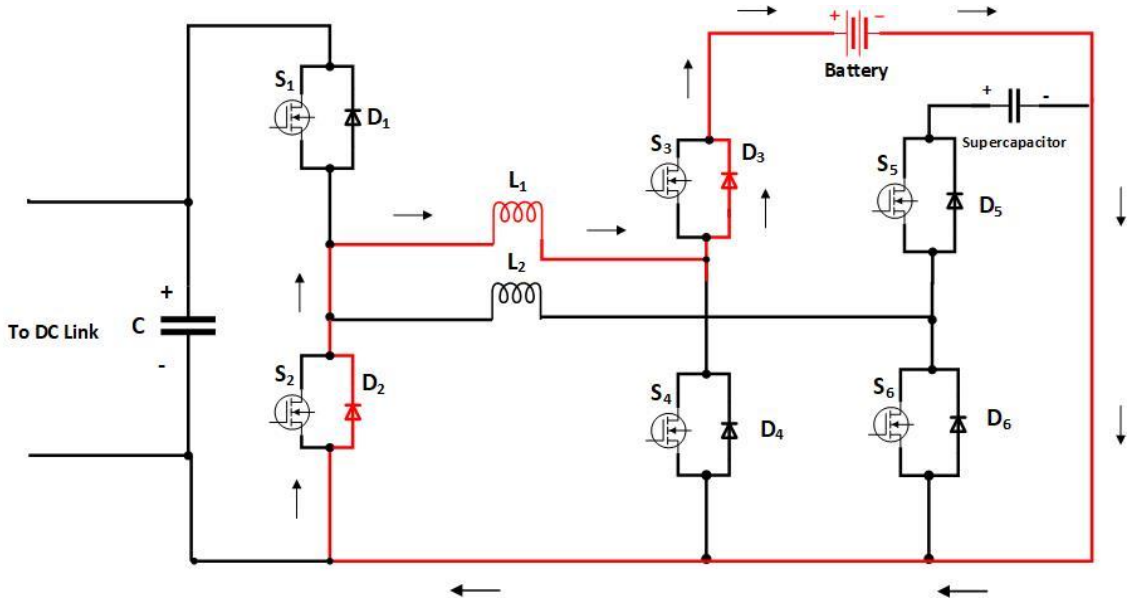

Figure 4.4 (b) Discharging from L1 in the battery through the diodes.

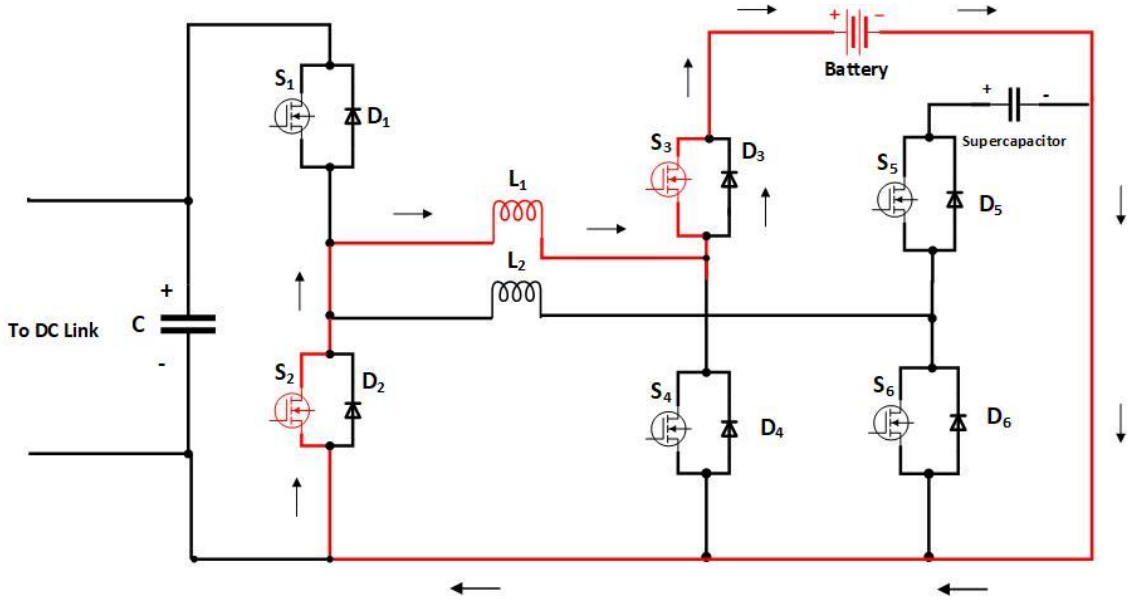

Figure 4.4 (c) Discharging from L1 in the battery through the switches.

4.2.2 Mode 2: Exchanging Power between the Supercapacitor and the DC link

In this mode of operation, the DC link is supplied from the supercapacitor only, so EV can be charged fast, thanks to the high-power density of the supercapacitor. Similar to mode 1, there are three-time intervals in this mode of operations. At the first interval T_1 the inductor L_2 is charged by turning on switches S_2 and S_5 as shown in Figure 4.5 (a). The following equation describes the voltage across the inductor L_2.

$$V_{L2} = L\frac{di_{L2}}{dt} = V_{sc} \qquad (4.12)$$

The stored energy in L_2, is transferred to the DC link during intervals T_2 and T_3 through diodes D_6 and D_1 and then through the switches S_2 and S_5 respectively as shown in Figures 4.5 (b) and 4.5 (c). During these intervals, V_{L2} can be described by the following equations:

$$V_{L2} = L\frac{di_{L2}}{dt} = -V_{DC} \qquad (4.13)$$

By applying the principle of volt-second balance for inductor L_2 using equations (4.12) and (4.13), the following equation can be deduced:

$$V_{L2} = D.V_{SC} + (1-D)(-V_{DC}) = 0 \qquad (4.14)$$

The following equation expresses the voltage of the DC link V_{DC} as a function of the supercapacitor V_{SC} voltage:

$$V_{DC} = \frac{T_1}{T_2+T_3}.V_{SC} = \frac{D}{1-D}.V_{SC} \qquad (4.15)$$

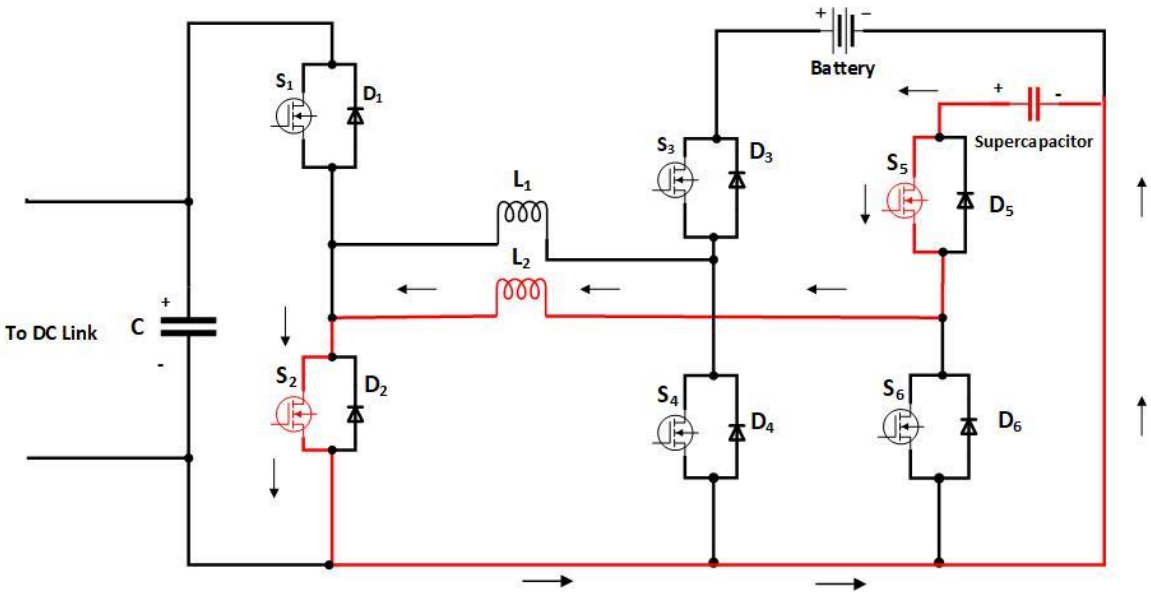

Figure 4.5 (a) Mode 1(b) T1 Charging L2 from the supercapacitor.

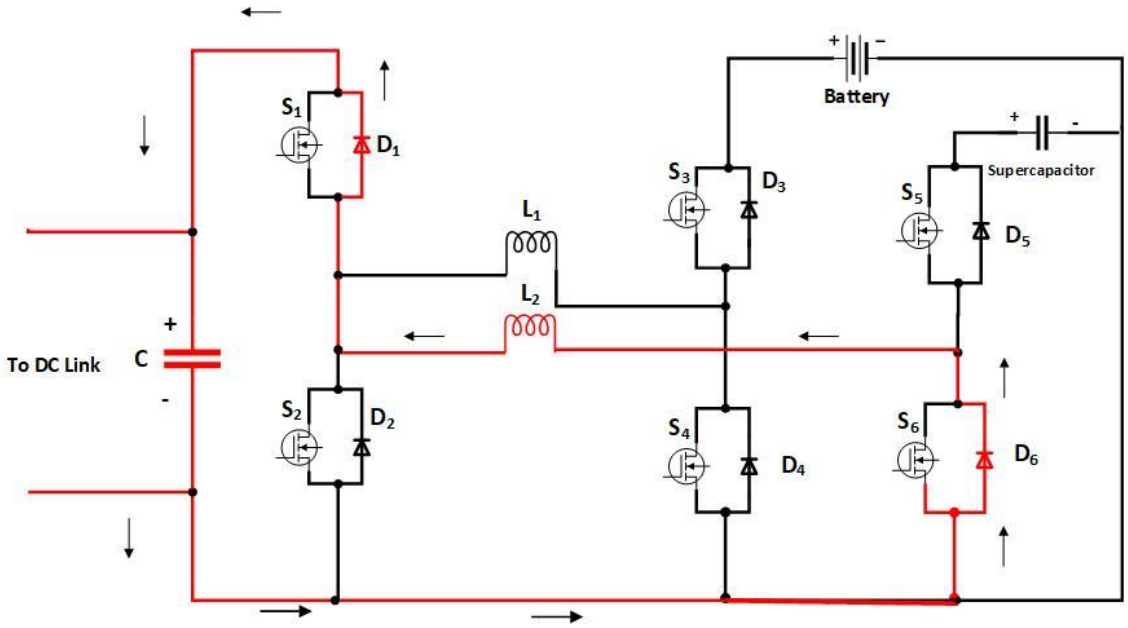

Figure 4.5 (b) Discharging from L2 in DC link through the diodes.

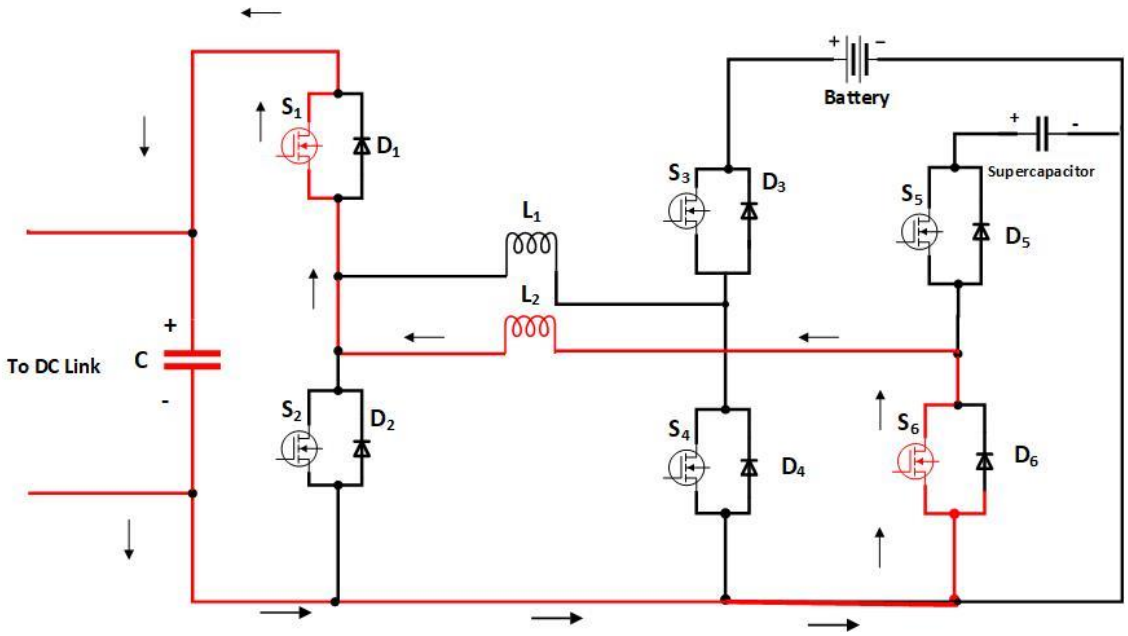

Figure 4.5 (c) Discharging from L2 in DC link through the switches.

In the opposite power flow direction, the power flows from the DC link to charge the supercapacitor by reversing the current flow in L_2. The inductor L_2 is charged in the time interval T_1 from the DC link through the switches S_1 and S_6 as shown in Figure 4.6 (a). The voltage across L_2 can be described by the following equation:

$$V_{L2} = L\frac{di_{L2}}{dt} = V_{DC} \qquad (4.16)$$

In T_2, the inductor L_2 discharges its energy to the supercapacitor through diodes D_2 and D_5 while switches S_2 and S_3 are turned off as shown in Figure 4.6 (b). The switches S_2 and S_5 are turned on in the last interval T_3 for continuous discharging of energy from L_2 to the supercapacitor as opposed to using the diodes in T_2 as shown in Figure 4.6 (c). The voltage across V_{L2} in T_2 and T_3 can be described by the following equation:

$$V_{L2} = L\frac{di_{L2}}{dt} = -V_{SC} \qquad (4.17)$$

By applying the principle of volt-second balance for inductor L_2 using equations (4.16) and (4.17), the following equation can be deduced:

$$V_{L2} = D.V_{DC} + (1-D)(-V_{SC}) = 0 \qquad (4.18)$$

Where D is the duty cycle ratio equal $\frac{T_1}{T_S}$, and T_S is the total period of the switching cycle. The following equation expresses the relation between input and output voltages:

$$V_{SC} = \frac{T_1}{T_2+T_3}.V_{DC} = \frac{D}{1-D}.V_{DC} \qquad (4.19)$$

And T_1 can be expressed as:

$$T_1 = L\frac{\Delta I_{L2}}{V_{DC}} \qquad (4.20)$$

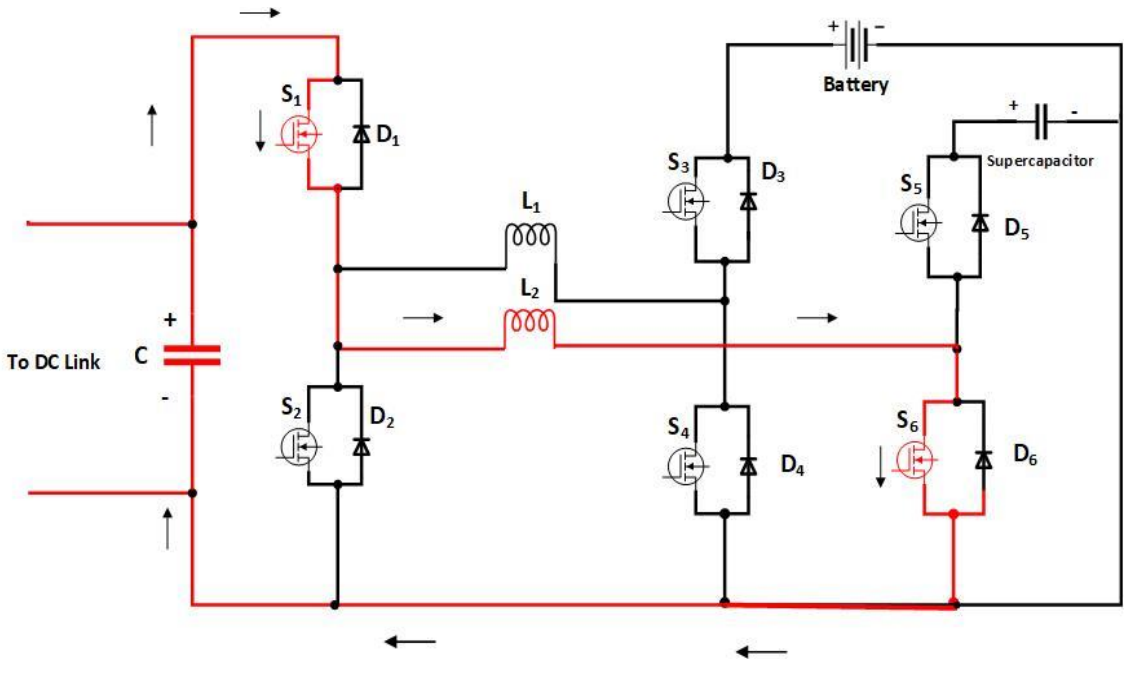

Figure 4.6 (a) Mode 2(b) T1 Charging L2 from DC link.

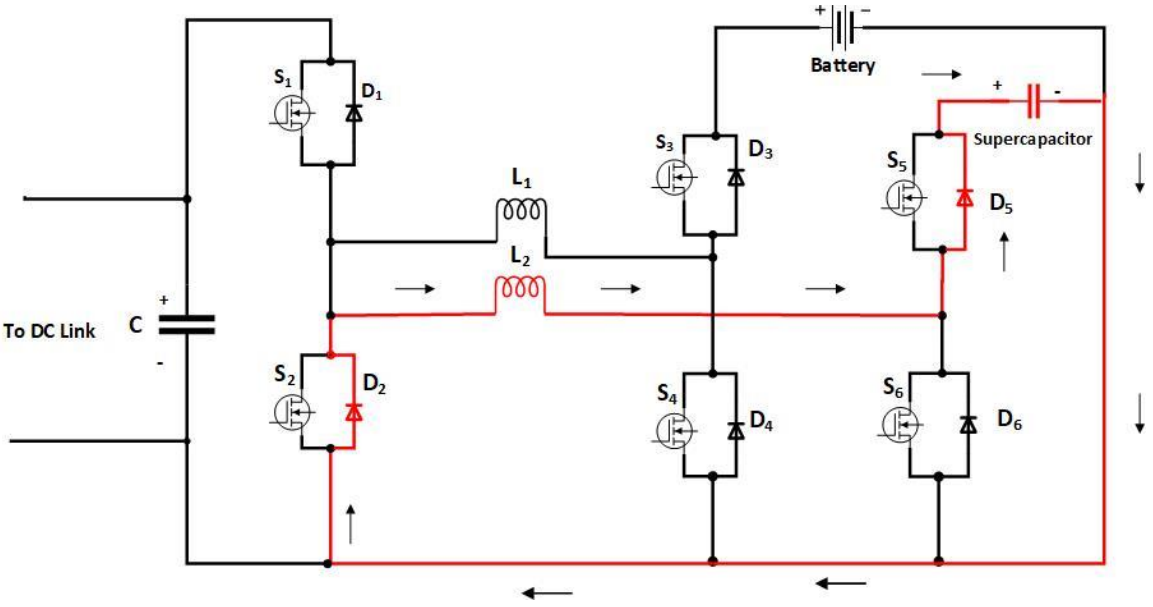

Figure 4.6 (b) Discharging from L2 in supercapacitor through the diodes.

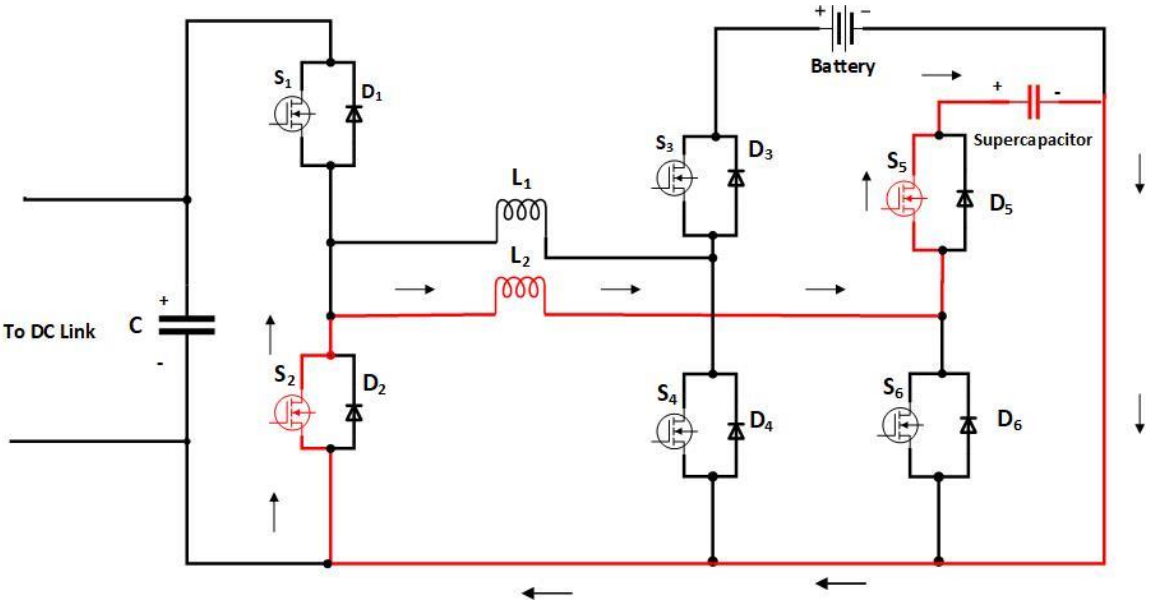

Figure 4.6 (c) Discharging from L2 in supercapacitor through the switches.

4.2.3 Mode 3: Exchanging Power between Battery and Supercapacitor

This mode is useful for increasing the lifetime of the battery by reducing the peak values of charging and discharging currents of the battery. When the ripple current in the battery is smaller than in the other two modes of operation, the boost mode is used. The buck mode is used when the ultracapacitor voltage is lower than the battery voltage. To

charge the supercapacitor inductors L_2 and L_1 are charged in the time interval T_1 from the battery through the switches S_3 and S_6 as shown in Figure 4.7 (a). The voltage across L_1 and L_2 can be expressed by the equation below:

$$V_{L2} + V_{L1} = V_{Bt} \qquad (4.21)$$

In T_2, inductors L_2 and L_1 discharge their energy to the supercapacitor through the switch S_3 and diode D_5 as shown in Figure 4.7 (b). Then switch S_5 is turned on in the last interval T_3 for continuous discharging of energy from L_2 and L_1 to supercapacitor as opposed to the diode D_5 in T_2 as shown in Figure 4.7 (c). The voltage across inductors L_1 and L_2 can be described by the following equation:

$$V_{L2} + V_{L1} = V_{Bt} - V_{SC} \qquad (4.22)$$

By applying the principle of volt-second balance for inductor L_2 and L_1 using equations (4.21) and (4.22), the following equation can be deduced:

$$V_{L2} + V_{L1} = D.V_{Bt} + (1-D)(V_{Bt} - V_{SC}) = 0 \qquad (4.23)$$

By simplifying equation (4.23), equation (4.24) can be obtained, and then the voltages of the battery V_{BT} and supercapacitor V_{SC} can be calculated in the boost operation mode.

$$V_{SC} = \frac{T_s}{T_2+T_3} . V_{BT} = \frac{1}{1-D} . V_{BT} \qquad (4.24)$$

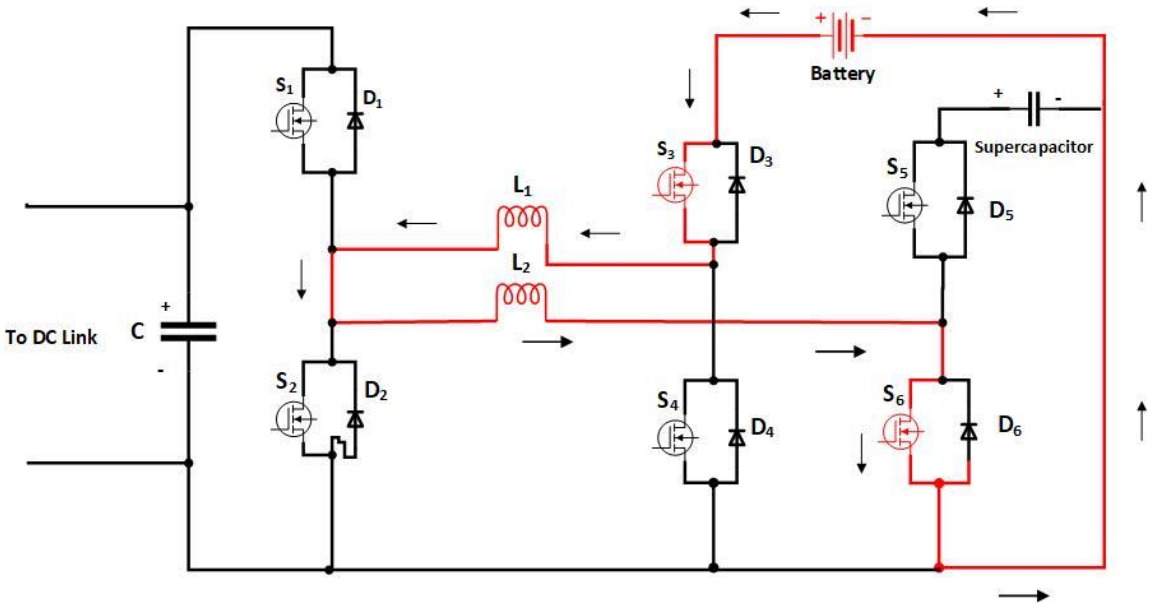

Figure 4.7 (a) Mode 3(a) T1 Charging L2 and L1 from the battery.

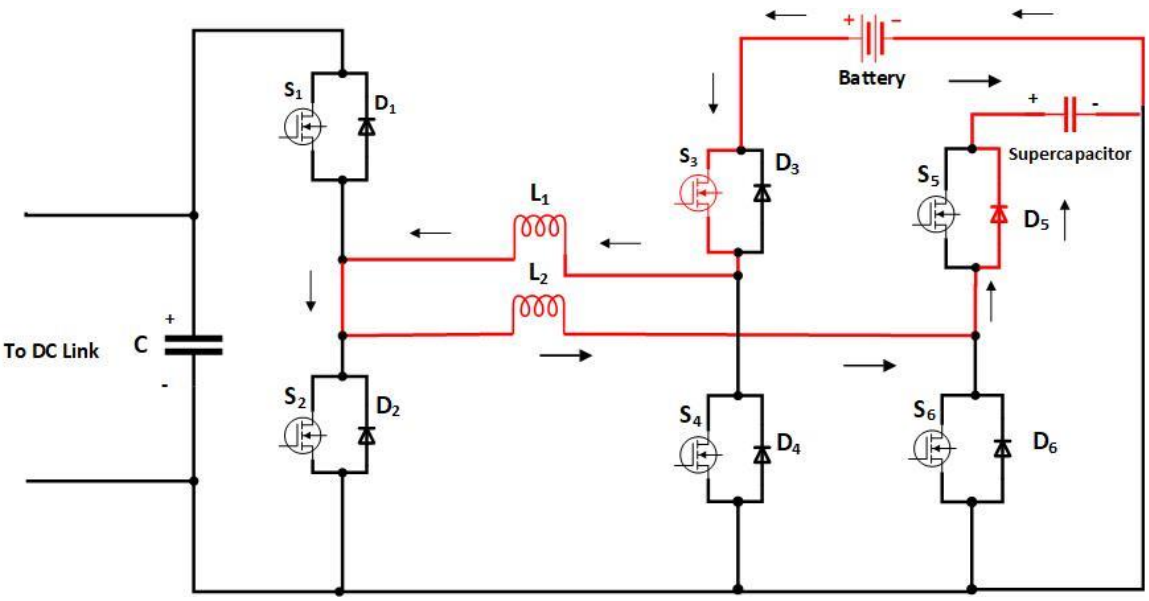

Figure 4.7 (b) Discharging from L2 and L2 in supercapacitor through the diode D5.

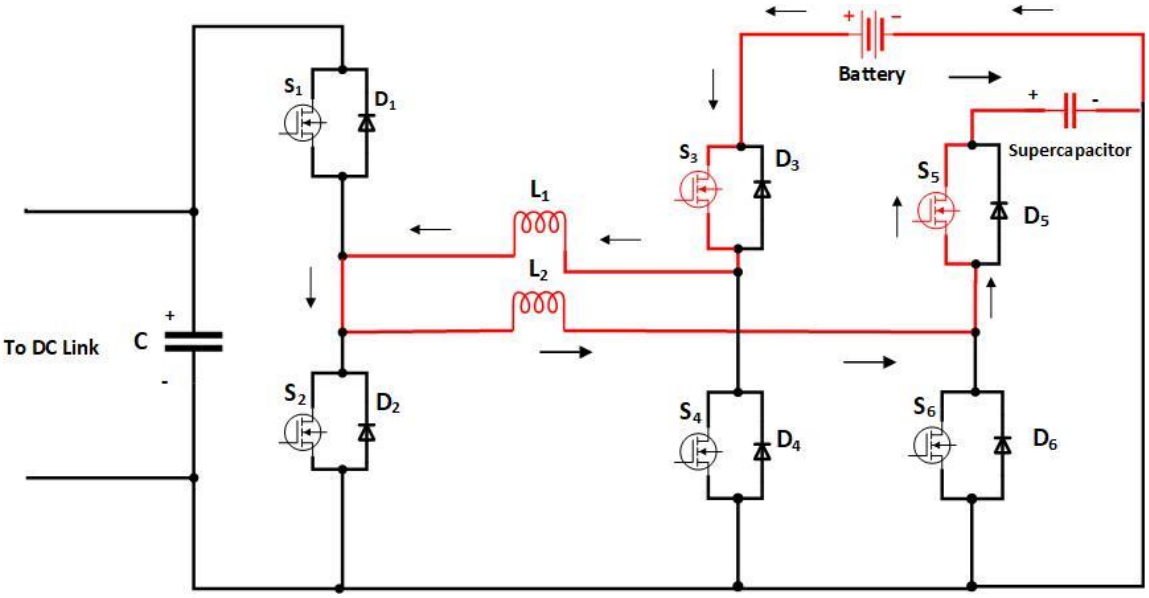

Figure 4.7 (c) Discharging from L2 and L2 in supercapacitor through the switch S5.

By reversing the charging current through the inductors by using the power switches S_3, S_5, S_6, and diode D_6, the battery can be charged in the buck operation mode from the supercapacitor, as shown in Figures 4.8 (a), 4.8 (b), and 4.8 (c). and using equation (4.6).

$$V_{BT} = \frac{T_1}{T_s} . V_{SC} = D . V_{SC} \qquad (4.25)$$

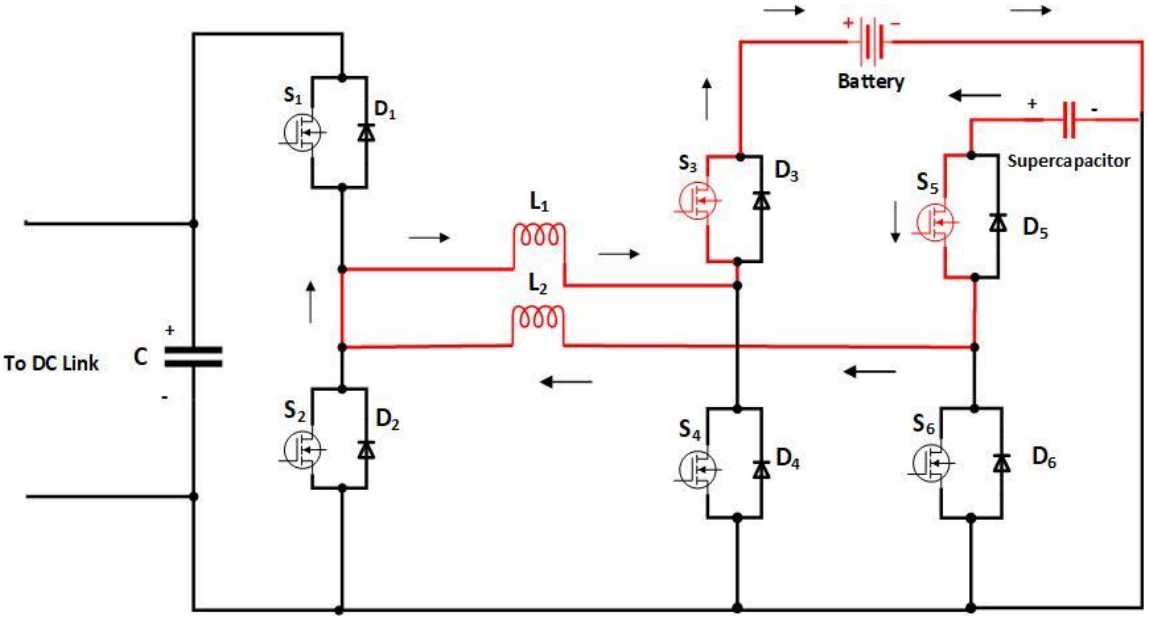

Figure 4.8 (a) T1 Charging L2 and L1 from the supercapacitor.

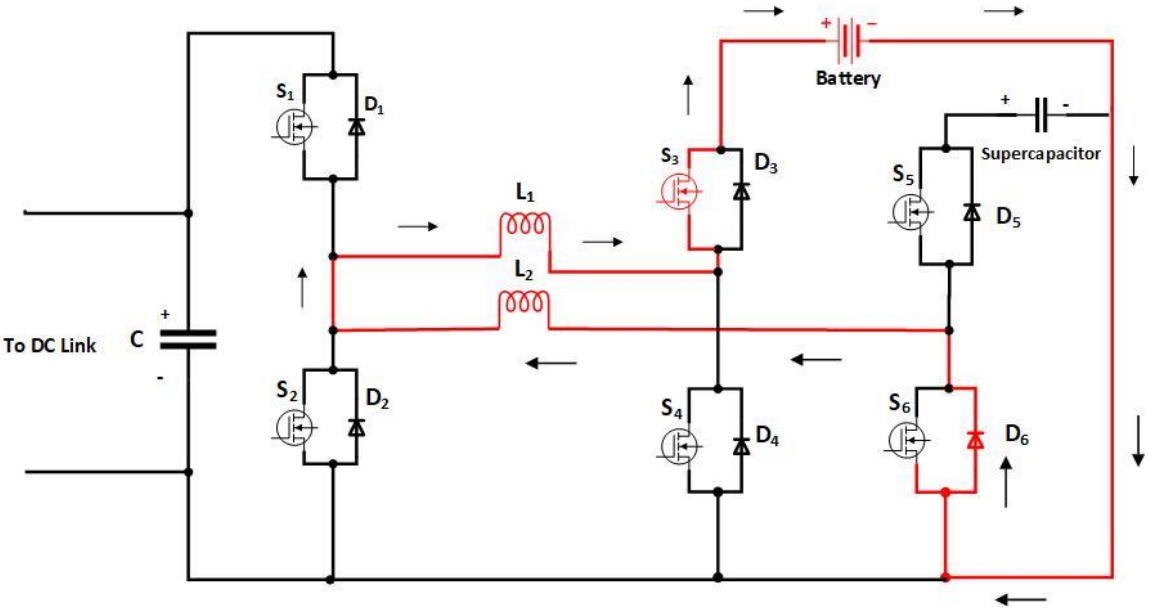

Figure 4.8 (b) Discharging from L2 and L2 in the battery through the diode D6.

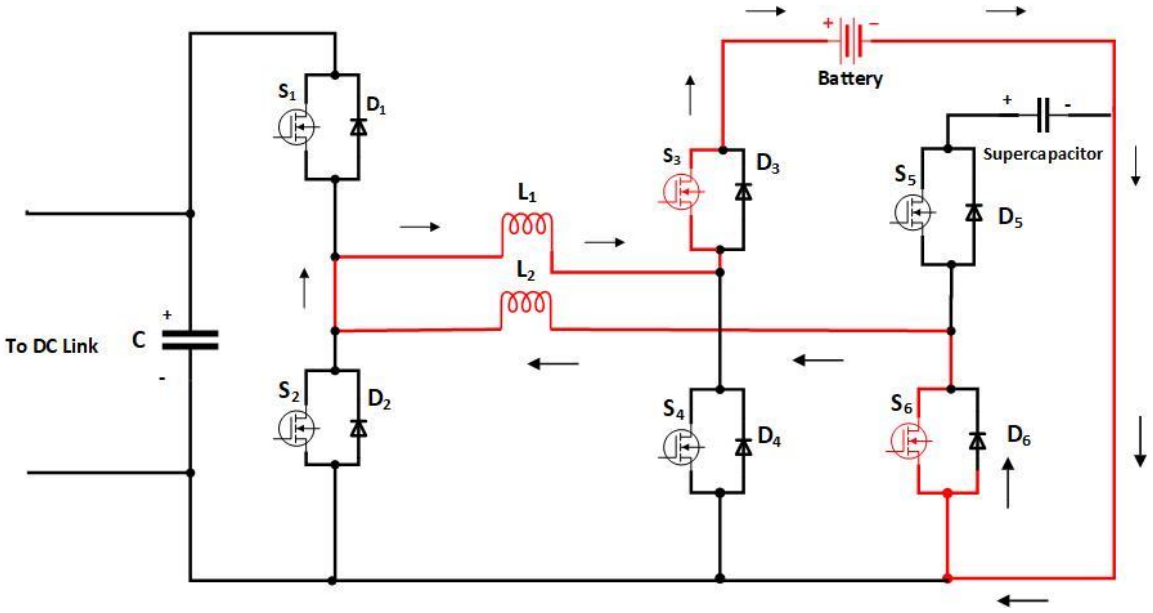

Figure 4.8 (c) Discharging from L2 and L2 in supercapacitor through the diode S6.

The switching sequence of the power switches in the three-time intervals of the previous operation modes is summarized in Table 4.3.

Table 4.3 Modes (1), (2), and (3) switching states.

	mode 1(a)	**mode 1(b)**	**mode 2(a)**	**mode 2(b)**	**mode 3(a)**	**mode 3(b)**
$\boldsymbol{T_1}$	S_2 , S_3	S_1 , S_4	S_2 , S_5	S_1 , S_6	S_3 , S_6	S_3 , S_5
$\boldsymbol{T_2}$	D_4 , D_1	D_2 , D_3	D_6 , D_1	D_2 , D_5	S_3, D_5	D_6 , S_3
$\boldsymbol{T_3}$	S_1 , S_4	S_2 , S_3	S_6 , S_1	S_2 , S_5	S_3 , S_5	S_6 , S_3

4.2.4 Mode 4: Supplying the DC link from the Combined Battery and Supercapacitor

This mode helps also increase the lifetime of the battery, especially in high-power demanding loads. When a battery is combined with a supercapacitor, the battery can supply the average current to the load while the supercapacitor can supply the transient currents. As illustrated in Figures 4.9 (a) and 4.9 (b), the transients caused by pulsed currents of source impedance are reduced.

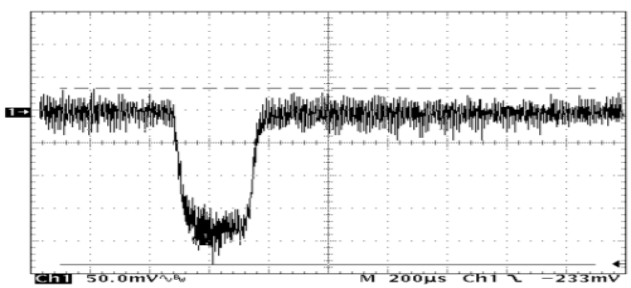

Figure 4.9 (a) Current pulse of the battery without supercapacitor [54].

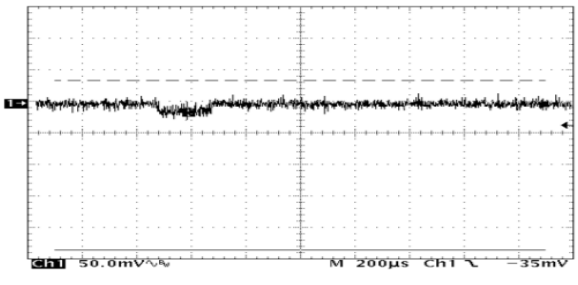

Figure 4.9 (b) Current pulse of the battery with supercapacitor [54].

This increases the lifetime of the battery, as pulsed currents can decrease battery life [59]. In addition, this mode of operation can be utilized in case of a grid failure or during peak hours to mitigate the load on the grid. Assuming most drivers will return home and plugin for charging between 4 -7 PM, which is the peak and mid-peak hours in Oshawa, Ontario [60]. The total number of zero-emission vehicles (ZEVs) registered in Ontario in 2020 is 10,515 [61], so approximately the number of ZEVs in Oshawa is 270 vehicles from the ratio of Oshawa population to Ontario population. On average, EVs have a typical energy consumption of 62.7 kWh/150 miles [62]. Assuming 70 vehicles will charge during the peak hours, the average energy consumption that can be reduced by using this operation mode in Oshawa will be 70 x 62.7 kWh = 4,389 kWh.

Furthermore, this operation mode can be useful to save money from the customer's perspective by using the hybrid energy system in FCS. Typically, drivers will return home and plug in between 4 and 8 PM, the customers or residents can take advantage of the time of use (TOU) energy prices in Oshawa, as shown in Figure 4.10 [60]. This can be done by varying station pricing according to the time of day, therefore reducing the cost of charging their vehicles.

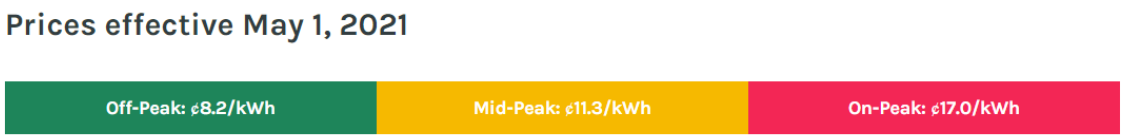

Figure 4.10 Time of Use (TOU) energy prices in Oshawa.

Assuming that, on average, EVs have a battery capacity of 62.7 kWh [62] and customers charge four times per month, the charging cost during peak hours can be calculated as follows:

- Per month = $0.17/kWh x 62.7 kWh x 4 = $42.6/month
- Per year = $42.6 x 12 = $511.6/year

Using the proposed converter and fast-charging station, and assuming the charging rate will be the same for the off-peak hours, $0.10, as shown in Figure 4.10 (more than the off-peak little bit), the charging cost can be calculated as follows:

- Per month = $0.10/kWh x 62.7 kWh x 4 = $25/month
- Per year = $25 x 12 = $300/year

The cost-saving will increase by increasing the number of charging times and the battery size of the vehicle. For example, suppose the customer has a Tesla Model Y (75 kWh/260 mi) [58] and charges it seven times per month.

In that case, the charging cost during the peak hours can be calculated as follows: \$0.17/kWh x 75 kWh x 7 = \$89/month, and the cost with the proposed converter and charging station = \$0.10/kWh x 75 kWh x 7 =\$53/month. The charging cost can be further reduced by charging the energy storage devices with renewable sources.

Transit companies like DRT or Go Transit can also benefit from the proposed station. On average, the battery capacity of electric buses is 245 kWh, and their average energy consumption is 1.4 kWh/km [63, 64]. Taking the 901B DRT bus as an example, its route from Ontario Tech University to Oshawa center is 8.6 km, and it takes approximately six trips during the peak hours, so 6 x 8.6 km = 52 km. During the peak hours, its energy consumption is 52 km x 1.4 kWh/km = 72 kWh, so one charge for a 901B DRT bus will be enough for the whole day. Therefore, the charging cost during peak hours:

- Per day = \$0.17/kWh x 245 kWh = \$42/day.
- Per month = \$42/day x 30 = \$1,260/month.
- Per year = \$1,260 x 12 = \$15,120/year.

Using the proposed converter and charging station and assuming the charging rate will be \$0.10 as shown in Figure 4.10 (more than the off-peak little bit), the charging cost can be calculated as follows:

- Per day = \$0.10/kWh x 245 kWh = \$24.5/day
- Per month = \$24.5/day x 30 = \$735/month
- Per year = \$735 x 12 = \$8,820/year

The cost savings using the proposed station and converter will be:
= 15,120 – 8,820 = \$6,300/year for each electric bus.

In this mode, the switching cycle T_s is divided into five-time intervals. In time-interval T_1, inductors L_1 and L_2 are charged from the combined sources V_{BT} and V_{SC} with current slopes V_{Bt}/L_1 and V_{SC}/L_2 respectively by turning on switches S_2 , S_3 , and S_5 as shown in Figure 4.11 (a). During time-interval T_2, switch S_3 is turned off to provide a freewheeling path for i_{L1} through D_4 as shown in Figure 4.11 (b). In time-interval T_3, L_2 continues

charging from the supercapacitor and switch S_4 is turned on to avoid any voltage drop across the diode D_4 as shown in Figure 4.11 (c). The stored energy in L_1 and L_2 is transferred to the DC link through D_1, as current passes through the antiparallel diodes of switches S_1 and S_6 as seen in Figure 4.11 (d). In T_5 switch S_1 acts as a synchronous rectifier to avoid the voltage drop across the diode D_1 and continue discharging the inductors in the DC link, as seen in Figure 4.11 (e). Finally, in the interval T_5 reversed logic signals are applied to switches S_2, S_3, and S_5 to start overcharging the inductors L_1 and L_2 and restart interval T_1. Figure 4.12 shows the voltage and current across both inductors under steady-state conditions in this mode. The relation between the DC link voltage, the battery voltage, and the supercapacitor voltage by applying volt–second balance for both inductors can be described by the following equations:

$$V_{BT} = \frac{T_4+T_5}{T_1} . V_{DC} = \frac{T_s-d_2T_s}{d_1T_s} . V_{DC} = \frac{1-d_2}{d_1} . V_{DC} \qquad (4.26)$$

$$V_{SC} = \frac{T_4+T_5}{T_1+T_2+T_3} . V_{DC} = \frac{T_s-d_2T_s}{d_2T_s} . V_{DC} = \frac{1-d_2}{d_2} . V_{DC} \quad (4.27)$$

Where d_1 is the ratio of the on-time of switch S_3 to total switching period T_S and, similarly, d_2 corresponds to switch S_2. From (4.27), it can be observed that the d_2 can be calculated for a required boost ratio of V_{SC} to V_{DC}.

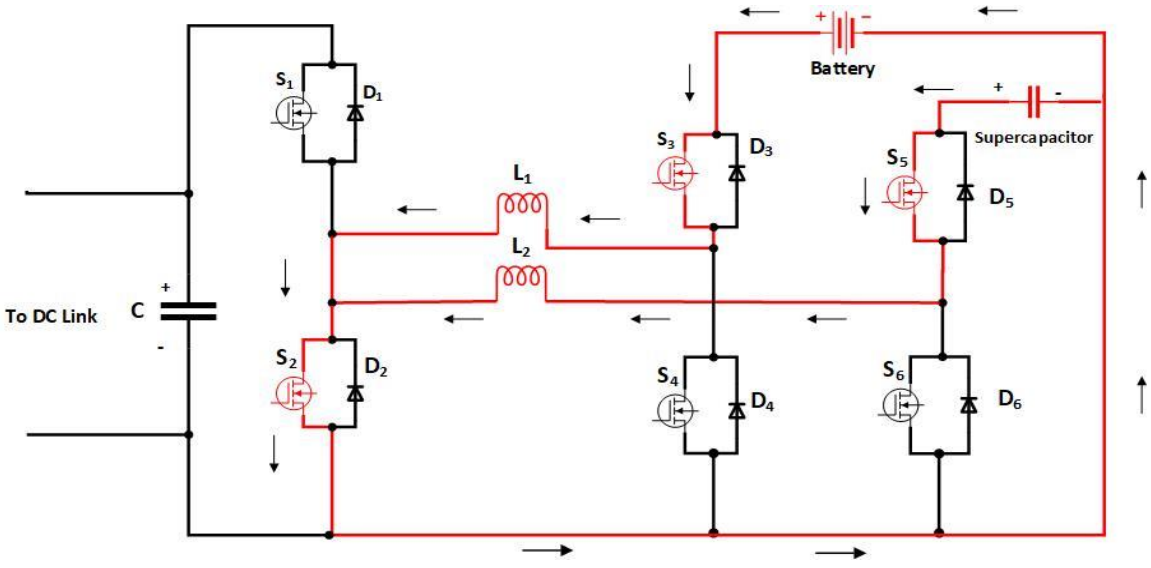

Figure 4.11 (a) Charging inductors L1 and L2 from the energy storage devices.

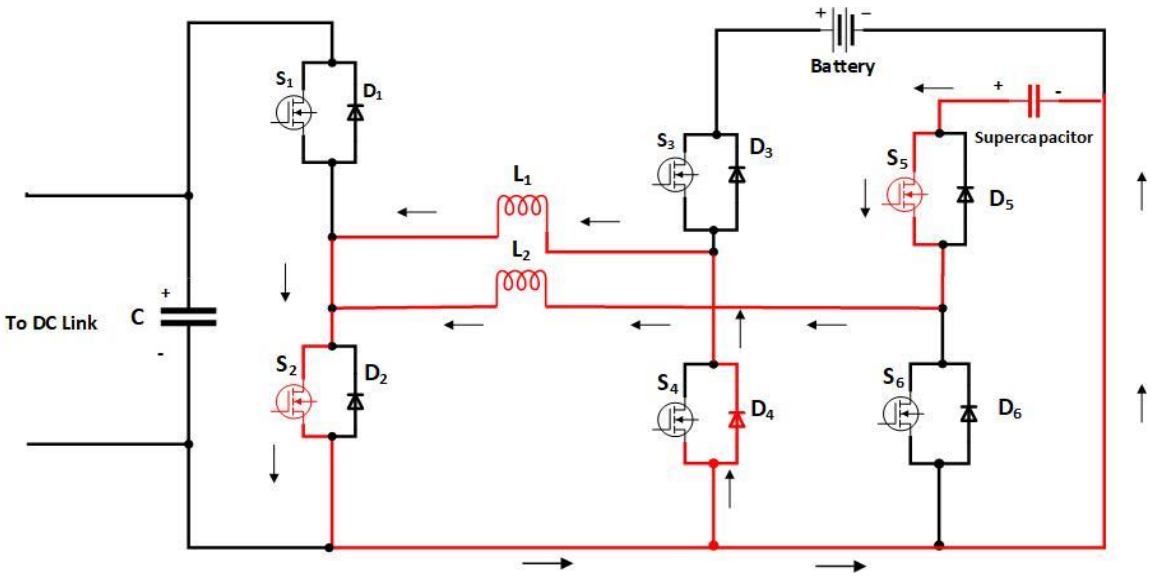

Figure 4.11 (b) Providing a freewheeling path for iL1 through D4 in T2.

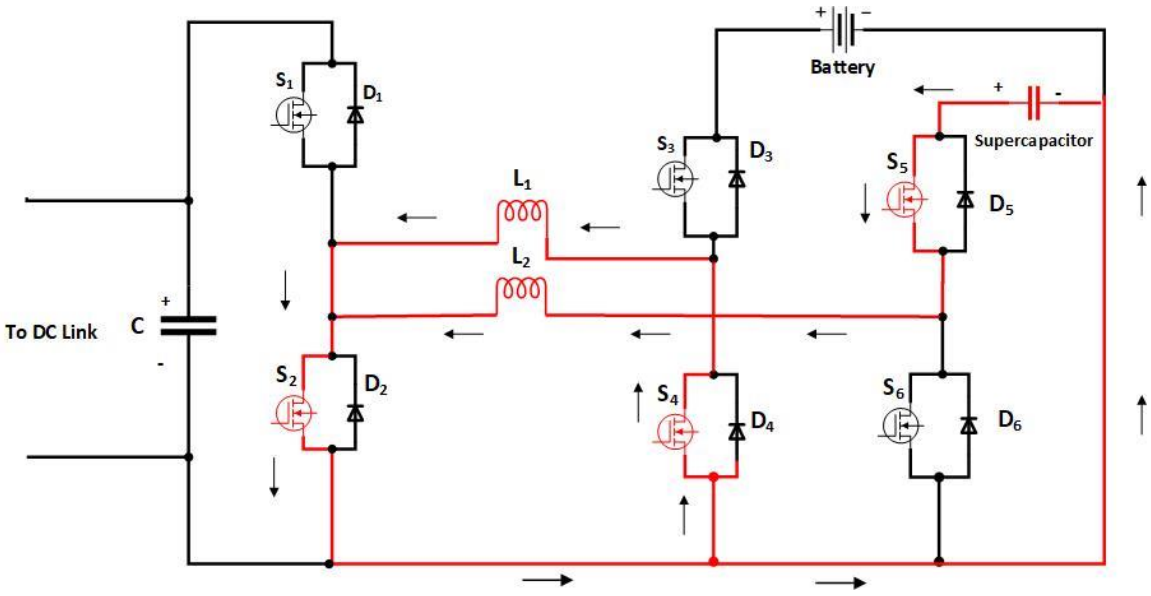

Figure 4.11 (c) Avoiding the voltage drop across the diode D4 by turning on S4 in T3.

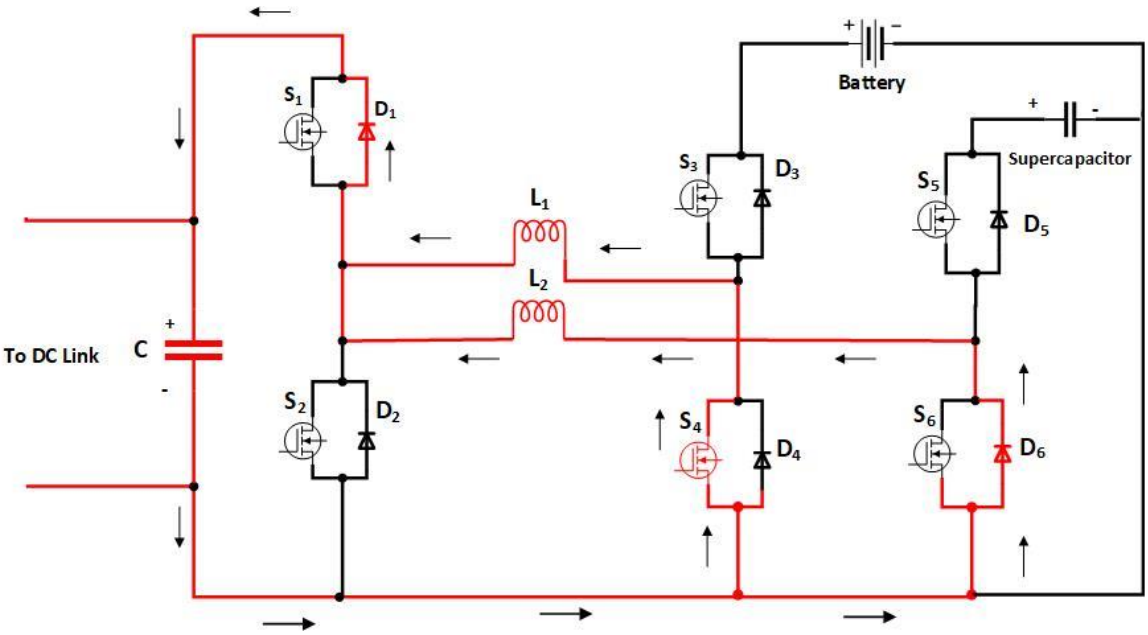

Figure 4.11 (d) Discharging from L1 and L2 in the DC link using D1.

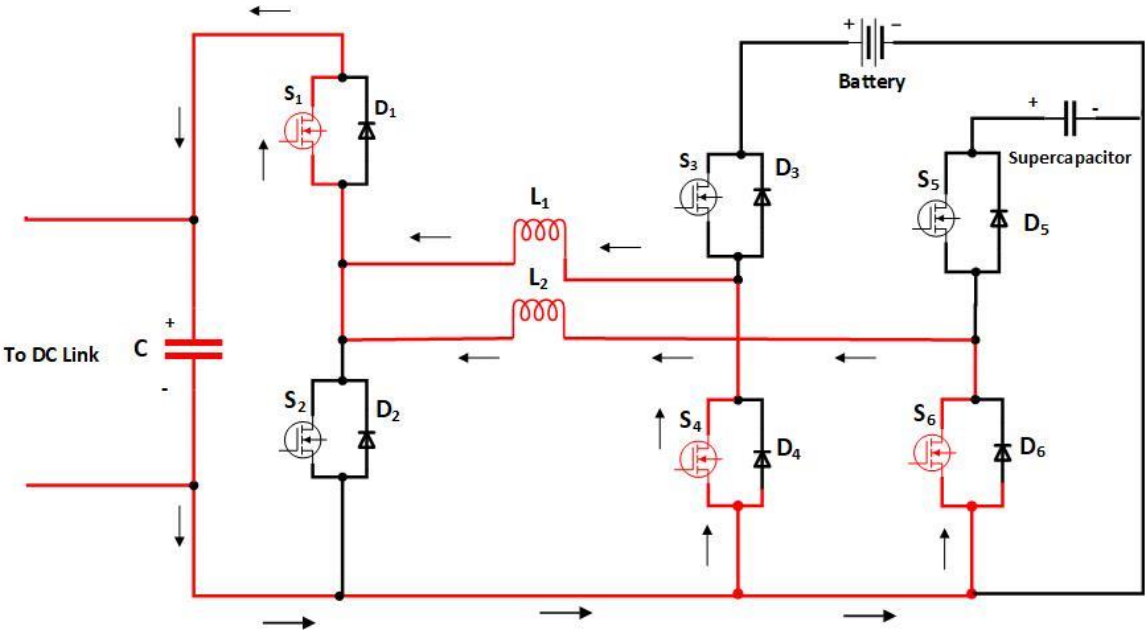

Figure 4.11 (e) Discharging from L1 and L2 in the DC link using S1.

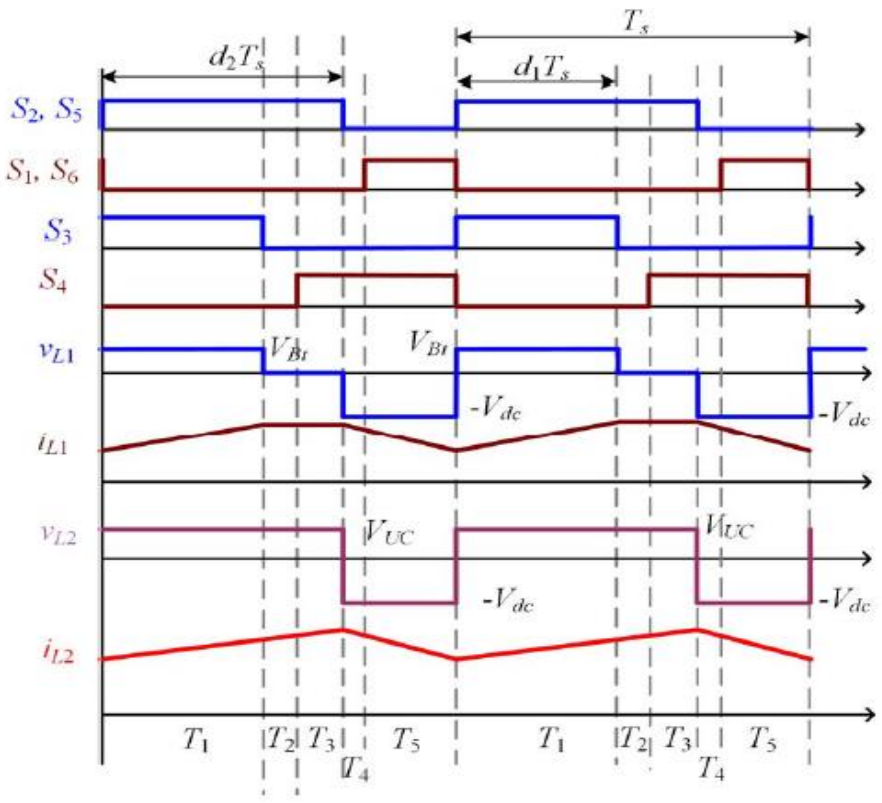

Figure 4.12 Steady-state waveforms for mode D.

4.2.5 Mode 5: Charging battery and supercapacitor from the DC link

In this mode of operation, the battery and supercapacitor can be charged from the grid during off-peak hours to reduce the energy cost. Firstly, switch S_5 is turned on while the switch S_6 is turned off to connect L_2 to the supercapacitor. The battery and supercapacitor sources are charged during the interval T_1 by turning on switches S_1, S_3, and S_5 as seen in Figure 4.13 (a). Then, inductor currents pass-through D_2 during interval T_2 while switch S_1 turned off as seen in Figure 4.13 (b). the voltage drop across the diode is avoided by turning on switch S_2 to work as a synchronous rectifier at the interval T_3 as seen in Figure 4.13 (c). Figure 4.13 (d) shows the current continues to flow in L_1 and the supercapacitor is charged by continuous inductor current i_{L2}, while switches S_3 is turned off, and S_4 is turned on at the interval T_4 . The battery and supercapacitor are charged from the DC link while switches S_1 and S_5 and diode D_3, as switches S_2 and S_4 are turned off at the end of the interval T_4. Finally, the cycle of this operation ended by turning on the switch S_3 , as the voltage dropped across it avoided providing a path for i_{L1} as seen in Figure 4.13 (e).

The relation between the voltages of the battery, DC link, and supercapacitor can be derived by applying volt–second balance across the inductors, as demonstrated in Figure 14.

$$V_{BT} = \frac{T_1+T_5}{T_1+T_2+T_3+T_5} . V_{DC} = \frac{T_1+T_5}{T_s-T_4} . V_{DC} = \frac{d_1}{d_2} . V_{DC} \qquad (4.29)$$

$$V_{SC} = \frac{T_1+T_5}{T_s} . V_{DC} = d_1 . V_{DC} \qquad (4.30)$$

Where $d_1 = \frac{V_{SC}}{V_{DC}}$, and $d_2 = \frac{V_{Bt}}{V_{DC}}$, as by regulating d_1 and d_2 the energy transferred from DC link to the battery and supercapacitor can be regulated.

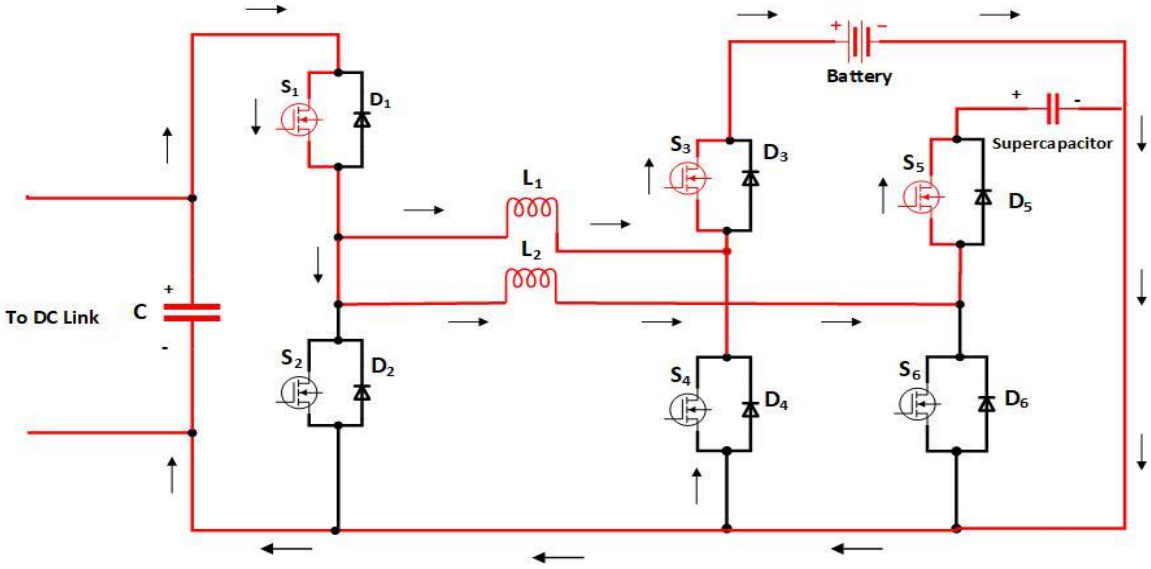

Figure 4.13 (a) Charging inductors L1 and L2 from the DC link in T1.

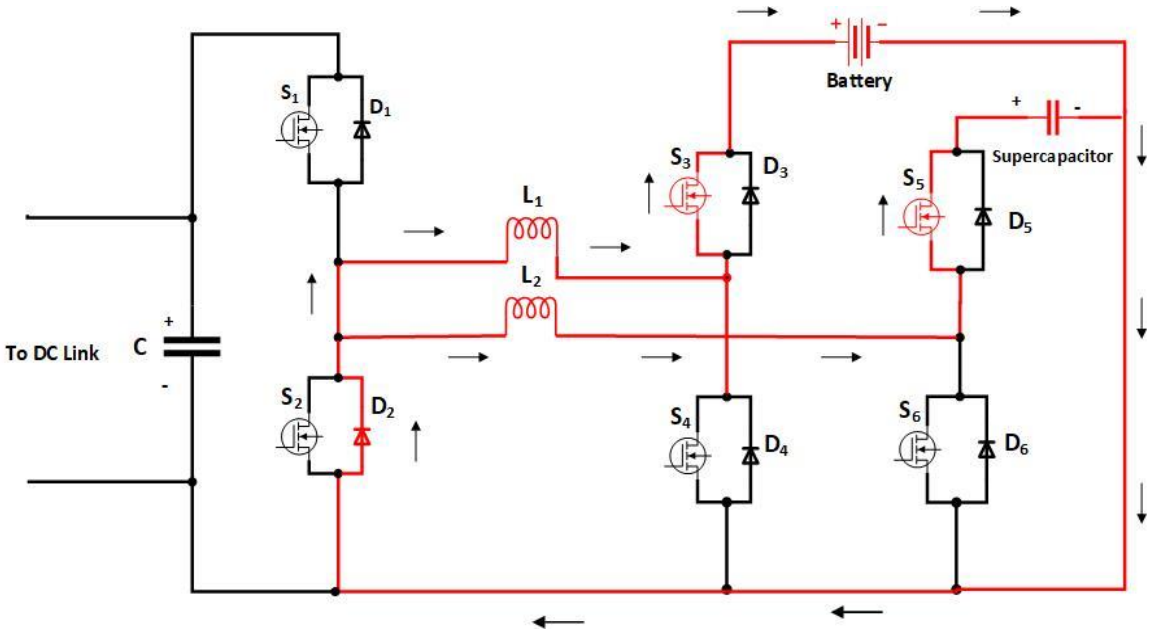

Figure 4.13 (b) Discharging from inductors L1 and L2 in the energy storage devices using D2 in T2.

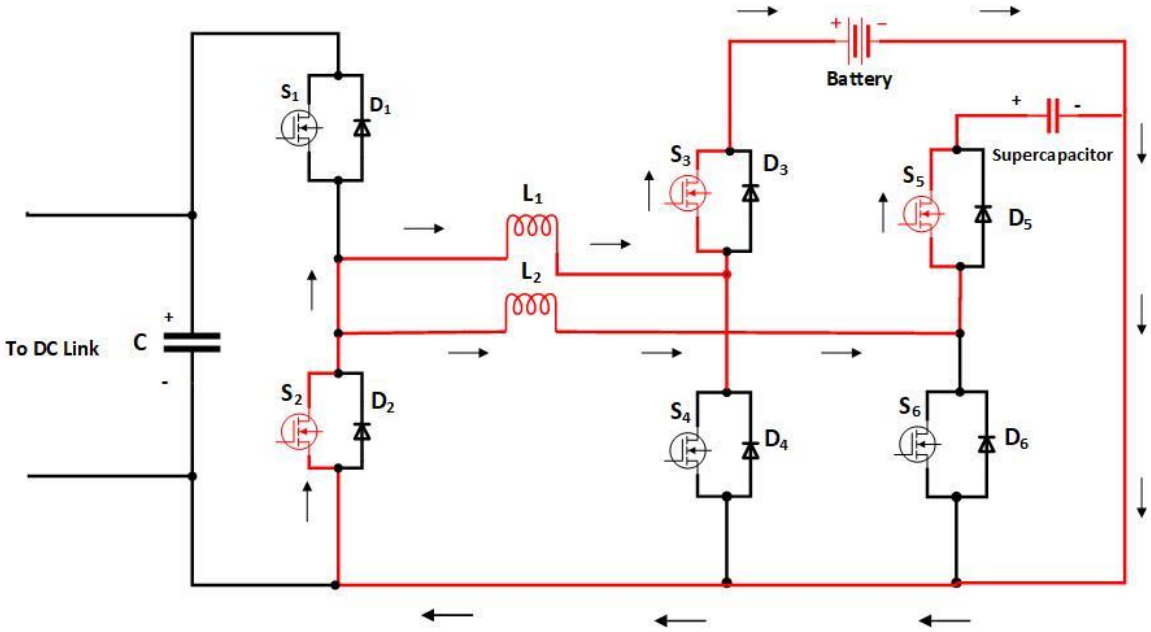

Figure 4.13 (c) Discharging from inductors L1 and L2 in the energy storage devices using S2 in T3.

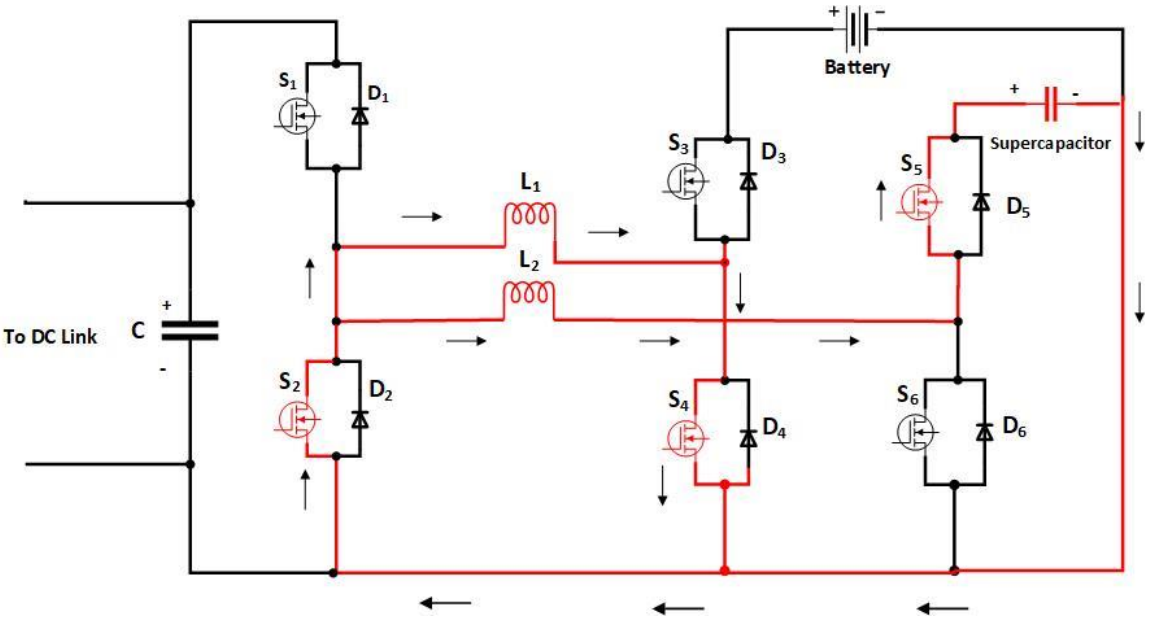

Figure 4.13 (d) Charging supercapacitor with continuous inductor current oft iL2, while switches S3 is turned off, and S4 is turned on at the interval T4.

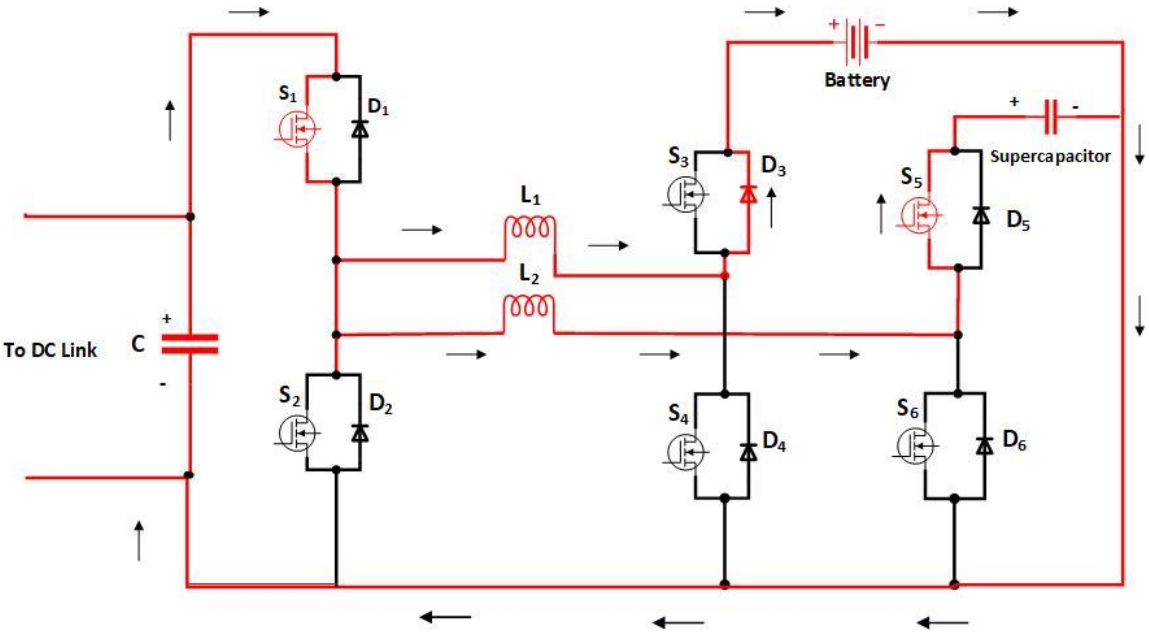

Figure 4.13 (e) Restarting the switching cycle Ts by turning on D3 and then switching S3 in T5.

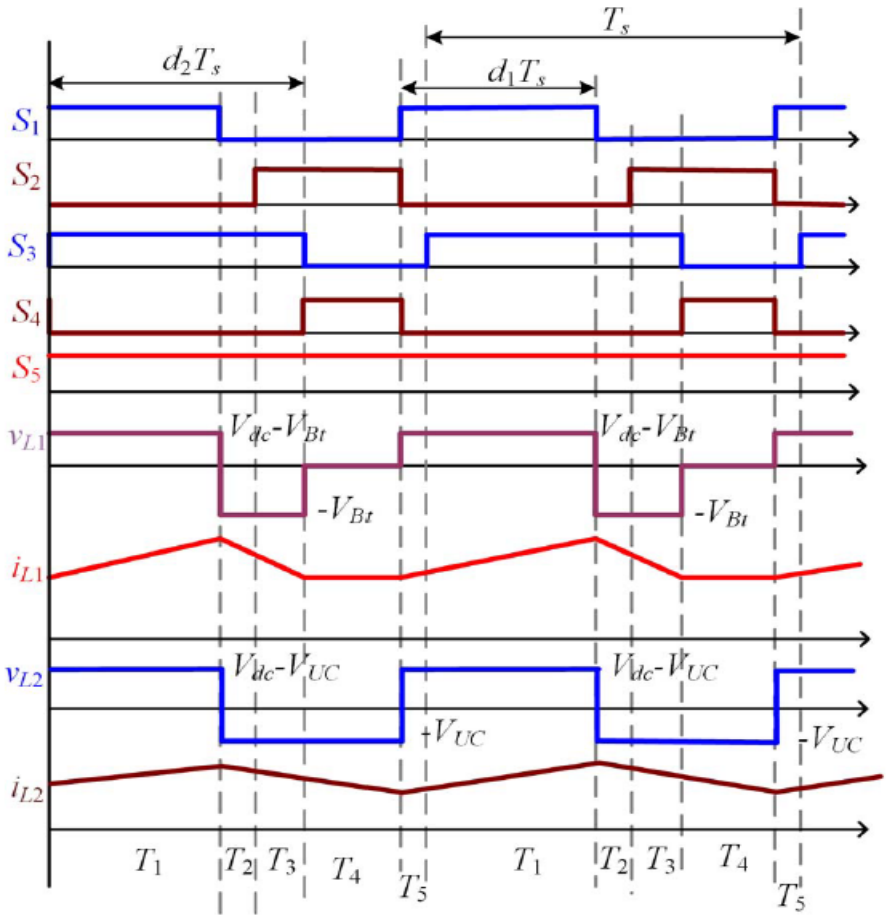

Figure 4.14 Steady-state waveforms for mode E.

The switching sequences of power switches in the operation modes (4) and (5) are listed in Table 4.4 [65].

Table 4.4 Switching states in modes (4) and (5).

	T_1	T_2	T_3	T_4	T_5
mode 4	S_2, S_3, S_5	S_2, D_4, S_5	S_2, S_4, S_5	D_1, S_4, D_6	S_1, S_4, S_6
mode 5	S_1, S_3, S_5	D_2, S_3, S_5	S_2, S_3, S_5	S_2, S_4, S_5	S_1, D_3, S_5

4.3 Control Design of the Converter

The PI controller is one of the most common control algorithms used in power electronics, especially the DC/DC converters. It has many advantages like simplicity, reliability, and ease of implementation in linear systems. It is part of the PID controller family with three integrated constants (Figure 4.15) that have a control loop mechanism employing feedback that is frequently utilized in power electronics circuits. Typically,

the proportional and the integrals (PI) constants are only used in the DC/DC converters, to control the steady-state and transient errors and as well to enhance the response time of the system. The proportional constant (P- controller) obtains the output by comparing the setpoint (the desired output) with the actual value coming from the feedback. The resulted value is multiplied with a proportional constant to get the desired output. To reduce the steady-state error to zero, the integral constant (I- controller) is used to integrate the error over time until the error value reaches zero. However, it is affecting the system stability by limiting the speed response; therefore, it is crucial to tune the PI constant to minimize the steady-state error, enhance the response time and the system stability. The output of the D-controller output depends on the rate of change of error to time, multiplied by the derivative constant.

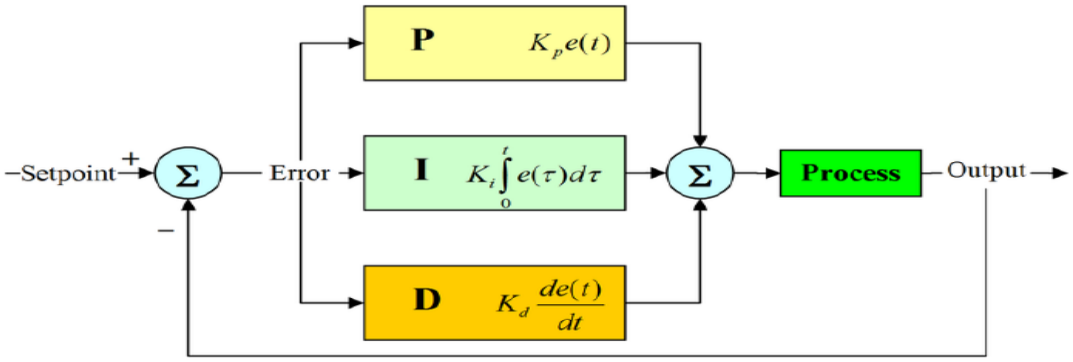

Figure 4.15 PID controller

The system performance and response can be optimized by tuning, the constants K_p, K_i, and K_d. However, as the constants Kp, and Ki are typically used only in the DC/DC converters, the output currents and voltages can be adjusted by tuning them and getting the desired process requirements. The error value is the difference between the feedback signal and the desired setpoint. The controller attempts to reduce it by modifying a controlled variable (e), the tracking error, as shown in Figure 4.16.The error signal will be delivered to the PID controller, and the signal immediately after the controller will match the proportional gain times the error magnitude plus the integral gain times the integral of the error plus the derivative gain times the derivative of the error where, this signal will be sent to the plant, to obtain the desired output.

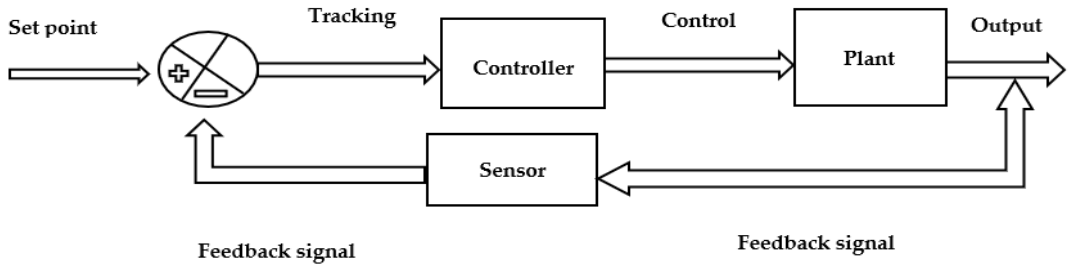

Figure 4.16 System block diagram with feedback control.

The PI controller is used for the voltage control for the buck and boost stages of the Multi-input DC-DC converter. The closed-loop transfer function of the PI controller's first order system is:

$$G(s) = \frac{\left(K_p + \frac{K_i}{s}\right).k}{\tau.s + 1 + \left(K_p + \frac{K_i}{s}\right).k} \qquad (4.31)$$

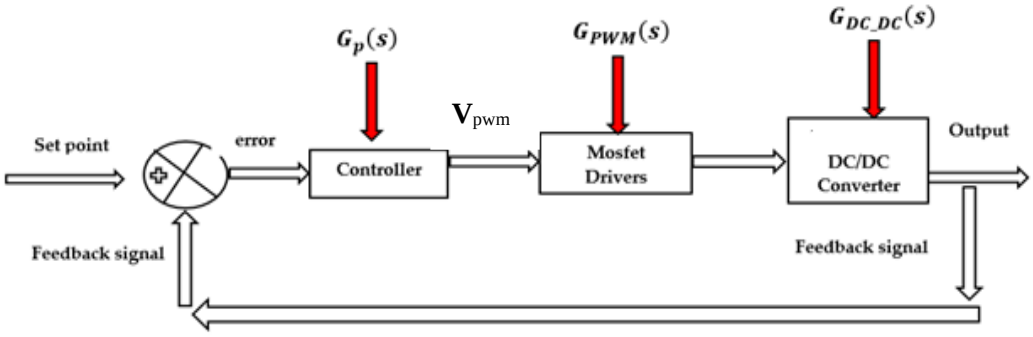

Figure 4.17 Multi-input DC-DC Converter Process with Closed-Loop Controller.

Where τ is the time constant, and K is the DC Gain. The equations below were used to implement the controller algorithm in Figure 4.17.

$$\frac{V_{out(s)}}{V_{set\ point(s)}} = \frac{G_{(s)}}{1 + G_{(s)}} \qquad (4.32)$$

$$G(s) = G_p(s).G_{PWM}(s).G_{DC\_DC}(s) \qquad (4.33)$$

$$G_{converter}(s) = G_{PWM}(s).G_{DC\_DC}(s) \qquad (4.34)$$

As shown in Figure 4.17, the output signals of the PI controller determine the suitable duty ratio for switching the MOSFETs gates to obtain the desired operation mode. The same algorithm is used in the downscale DC-DC converter to control the charging current of the EV. The system is underdamped by regulating the value of the proportional coefficient $K_p = 3$ and the integral coefficient $K_I = 5$ to minimize the steady-state error. To make the whole system stable, the lead-lag compensator was designed using the below equation, with Kp=3 and Ti= 7.5758x10−4.

$$C_{iL} = K_p(1 + \frac{1}{T_{iS}}) \qquad (4.35)$$

4.4 Design of the Proposed Fast-Charging Station

The proposed converter, as mentioned before, is used to charge the EVs from the energy storage devices individually and simultaneously. The energy storage devices connected with the grid utility to the DC link as shown in Figure 4.18. This DC link is connected to the step-down converter to reduce the voltage of the DC link and increase the charging current of the EV, in addition to controlling the charging rate. The proposed FCS uses off-board charging topology as the power conversion outside the vehicle, and it works at a high-power rate, as we will discuss later in the simulation work section. To form a hybrid energy storage system, a battery and supercapacitor are utilized to combine the high energy density of the battery and the high-power density of the supercapacitor. Furthermore, using the modularity feature of the converter, more renewable energies can be added easily to charge the energy storage devices; thus, the charging cost and the load on the gird can be reduced more.

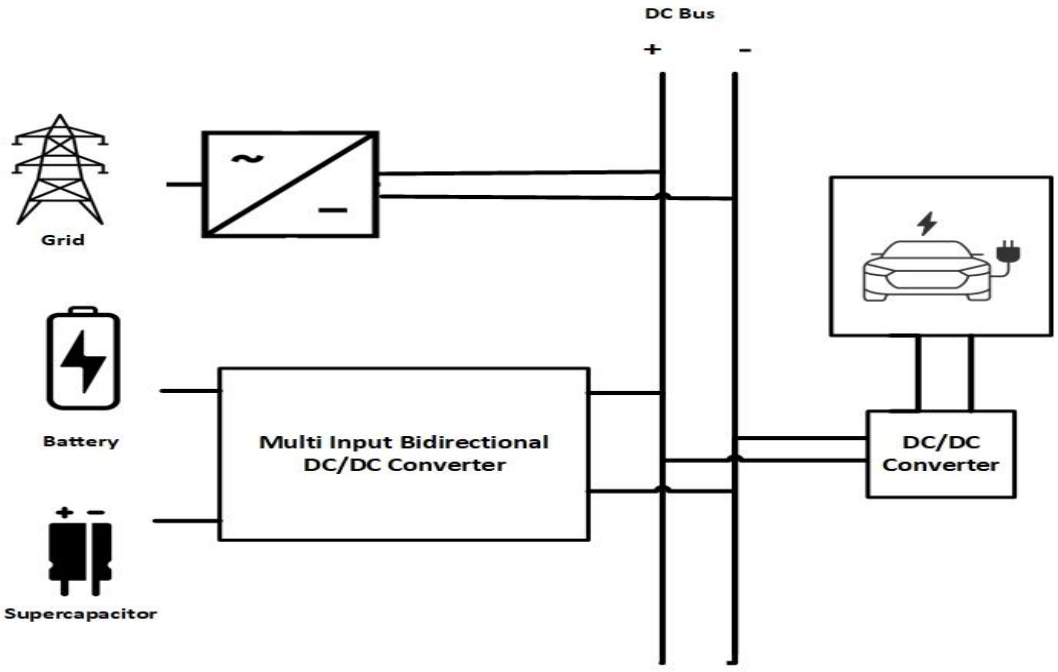

Figure 4.18 The proposed fast charging station.

4.4.1 The Design of the Buck Converter

The step-down DC/DC converter shown in Figure 4.19 consists of MOSFET switch *S* to charge and discharge the inductor *L* and diode *D* to prevent the current from passing through it during the on-state of the switch as its reversed biased by voltage. The capacitor *C* is used as a filter for voltage ripples.

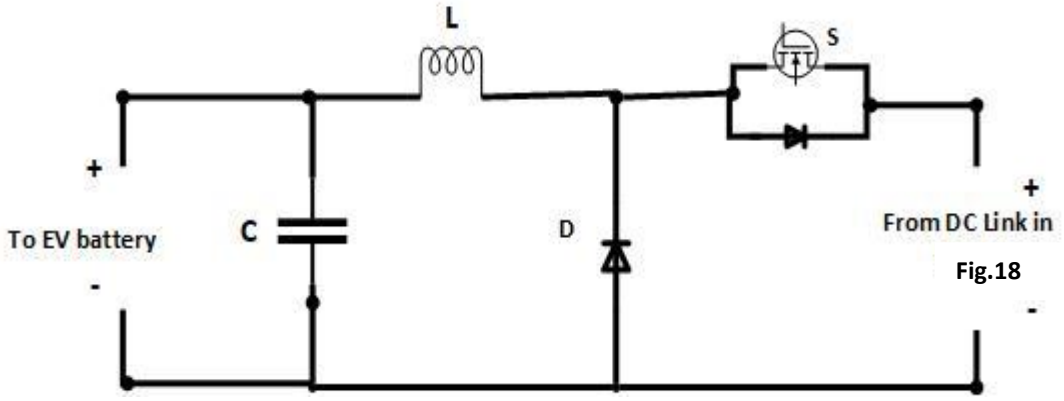

Figure 4.19 Circuit diagram of the buck converter.

During the on-state, the switch *S* is turned on, the current through inductor L is increased, and the voltage across the inductor will be:

$$V_L = V_{in} - V_O \qquad (4.36)$$

In this case the V_{in} will be the DC link voltage and the V_O the output voltage to charge the EV's battery. In the of- state, the switch *S* is turned off, the diode D will be forward biased, and the voltage across the inductor will be:

$$V_L = -V_O \qquad (4.37)$$

The current through the inductor will decrease and flow through the freewheeling diode *D*, and the EV's battery. The inductor has been selected to make the converter work in continuous operation mode and reduce the current ripples and has been calculated using equation (4.38)

$$L = \frac{(1-D)R}{2f} \qquad (4.38)$$

Similarly, the capacitor has been selected and calculated using equation (4.39) to reduce the output voltage ripples and handle the required ripple current stress.

$$\Delta V_C = \frac{V_S D(1-D)R}{8LCf^2} \qquad (4.39)$$

The buck converter works at a switching frequency f_s 30 kHz to reduce the size of the inductor and the capacitor. Table 4.5 shows the design specification of the proposed buck converter [66].

Table 4.5 Design specification of the buck converter.

Specifications	**Input voltage**	**Output voltage**	**Switching frequency (f_s)**	**Inductor (L)**	**Capacitor (C)**	**Power**
Values	500 V	350 V	30 kHz	5 mH	50 F	17 kW

4.4.2 The Control of the Buck Converter

The multi-input converter was based on voltage control to sustain the DC link voltage at 500 V. In contrast, the buck converter is based on current control, as shown in Figure 4.20 to control the charging current of the EV. The proportional-integral (PI) controller was also chosen to control the charging current. Figure 4.20 shows that the PI controller minimizes the error between the output current and the reference charging current to determine the desired duty ratio for generating the pulses of the switch of the buck converter. The system is underdamped by regulating the value of the Integral coefficient K_I = 5 and proportional coefficient Kp = 3 to minimize the overshoot and the steady-state error.

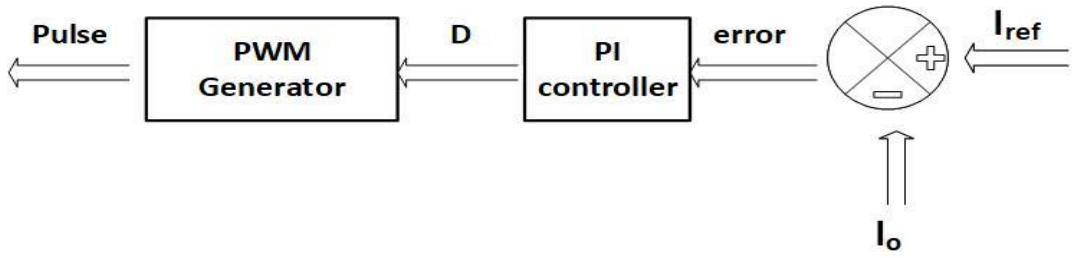

Figure 4.20 Buck converter controller.

Chapter 5. Simulation Results and Performance Analysis

5.1 Simulation Results of the Proposed Converter

The proposed converter was simulated in MATLAB/Simulink, as shown in Figure 5.1, in different operation modes to verify its topology and analysis. The built-in models of the battery and supercapacitor were used, and the gate signals were sent from the PID controller to determine which MOSFETs would switch on and which MOSFETs would switch off based on the operation mode.

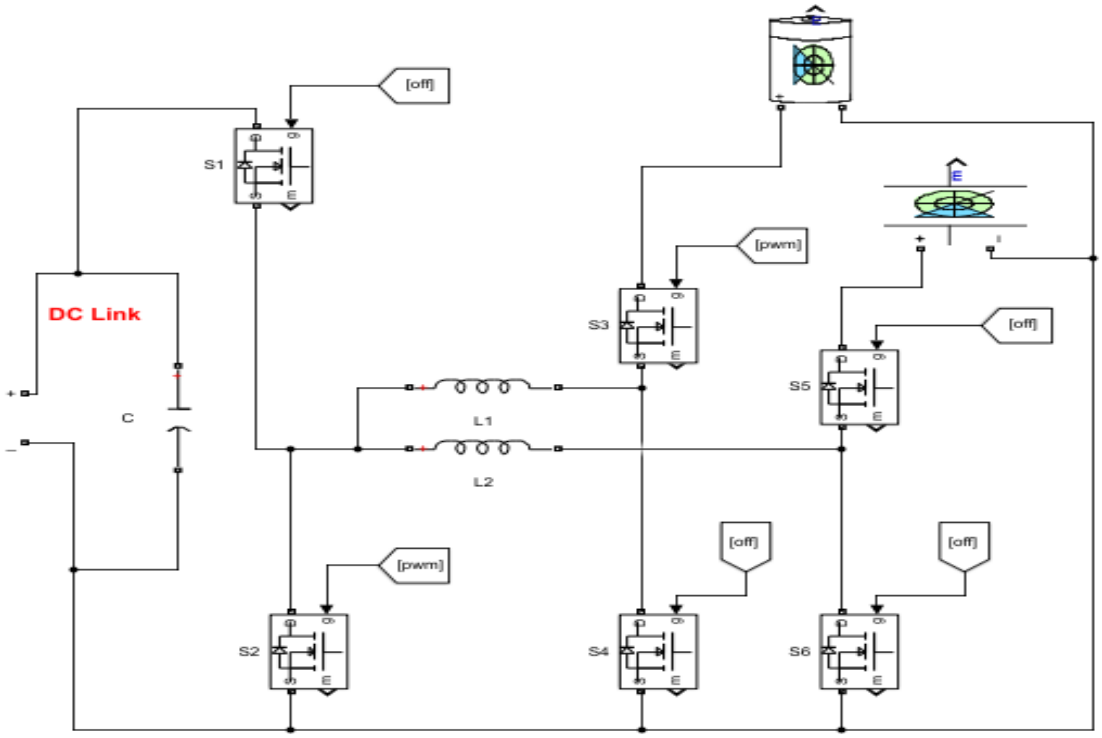

Figure 5.0:1 Design of the proposed converter in MATLAB/Simulink.

Figure 5.2 (a) shows the battery was boosted from 200 V to 500 V to discharge in the DC link through L_1 in mode 1(a), based on the switching sequence in this mode, the switch S_2 work in complementary wise with switch S_4 , as the voltage across S_2 present DC link voltage, and the voltage across S_4 present battery's voltage. In mode 1(b), the battery is charged from the DC link by reversing the current in the inductor L_1 in the average current of 15 A, as shown in Figure 5.2 (b), and similarly, the voltage across S_2 present DC link's voltage, and the voltage across S_4 present battery's voltage.

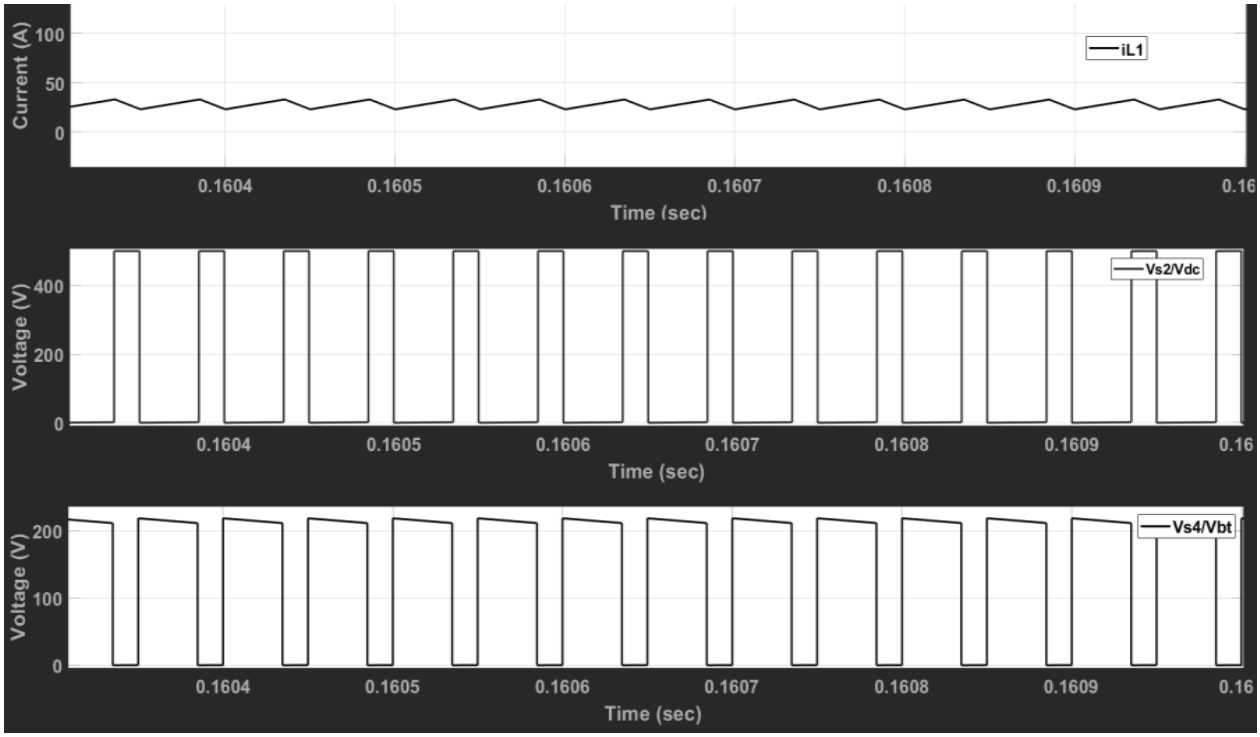

Figure 5.2 (a) Current of L1 and voltages across VS4 and VS2 in mode 1(a).

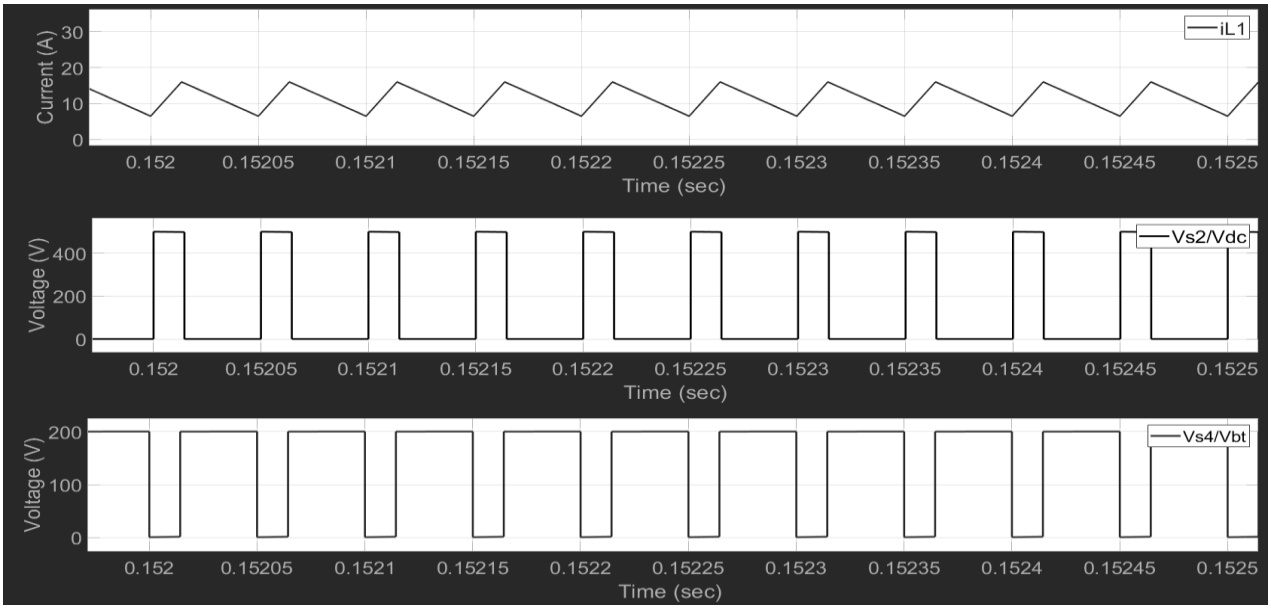

Figure 5.2 (b) Current of L1 and voltages across VS4 and VS2 in mode 1(b).

In mode 2(a), the energy transferred from the supercapacitor to the DC link as voltages across switches S_2 and S_6 show the DC-link and supercapacitor voltage, respectively, along with their states. As shown in Figure 5.3 (a), the supercapacitor's voltage is boosted from 160 V to the DC link's voltage of 500 V by charging the inductor L_2. By using the same switches and by reversing the current in the inductor L_2, the supercapacitor charged from the DC link by reducing the voltage from 500 V to 160 V, as shown in Figure 5.3 (b).

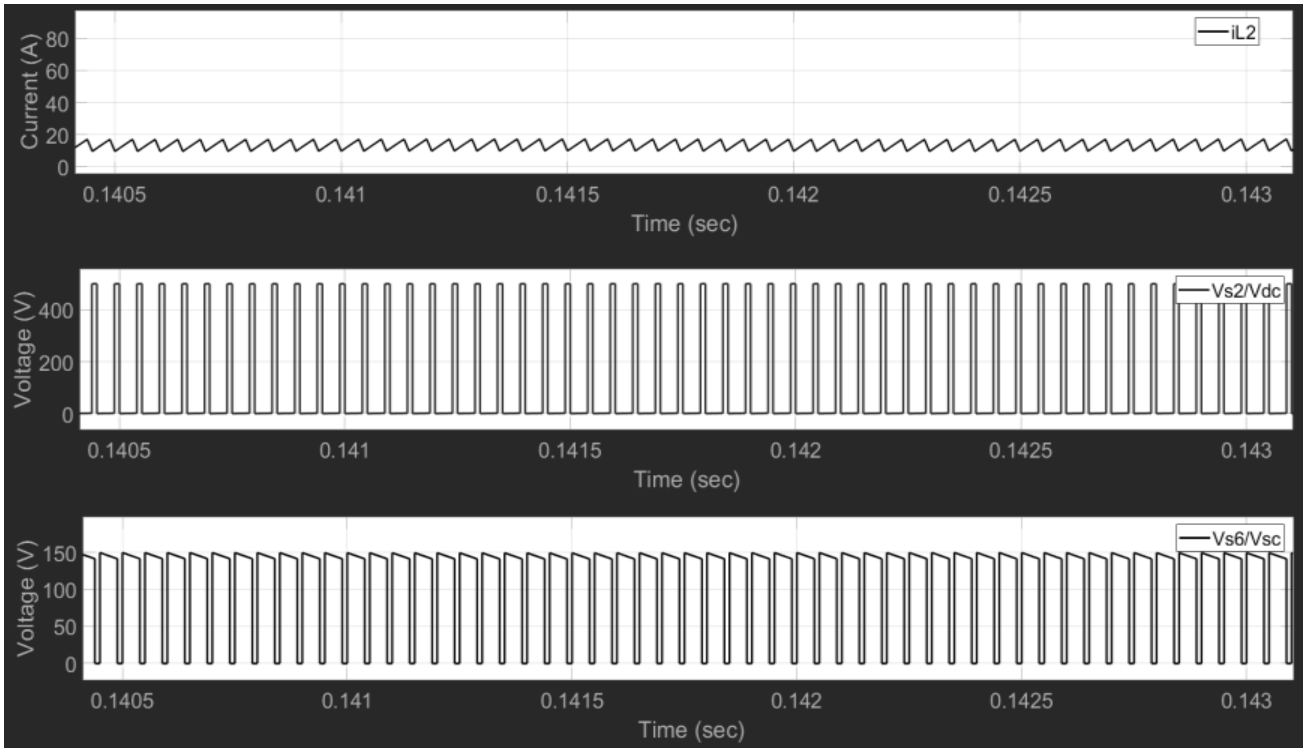

Figure 5.3 (a) Voltages across switches S_6 and S_2 and current of L_2 in mode 2(a)

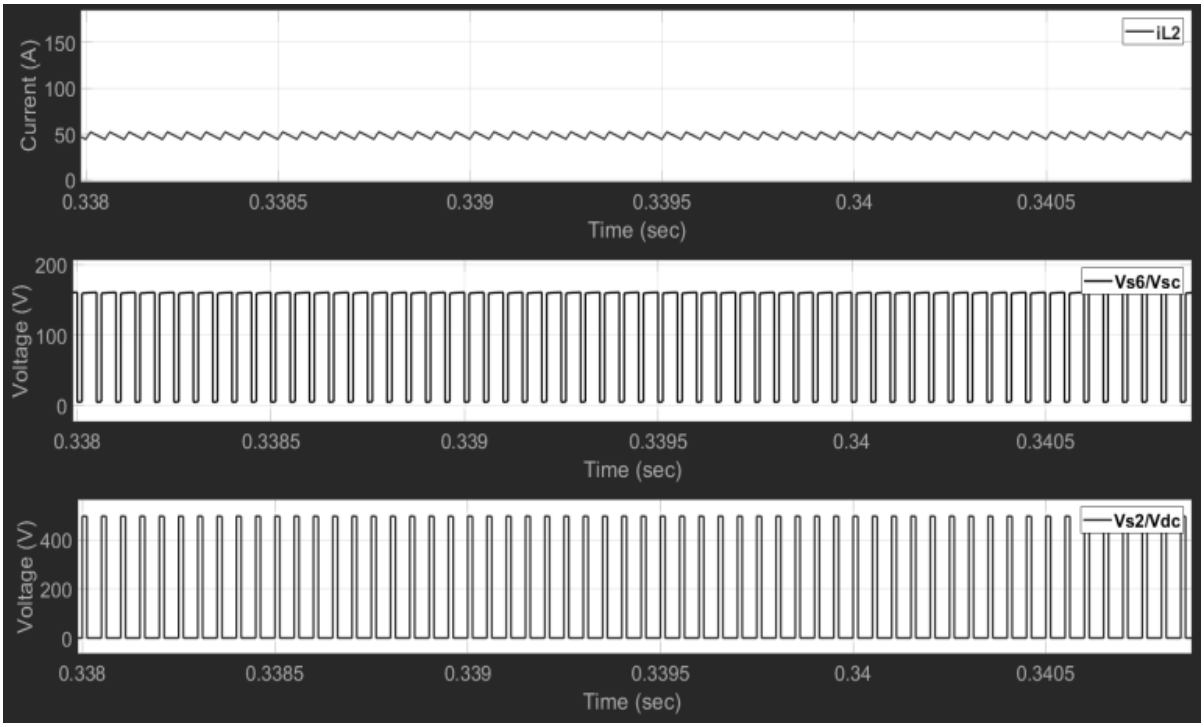

Figure 5.3 (b) Voltages of switches S6 and S2 and current of L2 in mode 2(b).

The power can be exchanged between the battery and supercapacitor as shown in Figure 5.4 (a) and Figure 5.4 (b), respectively, in mode 3(a) and mode 3(b) using switches S_3, S_5, and S_6. The SOC of the supercapacitor increases with a low voltage ripple of charging, and the charging current is negative, which means the current enters the supercapacitor, as shown in Figure 5.4 (a). Similarly, the voltage and current ripple of charging the battery from the supercapacitor was less than 0.2 V, as shown in Figure 5.4 (b).

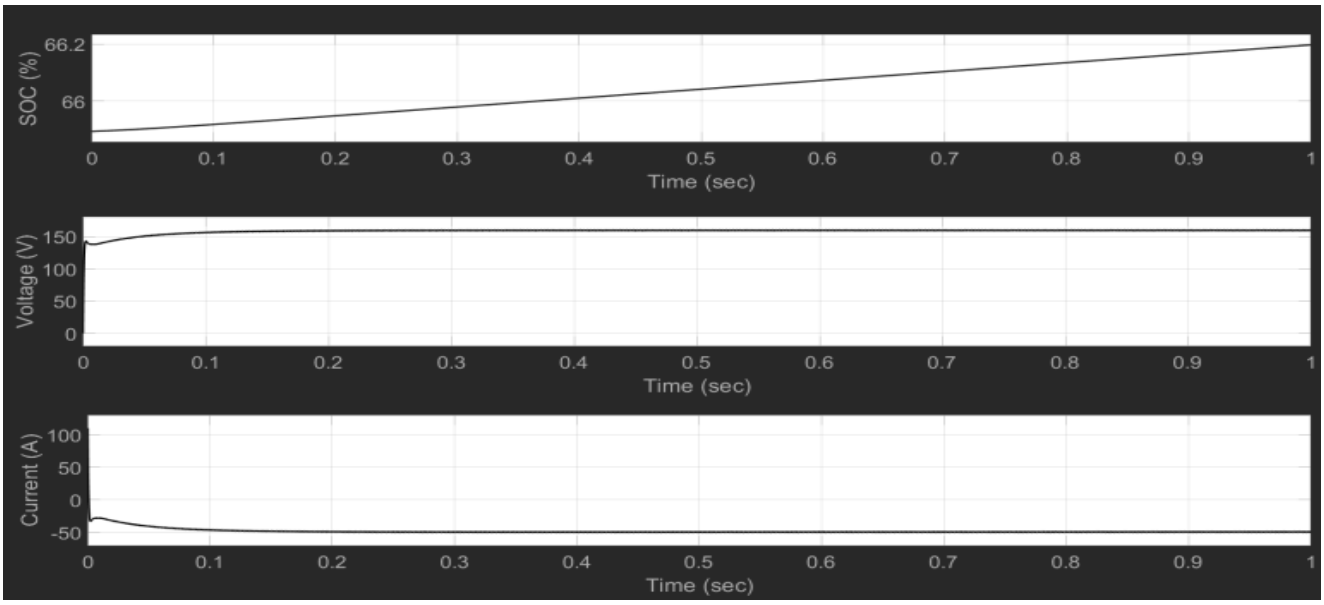

Figure 5.4 (a) SOC, voltage and current of supercapacitor in mode 3(a).

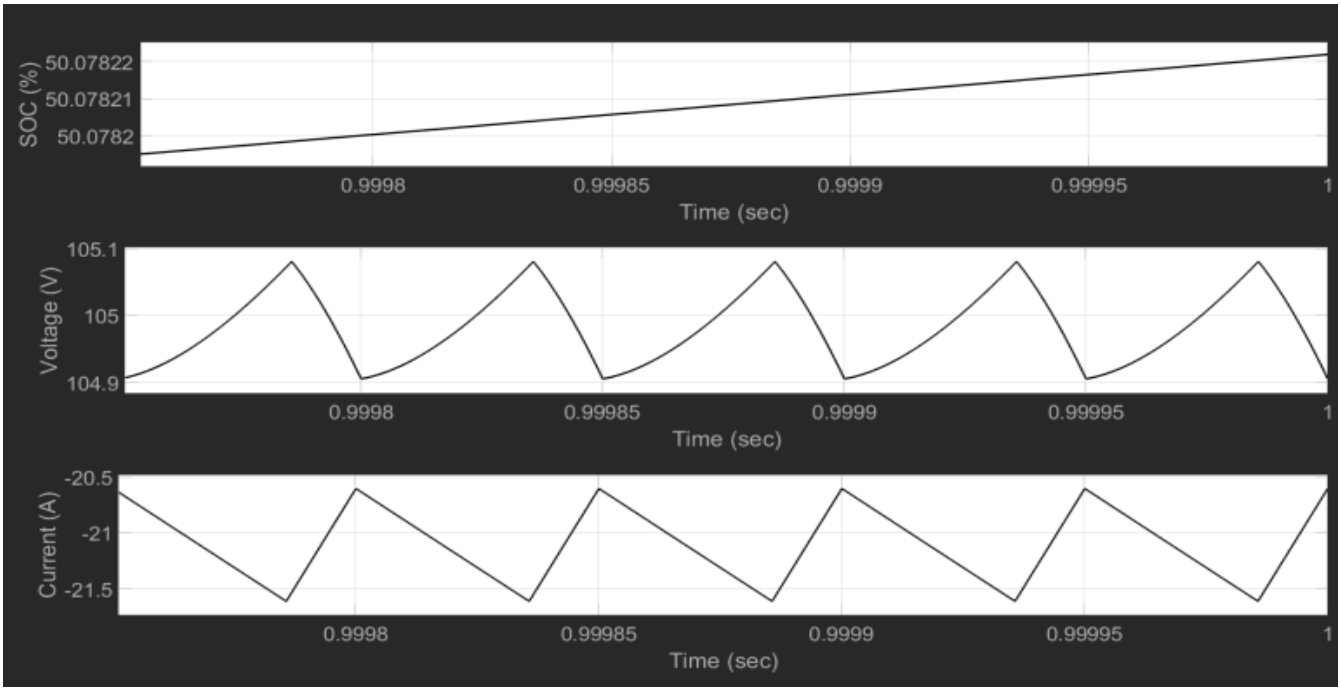

Figure 5.4 (b) SOC, voltage and current of battery in mode 3(b).

In mode four, the DC link is boosted to 500 V from the battery's voltage of 200 V and supercapacitor's voltage of 160 V simultaneously with low voltage ripples through inductors L_1 and L_2 as shown in Figure 5.5. Simultaneously, the supercapacitor and the battery can be charged from the DC link to their voltages by reversing the currents through inductors L_1 and L_2 also, as shown in Figure 5.6. Their SOC increased, and the charging currents were negative, which means the currents entered the energy storage devices.

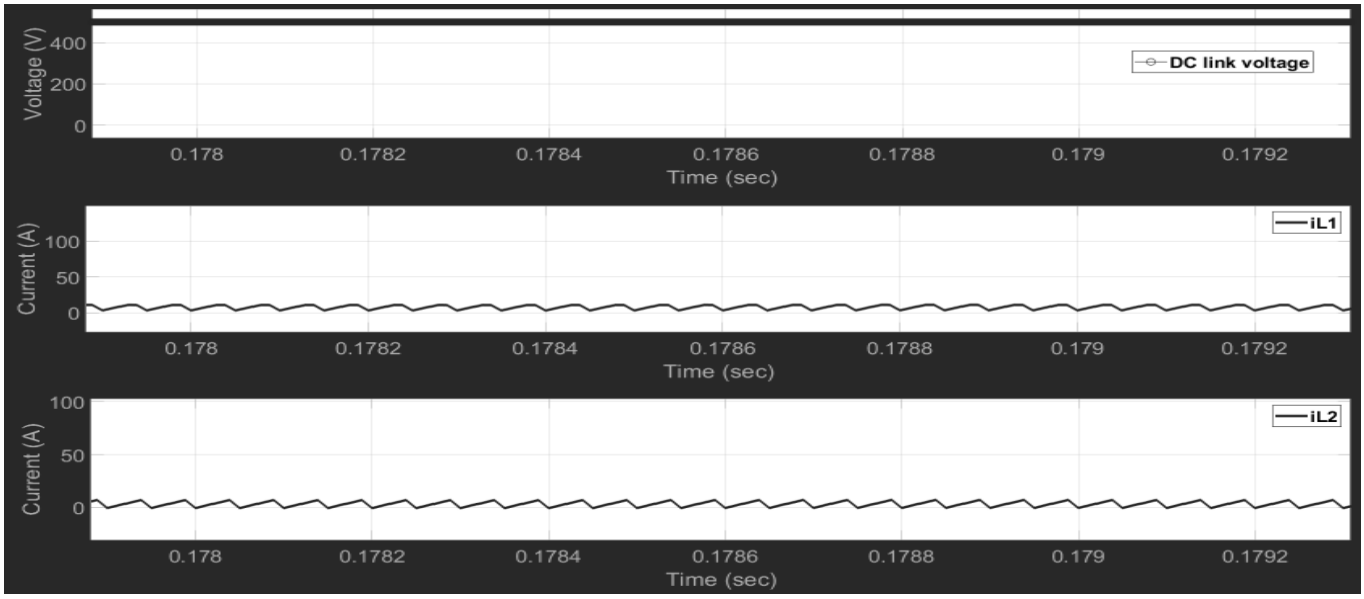

Figure 5.5 Currents of L2 and L1 and DC link voltage in mode 4.

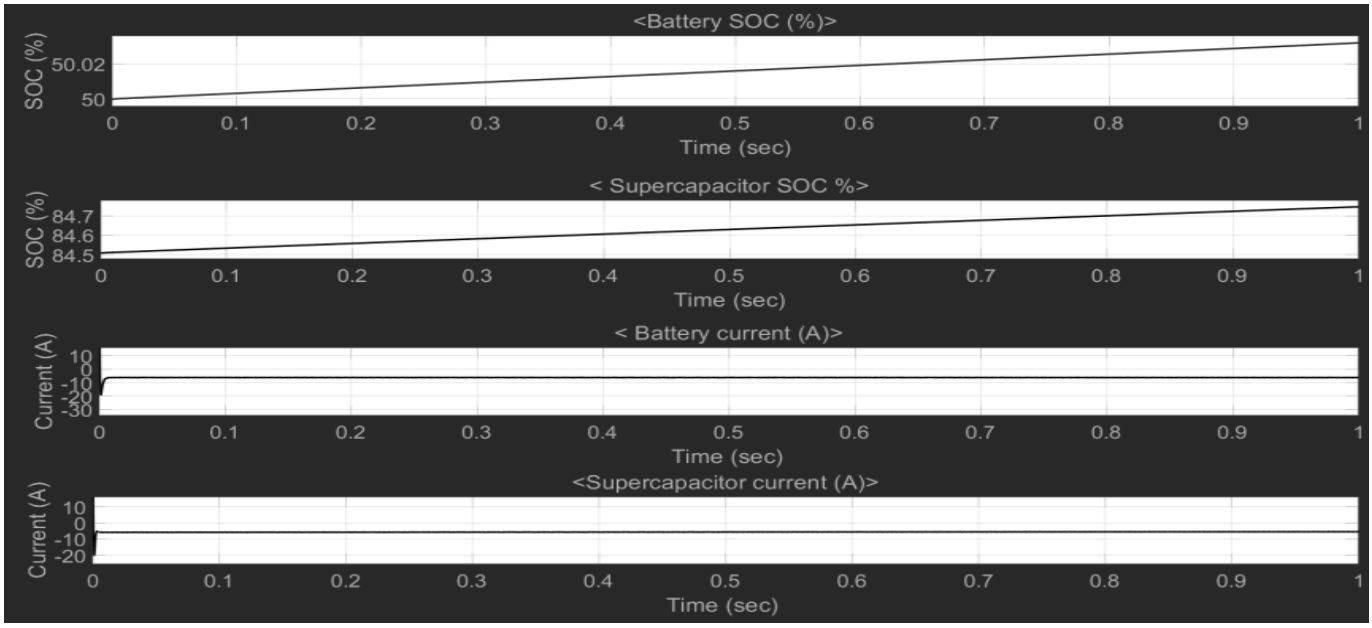

Figure 5.6 Currents and SOC of the battery and the supercapacitor in mode 5.

The simulation results also show the optimization of the PID control algorithm, as the results show the steady-state error, and the overshoot values were low and in the acceptable range. For example, Figure 5.7 (a) shows the steady-state error was less than 2 V and the rising time was less than 0.2 sec in mode 1(a), and the same for charging the battery from the DC link as seen in Figure 5.7 (b) the output voltage was very smooth by charging the battery with 200 V.

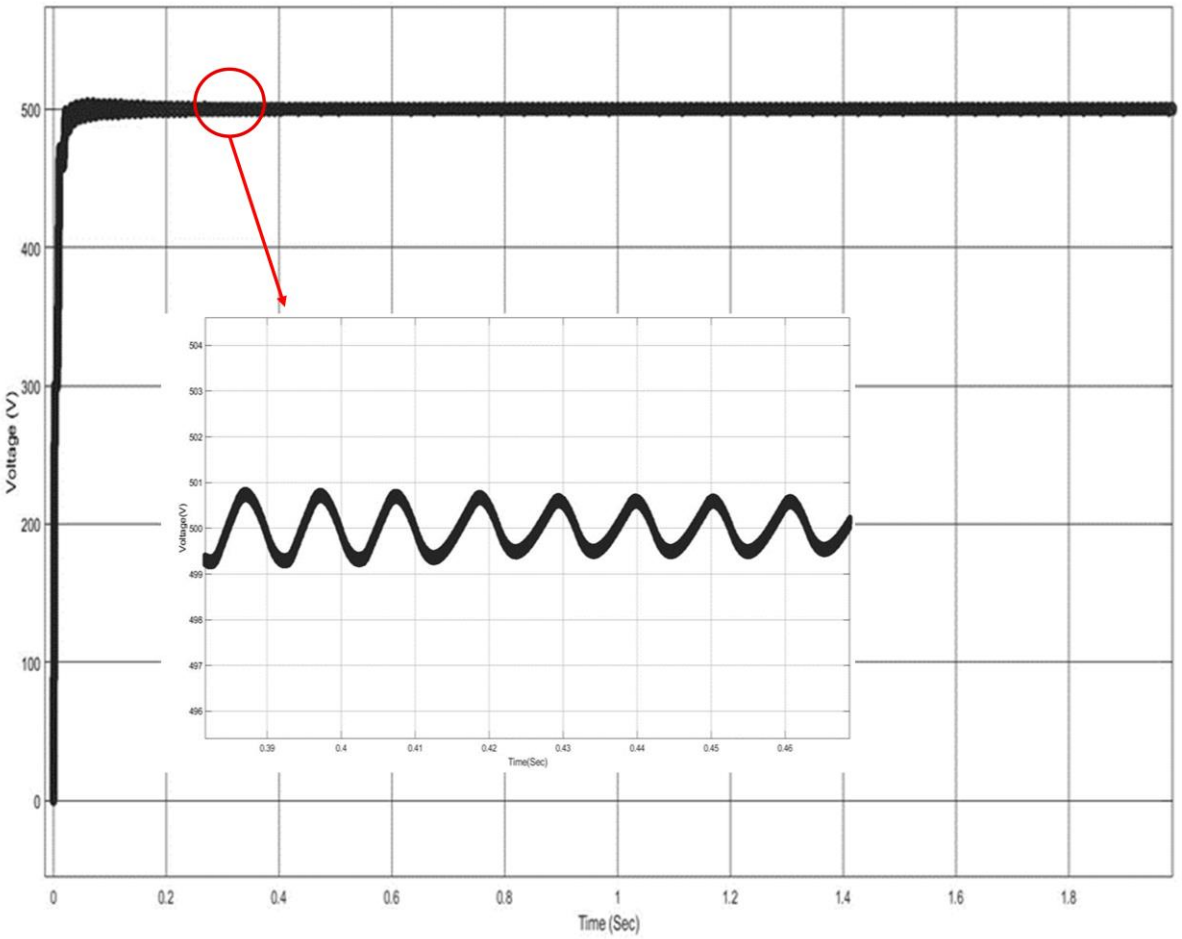

Figure 5.7 (a) Steady-state error of the output voltage in mode 1(a).

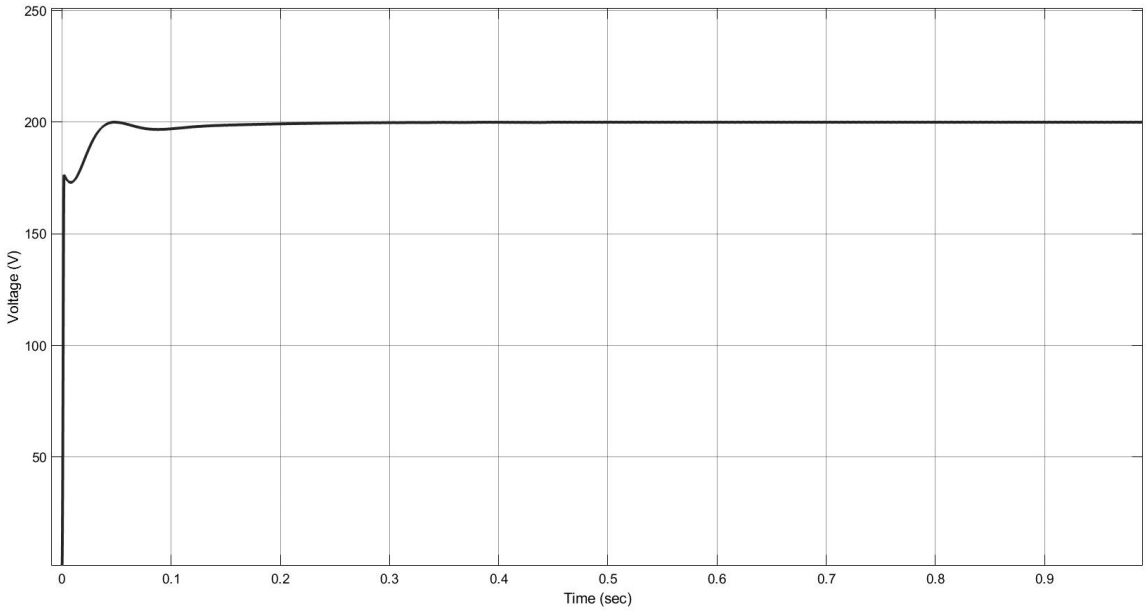

Figure 5.7 (b) Battery's voltage in mode 1(b).

Similarly, the steady-state error was less than 7 V, meaning 0.014 voltage ripples, and the rising time was less than 0.1 sec in mode 2(a), as seen in Figure 5.8 (a). As seen in Figure 5.8 (b), the output voltage was very smooth in charging the supercapacitor from the DC link with an output voltage of 160 V.

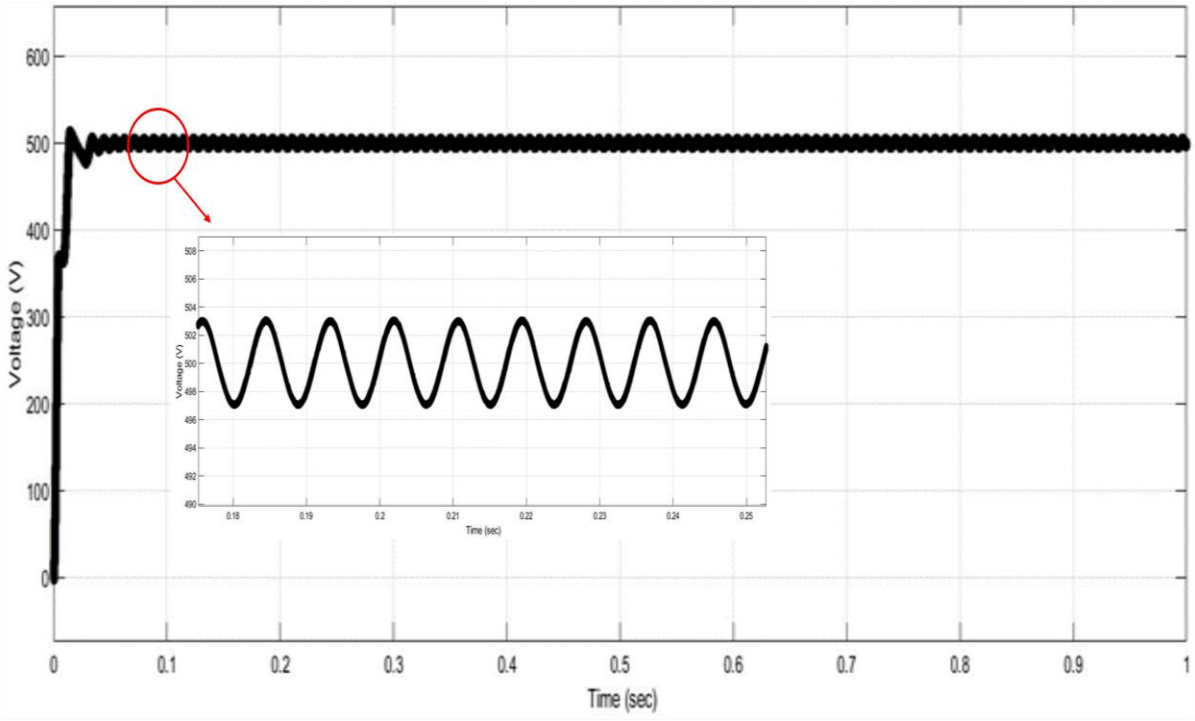

Figure 5.8 (a) Steady state error of the output voltage in mode 2(a).

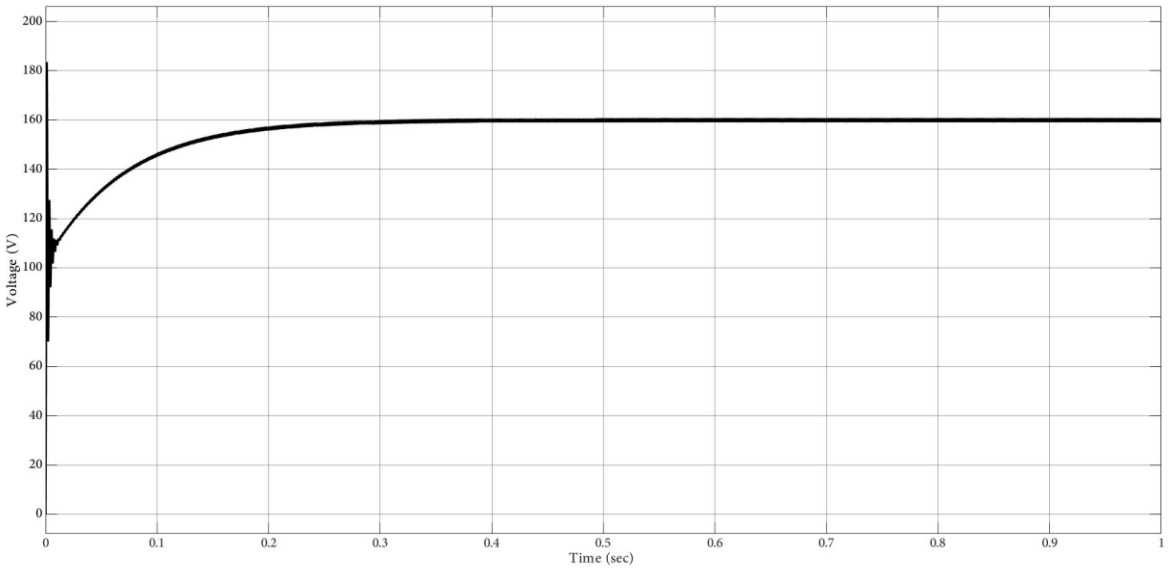

Figure 5.8 (b) Supercapacitor's voltage in mode 2 (b).

Moreover, Figure 5.9 present the battery and supercapacitor were charged from the DC link in low overshot and voltage ripples with different current and voltage rates.

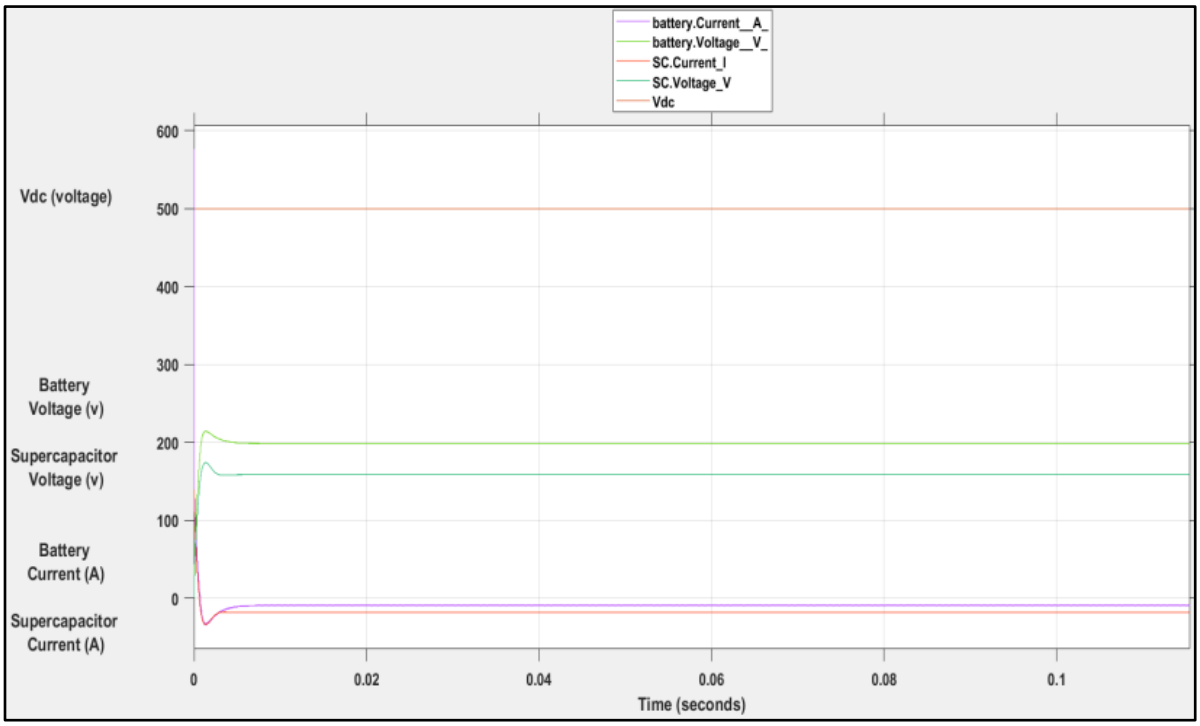

Figure 5.9 The current and voltage of the supercapacitor and battery while charging from the DC link at mode 5.

5.2 Losses and Efficiency of the Proposed Converter

The switching losses and conduction losses are the main losses of the proposed converter. As the MOSFETs of the converter exposes to high voltage and current during a transition between the on and off states, as shown in Figure 5.10, this creates switching losses in the converter. By using equation (5.1), the switching losses in the different operation modes can be calculated.

$$P_S = \int V_D \, I_D \, dt \qquad (5.1)$$

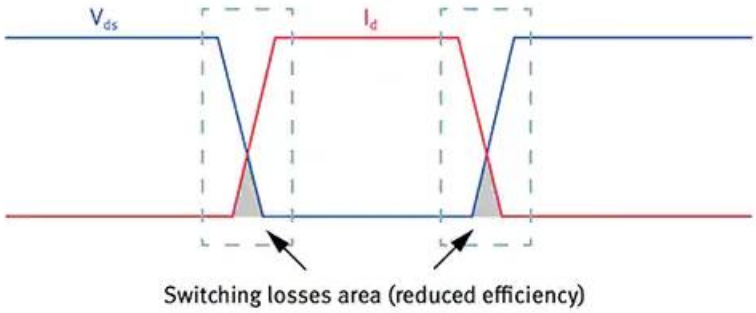

Figure 5.10 Switching losses during the overlap transaction between the current and the voltage of the MOSFET

Where V_D and I_D , the voltage and current drain of the MOSFET in on and off states. The resistive elements of the MOSFETs dissipate power and create conduction losses as current is conducted through the power switch. The resistive parameter is described as on-resistance, or R_{DSon} , and it is equal to 0.1 Ω in the proposed converter. The average value of the conduction losses can be calculated using equation (5.2)

$$P_c = I_{Drms}^{\,2} \, R_{DSon} \qquad (5.2)$$

Where is I_{Drms} is the rms value of the MOSFET on-state current, therefore the total losses will be:

$$P_T = P_s + P_c \qquad (5.3)$$

The switching and conduction losses in the different operation modes are summarized in Tables 5.1 and 5.2 based on equations (5.1) and (5.2).

Table 5. 1 Switching losses of the five operation modes.

	S_1	S_2	S_3	S_4	S_5	S_6	**Total**
mode 1(a)	2.8 W	6.6 W	55.9 W	23. 7 W	-	-	89 W
mode 1(b)	6.7 W	16.3 W	9.5 W	3.8 W	-	-	36.3 W
mode 2(a)	3 W	13.11 W	-	-	14.2 W	4 W	33 W
mode 2(b)	63 W	183 W	-	-	176 W	57 W	479 W
mode 3(a)	-	-	48 W	-	32 W	13 W	96 W
mode 3(b)	-	-	45 W	-	32 W	13 W	90 W
mode 4	3 W	12 W	3.2 W	3.7 W	1.2 W	0.38 W	23 W
mode 5	5.6 W	12.4 W	4.3 W	0.9 W	3.8 W	0 W	27 W

Table 5.2 Conduction losses of the five operation modes.

	S_1	S_2	S_3	S_4	S_5	S_6	**Total**
mode 1(a)	0.25 W	6.6 W	52 W	2.12 W	-	-	63.97 W
mode 1(b)	6.7 W	1.5 W	0.87 W	3.8 W	-	-	12.87 W
mode 2(a)	0.27 W	13.2 W	-	-	14.24 W	0.37 W	28.08 W
mode 2(b)	62.7 W	16.5 W	-	-	15.8 W	57 W	152 W
mode 3(a)	-	-	855 W	-	40 W	400 W	1295 W
mode 3(b)	-	-	4 W	-	31.7 W	1.6 W	37.3 W
mode 4	0.28 W	12 W	3.25 W	0.33 W	1.26 W	0.035 W	17.16 W
mode 5	5.6 W	1.12 W	0.39 W	0.94 W	0.35 W	0 W	8.4 W

The efficiency of the proposed converter in the different operation modes is summarized in Table 5.3 based on equation (5.4).

$$\text{efficiency} = \frac{P_{op}}{P_{in}} \qquad (5.4)$$

Table 5.3 The efficiency of the converter in the five operation modes.

	mode 1(a)	mode 1 (b)	mode 2(a)	mode 2 (b)	mode 3 (a)	mode 3(b)	mode 4	mode 5
P_{in}	4000 W	2100 W	1520 W	2100 W	9000 W	2200 W	1200 W	2100 W
P_{op}	3847 W	2051 W	1471 W	1469 W	7609 W	2073 W	1160 W	2065 W
Efficiency	96.18%	97.60%	96.70%	70%	85%	98.70%	96.70%	98.30%

5.3 Simulation Results of the Fast Charging Station

To test the charging capability of the proposed multi-input converter for charging an EV's battery from the energy storage devices individually or simultaneously without the grid utility, a battery is connected to the buck converter with specifications similar to the Nissan leaf battery (350 V, 60 Ah). The storage battery successfully charged the EV battery with a charging current of more than 25 A and with a charging power rate of 8750 W, as shown in Figure 5.11. Using the supercapacitor, the SOC of the EV's battery increased linearly with a charging current of 25 A and a charging power rate of 8750 W, as shown in Figure 5.12. To increase the charging current rate and reduce the charging time, the EV's battery is simultaneously charged from the battery and supercapacitor, as shown in Figure 5.13. During the first one second of the simultaneous charging, the charging current was 50 A and the SOC was higher than the SOC in the same charging time for individual charging.

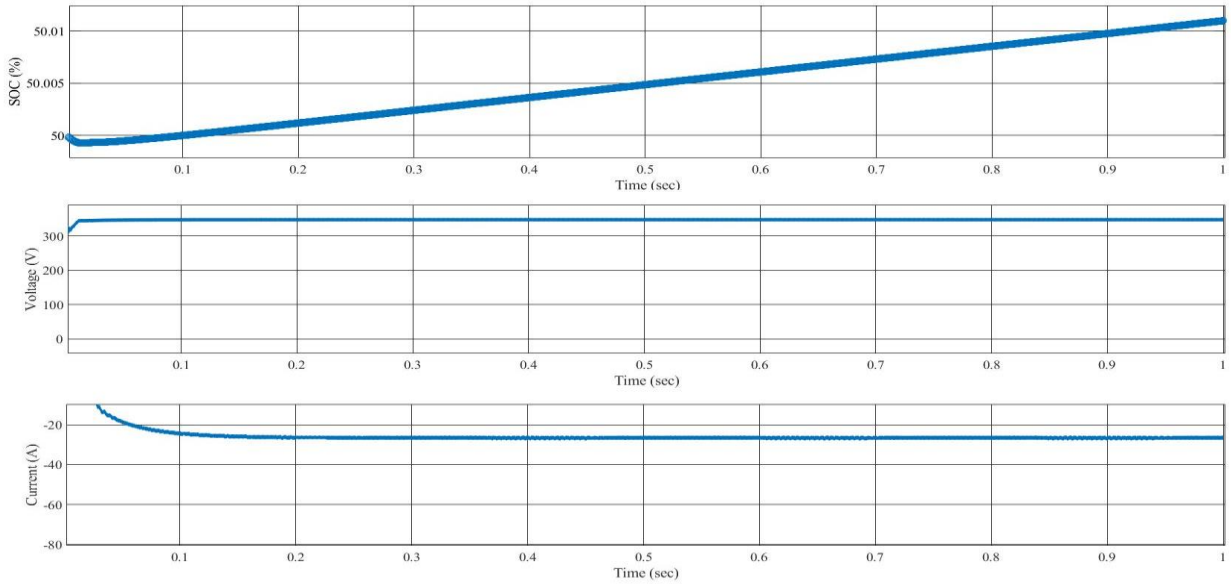

Figure 5.11 Charging the EV's battery from the battery only.

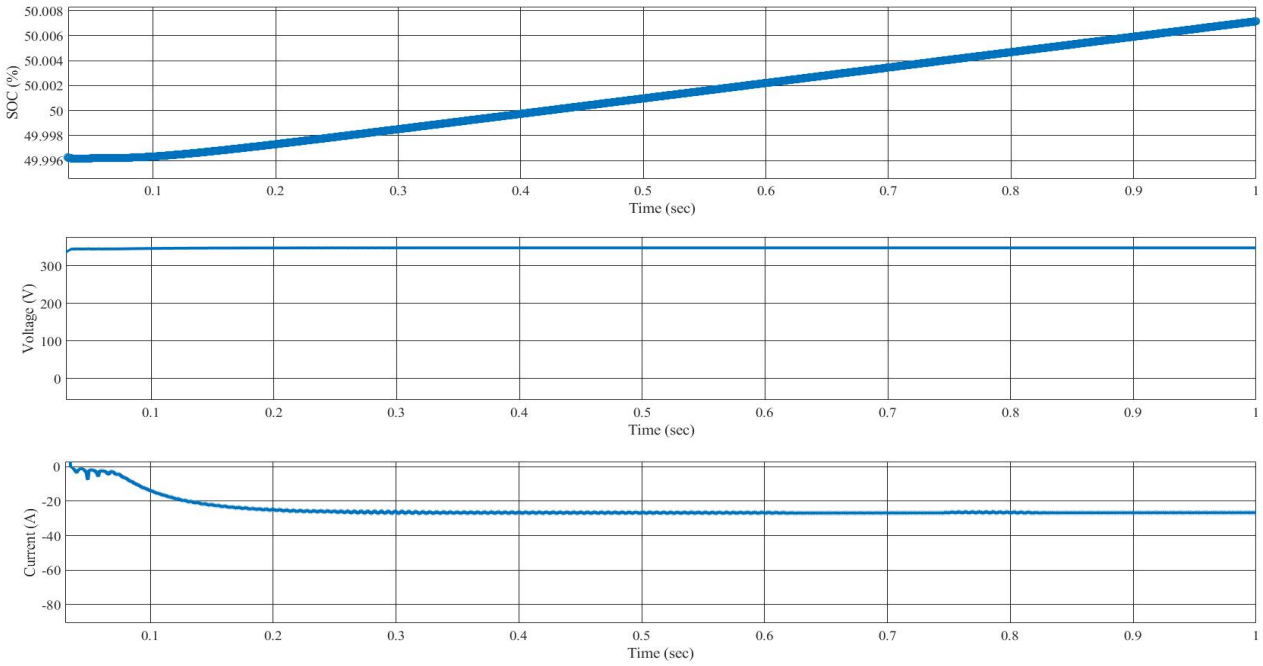

Figure 5.12 Charging the EV's battery from the supercapacitor only.

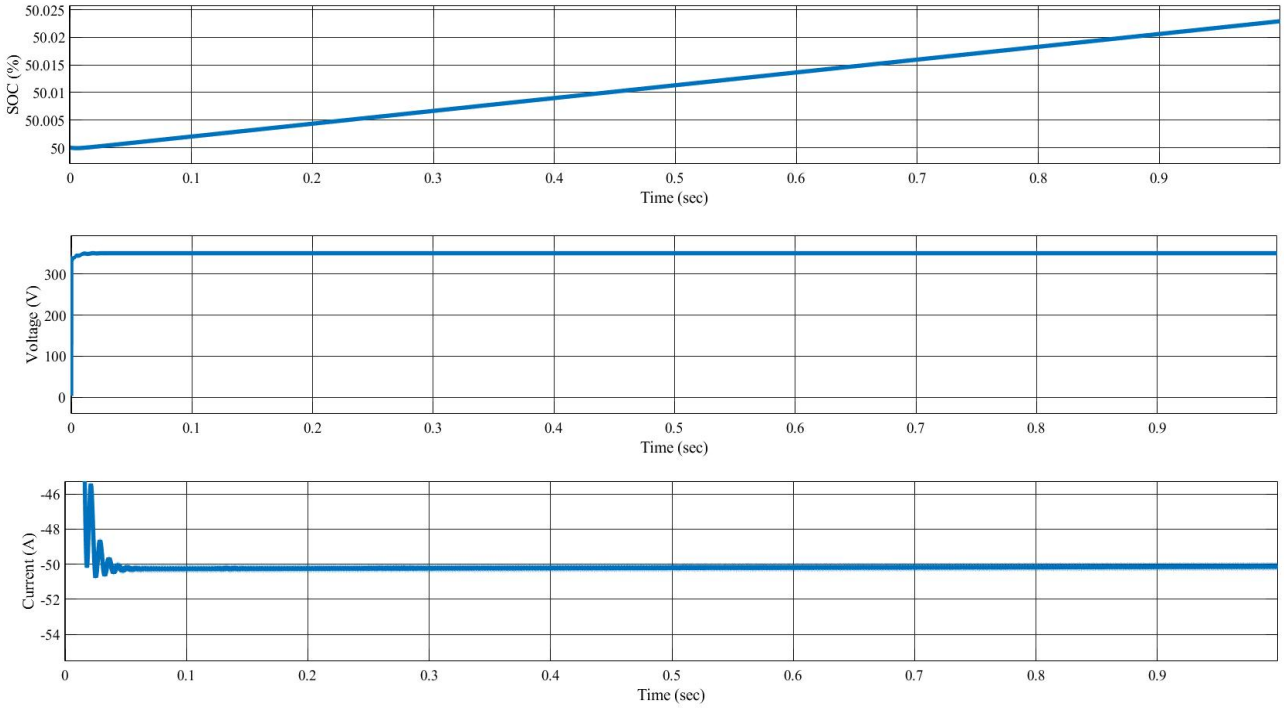

Figure 5.13 Charging the EVs from both sources simultaneously.

The simulation results show that the converter can work and charge the EVs at a power rate up to 17 kW, which is considered level 2 in the SAE J1772 standard [67].

Chapter 6. Experimental Results of the Proposed Converter

Battery, supercapacitor bank, and restive loads in different values are used in the prototype to validate the switching sequence of the converter and the topology concept. In addition, Arduino UNO is used as a controller with IRS 2186 MOSFET gate driver for switching the MOSFETs of the multi-input converter prototype. In addition, for maintaining the voltage across the gate and source of the high-side MOSFETs with 12 V. The prototype of the multi-input DC/DC converter in Figure 6.1 was tested at a low power rate (up to 100 W) to test the functionality of the converter in different operation modes in different switching sequences and to prove the concept of the topology Table 6.1 shows the design specifications of the multi-input converter prototype. The supercapacitor as mentioned before has a long lifetime compared to the battery, as the one used in this prototype can charge and discharge for 500,000 cycles, and the lithium-ion battery is around 5 years or at least 2,000 charging cycles [68].

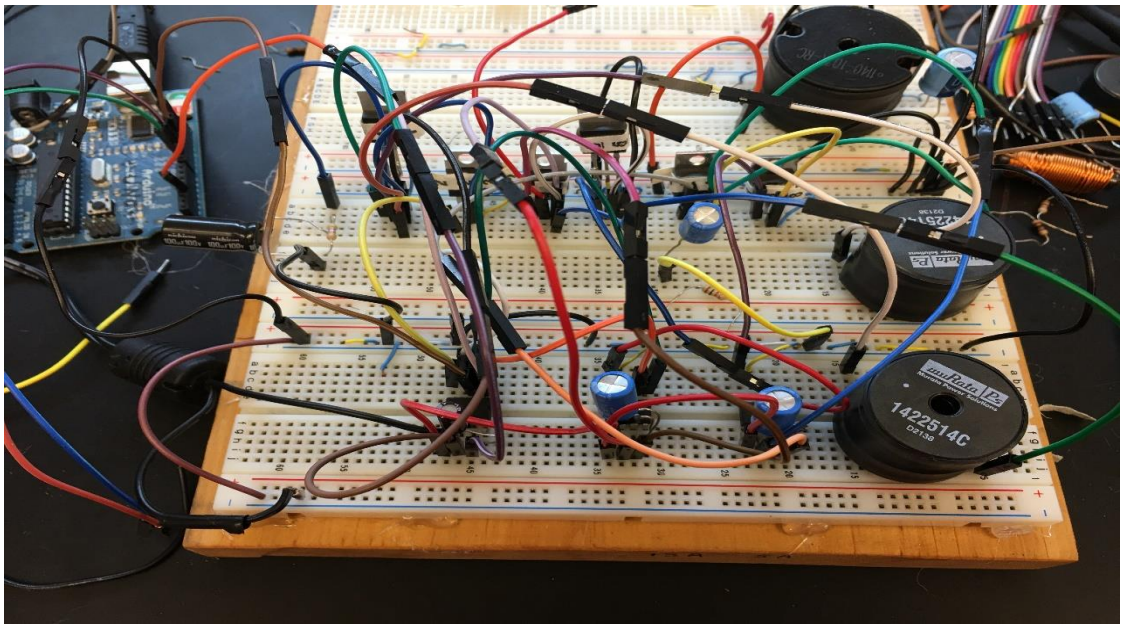

Figure 6.1 Multi input converter prototype.

Table 6.1 Design specification of the multi-input converter prototype.

Specifications	**Battery**	**Supercapacitor**	**DC link**	**Inductor (L_1)**	**Inductor (L_2)**	**Capacitor (C)**	**Switching frequency (f_s)**	**Load**	**Power**
Values	12 V/ 2.2 Ah	15 V/ 400 F	24 V	2 mH	2 mH	100 µF	30 kHz	10 k Ω	100 W

6.1 Experimental Results of the Converter in Different Operation Modes

6.1.1 Supplying the DC link from the Battery Only

The battery's voltage was boosted from 12 V to 24 V with complementary switching signals, as shown in Figure 6.2 (a), by switching the MOSFETs S_3 and S_2 complementary with S_1 and S_4. Inductor L_1 is charged when switches S_3 and S_2 are turned on from the battery, and discharged in the DC link when the S_1 and S_4 are turned on as shown in Figure 6.2 (a). The voltage across S_2 present DC link's voltage, and the voltage across S_4 present battery's voltage. Vice versa, the DC link voltage was reduced from 24 V to 12 approximately, as shown in Figure 6.2 (b), by operating switches S_1 and S_4 complementary with S_3 and S_2. The charging current is reversed in L_1, as seen in Figure 6.2 (b), to charge the battery from the DC link, which also shows the reversal of direction of power to approve the bidirectional power flow capability of the proposed converter.

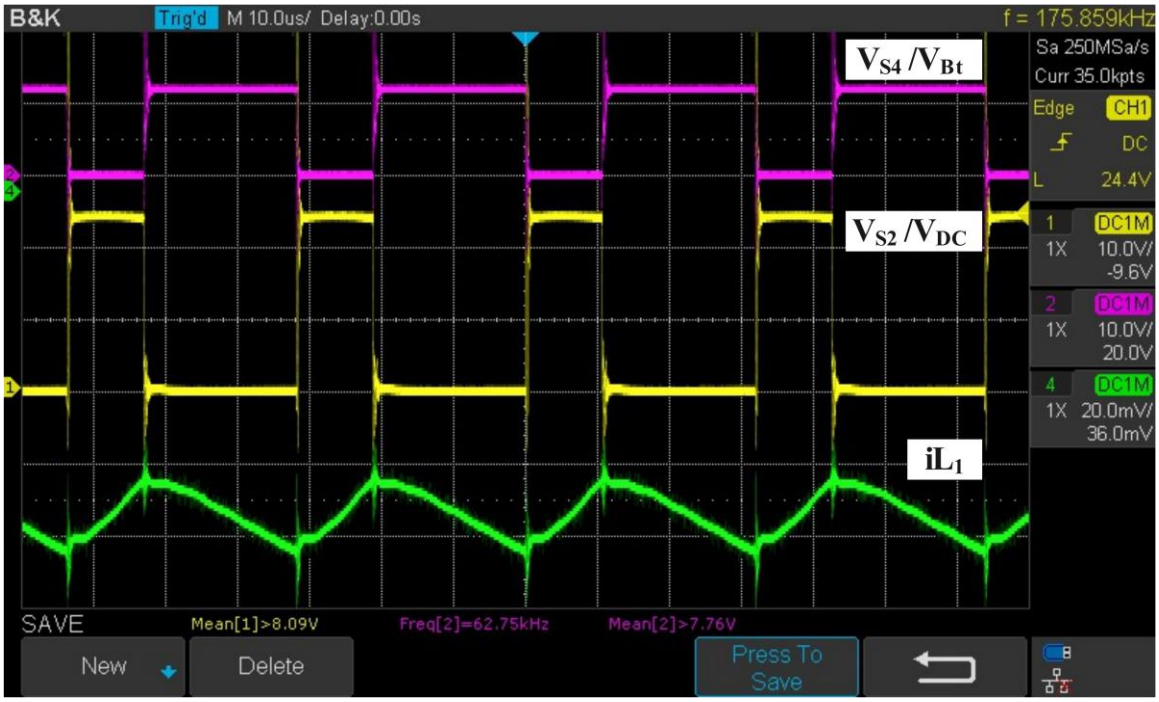

Figure 6.2 (a) Voltage across switch S2, VS2 (scale: 10 V/div), and voltage across switch S4, VS4 (scale: 10 V/div) .

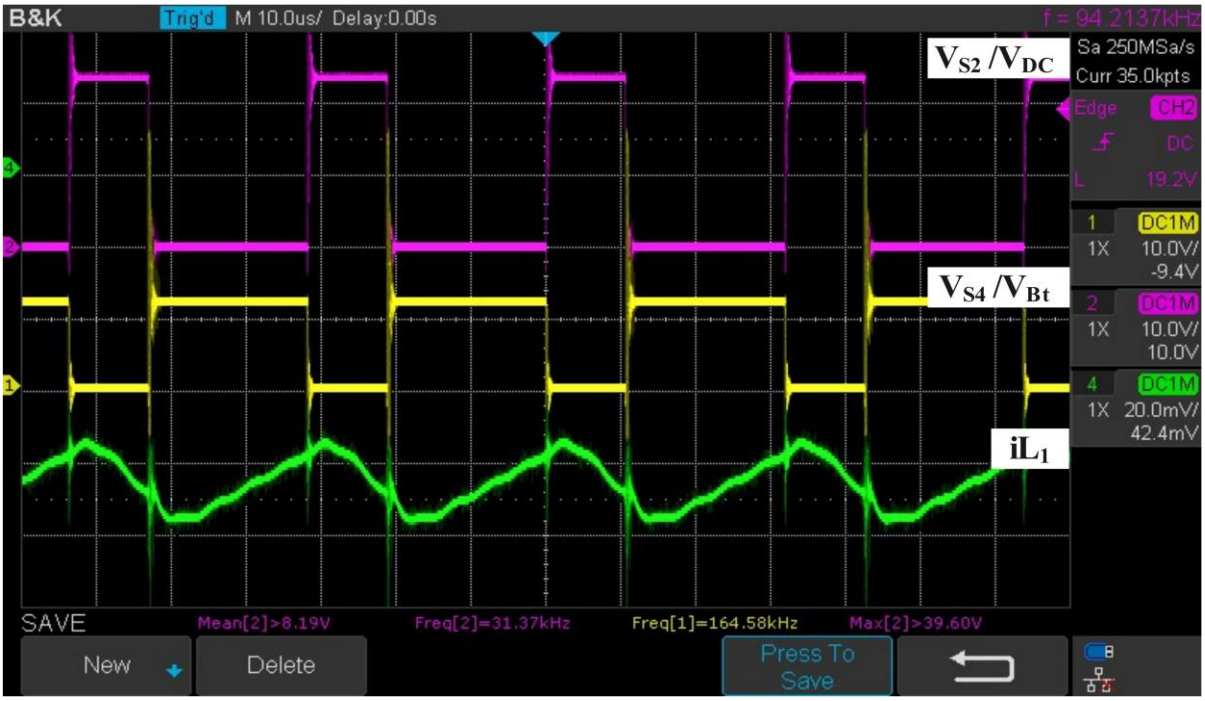

Figure 6.2 (b) Voltage across switch S2, VS2 (scale: 10 V/div), and voltage across switch S4, VS4 (scale: 10V/div) .

6.1.2 Supplying the DC link from the Supercapacitor Only

Same to the previous mode, the supercapacitor's voltage was boosted from 15 V to 24 V with complementary signals, as shown in Figure 6.3 (a), but by switching the MOSFETs S_5 and S_2 complementary with S_1 and S_6. At this operation mode, the inductor L_2 is charged and discharged to transfer the power from the supercapacitor to the DC link. Inductor L_2 is charged when the switches S_5 and S_2 are turned on and releases its energy in the DC link when the switches S_1 and S_6 are turned on, as shown in Figure 6.3 (a). Vice versa, the DC link voltage was reduced from 24 V to 15 approximately, as shown in Figure 6.3 (b), by operating switches S_1 and S_6 complementary with S_5 and S_2. As presented in Figure 6.3 (b), inductor L_2 reversed its current in mode 2 (b), so the iL_2 slope returned to zero, which means the inductor L_2 is discharging when the switches S_5 and S_2 are turned on.

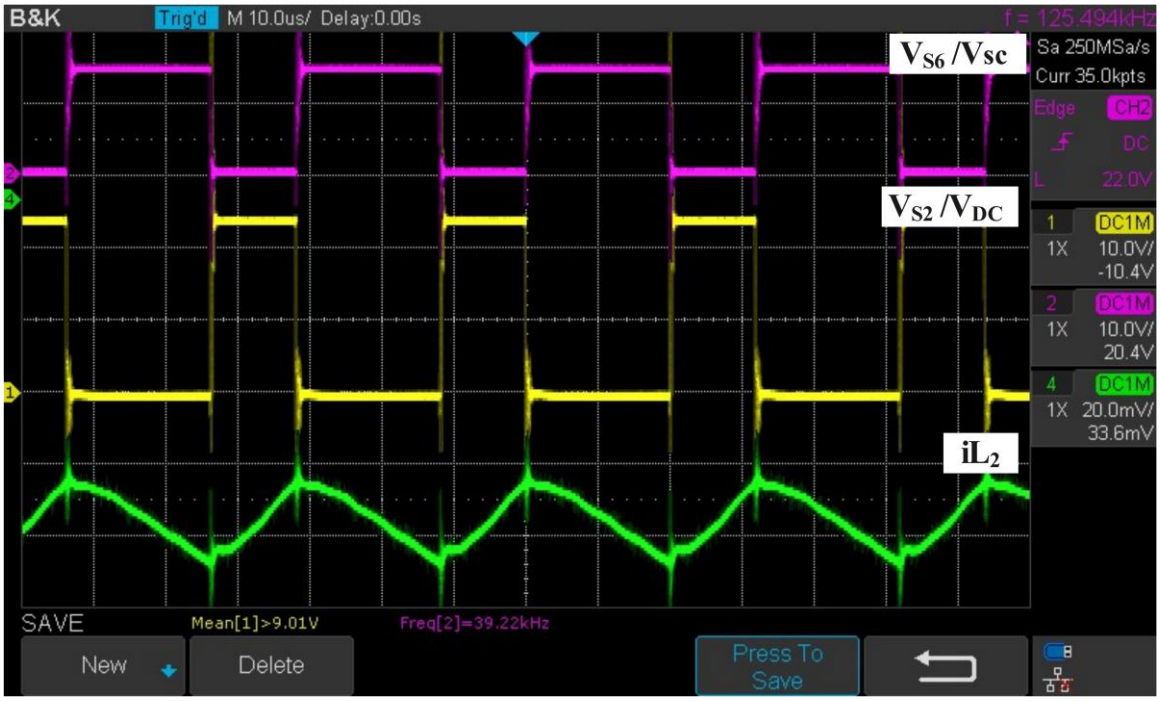

Figure 6.3 (a) Charging and discharging of inductor L2 in mode 2(a).

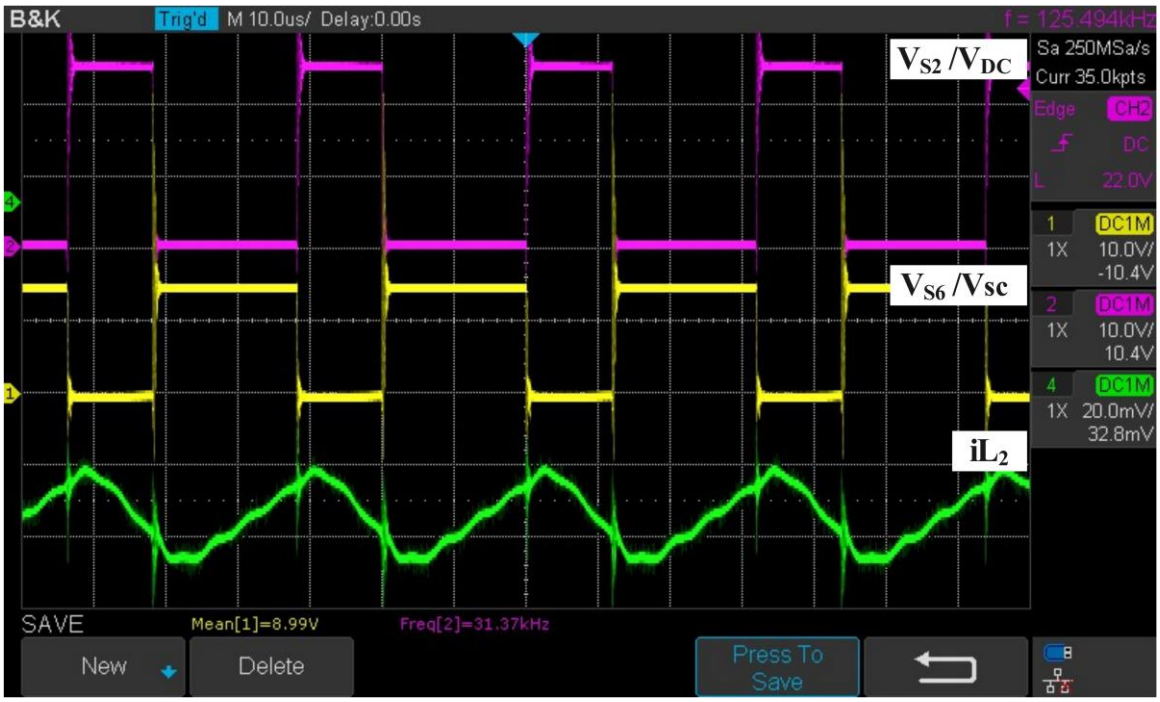

Figure 6.3 (b) Charging and discharging of inductor L2 in mode 2(b).

6.1.3 Supplying the Battery from the Supercapacitor

This operation mode was used and tested to extend the battery's lifetime as the supercapacitor voltage reduced from 15 V to 12 V using switches S_3, S_5, and S_6. As seen in figure 6.4 (a), the inductors L_1 and L_2 are charged at the same time from the supercapacitor to discharge in the battery, and vice versa, the battery voltage was boosted from 12 V to 15 approximately to charge the supercapacitor, as shown in Figure 6.4 (b) by reversing the currents in inductors L_1 and L_2. Also, the figures below show the current ripples of the inductors reduced compared to the previous operation modes because the inductors were in series.

Figure 6.4 (a) Charging battery from the supercapacitor using inductors L1 and L2

Figure 6.4 (b) Charging supercapacitor from the battery by reversing the currents in inductors L1 and L2

6.1.4 Supplying the DC link from the Battery and the Supercapacitor

The inductors L_1 and L_2 are charged simultaneously in this operation mode from the battery, and the supercapacitor uses switches S_2, S_3, and S_5, as shown in Figure 6.5. Then the inductors discharge their energy at the DC link using switches S_1, S_4, and S_6 to boost the DC link voltage to 24 V, as shown in Figure 6.5. The voltage across switch S_2 represents the DC link's voltage, and the voltage across switch S_6 shows the supercapacitor's voltage.

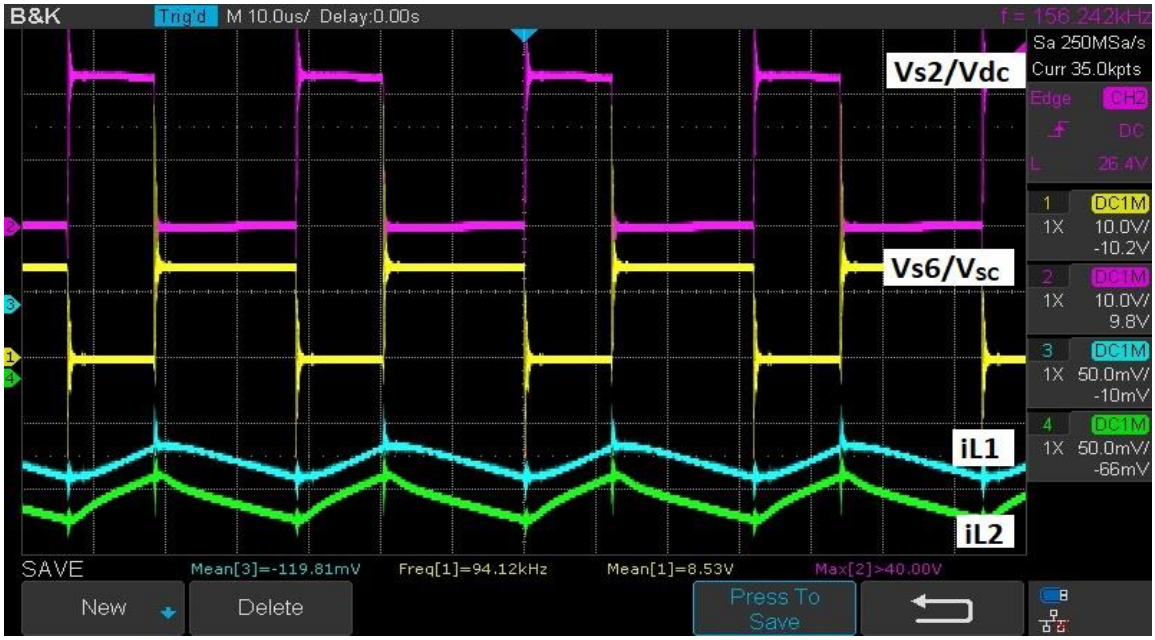

Figure 6.5 Charging simultaneously the DC link from the battery and supercapacitor

6.1.5 Charging the Battery and the Supercapacitor from the DC link

In this operation mode, the battery and supercapacitor are charged simultaneously from the DC link by reversing the inductors' L_1 and L_2 currents compared to the previous mode. Same to the last operation mode, the inductors L_1 and L_2 are charged simultaneously from the DC link using switches S_1, S_4, and S_6, as shown in Figure 6.6. Then the inductors discharge their energy at the battery and the supercapacitor using S_2, S_3, and S_5, as shown in Figure 6.6. The voltage across switch S_2 represents the DC link's voltage, and the voltage across switch S_6 shows the supercapacitor's voltage.

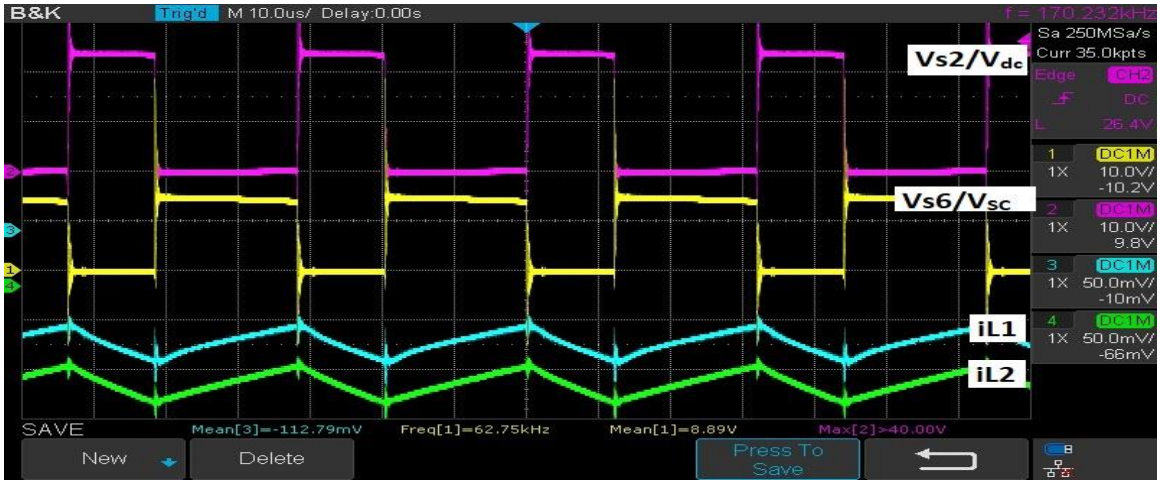

Figure 6.6 Charging simultaneously the battery and supercapacitor from the DC link

6.2 Validation and Comparison between Simulation and Experimental Results

The experimental results validate the concept topology of the converter, specifically the switching sequence to charge and discharge the energy storage devices in different scenarios. It also shows the bidirectional power flow capability of the converter and charging and discharging simultaneously from two sources. Figure 5.2 (a) shows similar waveforms to Figure 6.2 (a) but in different values, which proves the functionality of the converter, especially the switching sequence. Similarly, the output results in Figure 5.3 (b) are identical to Figure 6.3 (b), validating the simulation results and the bidirectional power flow capability. Figure 6.4 validates the functionality of the converter to exchange the power between two energy storage devices, as presented before in the simulation results. Figures 6.5 and 6.6 shows the capability of the converter to charge and discharge two sources simultaneously. Therefore, to operate the converter at a high power rate, we need to adjust the values of the specification design to match the high power rate applications.

6.3 Discussions

The five operating modes of the converter have been simulated successfully as well as the losses, and the converter's efficiency was calculated in the different operation modes. The voltage ripples during most operation modes were less than 5%, and the efficiency was higher than 90% in the simulation work. The proposed converter was tested on a simulation scale to charge a Nissan Leaf battery (350 V, 60 Ah) individually and simultaneously from the energy storage devices. The output results show the converter successfully charges the EV’s battery separately on average with 25 A, and simultaneously on average with 50 A, which means the charging time can be reduced using this operation mode. The charging rate can be controlled by adjusting the reference charging current in the PI controller of the buck converter. The simulation results were validated on a hardware scale at a low power rate (100 W) to validate the topology of the converter and switching sequence. The experimental results show the capability of the converter to operate in different operation modes at bidirectional power flow, similar to the simulation results but at low power rates. To upgrade the converter to work at a high-power rate of 17 kW, similar to the simulation work, we need to adjust the design specification of the converter, as well as add more protection elements to increase the safety of the converter.

Chapter 7. Conclusion and Future Work

7.1 Conclusions

This thesis discusses the designing, modeling, analysis, and simulation of a multi-input DC/DC converter to integrate a hybrid energy system for a proposed fast-charging station of electric vehicles and the experimental work for validating the simulation work.

Chapter 1 presented a general idea about the motivation of the Canadian Government to set a goal to increase the sales of electric vehicles to reduce CO2 emissions and face global climate change, as well as the importance of increasing the number of fast-charging stations to achieve this target. It also discusses different topologies of the DC/DC converters and the multi-input DC/DC converters and their merits over the traditional DC/DC converters.

Chapter 2 discusses in detail the different fast charging technologies and infrastructure of electric vehicles. In addition, it presents different global and recognized fast charging standards, protocols, and power rates of each standard. Moreover, the recent topologies of the multi-input converters were presented and compared with the proposed multi-input converter in terms of the number of components, power flow capability, number of operation modes, and the modularity of the design.

Chapter 3 presents different energy storage devices like batteries and supercapacitors with their different characteristics, advantages, and disadvantages. In addition, it discusses the merits of supercapacitors over batteries as energy storage devices.

In chapter 4, the design of the proposed converter was presented in detail with its merits over the recent topologies of the multi-input converter, and the equations used for this design. In addition, the converter's modeling, analysis, and operation modes are discussed in detail in this chapter. The control algorithm was also presented, and the reasons for the selection of the PI controller and the equations used for calculating the constants of the controller were stated. The proposed fast-charging station design also mentioned how it could reduce the charging time, charging cost, and the load in the grid during peak hours with the proposed converter. A simple buck converter was used to charge the EV’s battery to reduce the voltage of the DC link and increase the charging

current, and its controller was presented as the buck converter was based on the current control, not voltage control like the multi-input converter.

Chapter 5 shows the simulation results obtained using MATLAB/Simulink with testing the converter in different operation modes with power rates (0-500 V DC, 0-60 A, and 17 kW). The results show the efficiency of the controller as the rising time, steady-state error were low, and the overshot was damped well. In addition, the voltage ripples were in the acceptable range, less than 5%. The conduction and switching losses were calculated, and the efficiency of the proposed converter was higher than 90% in most of the operation modes. The simulation results of the whole system show the converter successfully charged the EV's battery individually and simultaneously, as the charging current in individual charging mode was on average 25 A, and in simultaneous mode was 50 A. The charging rate can be controlled by adjusting the reference charging current in the PI controller of the buck converter.

Chapter 6 represents the experimental results for validation of the simulation work, but at a low power rate (100 W) and with different loads to validate the converter's switching sequence and topology.

7.2 Contributions

The first chapter looked at DC-DC converters and the purpose and merits of multi-input converters over the traditional ones. Multiple-input converters can play an essential role in reducing charging time, charging cost, and the load on the grid during peak hours by utilizing them with a hybrid energy system in the fast-charging station of electric vehicles with effective energy management.

The merits and drawbacks of recent topologies of the multi-input converters are investigated to address the main concerns and introduce the efficient proposed converter. The proposed converter focus on reducing the components numbers, increasing the operation modes, working in bidirectional power flow, and reducing the cost and weight of the converter compared to other topologies. In addition, to add modularity to the proposed design, so it can easily add more energy sources to the converter. In Further detail, compared to other topologies mentioned in the literature review in chapter 2, the novelty and contribution of this proposed topology it can work in five operation modes as it can charge and discharge the power sources simultaneously or individually. Moreover, it can exchange the power between them,

showing the bidirectional power flow capability of the converter as presented in the simulation and experimental results with minimum components parts. The proposed converter also shows it can be less weight and cost compared to other topologies, as discussed in chapter 4. In addition, the converter has the advantage of modularity by adding a switching leg consisting of two power switches and one inductor to increase power sources or energy storage devices based on the application.

A new fast-charging station for EVs was developed with a hybrid energy system to combine the high energy density of the battery, and the high-power density of the supercapacitor. With this design, the load in the grid during the peak hours can be mitigated, as discussed in detail in chapter 4, and the lifetime of the energy storage devices can be extended. The EVs can be charged faster using the merit of the supercapacitor as it has a high-power density or by charging simultaneously from two power sources or more. In addition, with the modular design of the proposed converter, more power sources like PV arrays can be integrated into the station, reducing the charging cost on the customers and the consumption from the grid.

A modular multiple-input non-isolated DC-DC converter was developed to give a reliable output power while managing energy storage devices for effective energy management of FCS of EVs. The losses and the efficiency of the converter were discussed in detail in different operation modes. The converter design was tested at a hardware scale using a small prototype to validate the simulation work. The topology shows it can be helpful for FCS and other industrial applications like microgrids and motor traction of EVs or PHEVs.

7.3 Limitations

The efficiency of the converter during charging the supercapacitor was very low compared to other operation modes, which could cause a high cost to charge it from the grid. As the non-isolated converters have less safety than the isolated converter, this could be an issue with using this converter in high-power applications like FCS. To solve this issue, it is recommended to use protection devices like circuit breakers and fuses in the DC link and near the input source to increase the safety of the FCS or any application. The present control algorithm is simple and reliable, but it cannot switch from operation mode to another mode automatically, as it needs high skills in control algorithms, as well as to understand more the behavior of the application and the conditions to know when to

switch from one mode to another. Also, the control algorithm of the prototype needs more optimization, as the voltage ripples and the overshot voltage in some operation modes were high. The efficiency of the converter in hardware scale was not calculated due to limitation of the devices to calculate it, as to calculate the switching and conductions losses its, need high cost and advanced devices.

7.4 Future Work

To charge the EV's battery using the constant current constant voltage control technique as its better than constant current control as this technique can extend the lifetime of the battery and charge it faster than the current control technique. To test the prototype at a high-power rate similar to the FCS power rate, hence adjusting the design specification of converter parameters to match the power rate of the application. Thus, to identify the issues the proposed topology can face while using it in high power rate applications. Furthermore, to calculate the efficiency of the converter in hardware scale to compare it with efficiency calculations in the simulation work. Furthermore, to test the number of power sources that can be easily added to the proposed converter using the advantage of the modularity without affecting the whole system stability. The topology was tested using the Arduino controller, an advanced controlling method, such as PLC, raspberry pi, and nonlinear control must be employed to get optimized results and to be implemented at high power rate applications like FCS. Moreover, to optimize the control algorithm so that the converter can work automatically from one operation mode to another. Finally, use suitable heatsinks to cool MOSFETs as the MOSFETs were burned out quickly because of the exceeding heat during the switching operations.

REFERENCES

[1] G. Zhang, Z. Li, B. Zhang, and W. A. Halang, "Power electronics converters: Past, present and future," *Renewable and Sustainable Energy Reviews*, vol. 81, pp. 2028-2044, 2018/01/01/ 2018, doi: https://doi.org/10.1016/j.rser.2017.05.290.

[2] A. R. Hasan, "Modeling, Design, Control and Validation of a Multiple-input DC-DC Converter Topology for Effective Renewable Energy Management," Ontario Tech University, Oshawa, 2019.

[3] A. Lavanya, J. D. Navamani, K. Vijayakumar, and R. Rakesh, "Multi-input DC-DC converter topologies-a review," in *2016 International Conference on Electrical, Electronics, and Optimization Techniques (ICEEOT)*, 2016: IEEE, pp. 2230-2233.

[4] G. o. Canada. "Greenhouse gas emissions – Transportation sector greenhouse gas emissions,Canada." (accessed 17-Jan-2022, 2022).

[5] "Canada targets 100% zero-emission vehicle sales by 2040." Clean Energy Canada. (accessed 17-Jan-2022, 2022).

[6] J. Song, A. Toliyat, D. Turtle, and A. Kwasinski, "A rapid charging station with an ultracapacitor energy storage system for plug-in electrical vehicles," in *2010 International Conference on Electrical Machines and Systems*, 2010: IEEE, pp. 2003-2007.

[7] E. D. Kostopoulos, G. C. Spyropoulos, and J. K. Kaldellis, "Real-world study for the optimal charging of electric vehicles," *Energy Reports*, vol. 6, pp. 418-426, 2020.

[8] S. Chakraborty, H.-N. Vu, M. M. Hasan, D.-D. Tran, M. E. Baghdadi, and O. Hegazy, "DC-DC converter topologies for electric vehicles, plug-in hybrid electric vehicles and fast charging stations: State of the art and future trends," *Energies*, vol. 12, no. 8, p. 1569, 2019.

[9] V. H. Sierra, "Design, simulation and experimental validation of a multiport electrical converter for Standalone Building-Integrated Photovoltaic systems."

[10] M. Yilmaz and P. Krein, "Review of charging power levels and infrastructure for plug-in electric and hybrid vehicles and commentary on unidirectional charging," in *IEEE international electrical vehicle conference*, 2012.

[11] A. Zidan and H. Gabbar, "Design and control of V2G," in *Smart Energy Grid Engineering*: Elsevier, 2017, pp. 187-205.

[12] N. Sakr, D. Sadarnac, and A. Gascher, "A review of on-board integrated chargers for electric vehicles," in *2014 16th European Conference on Power Electronics and Applications*, 2014: IEEE, pp. 1-10.

[13] S. Kalker *et al.*, *Fast-charging technologies, topologies and standards*. E. ON Energy Research Center, RWTH Aachen University, 2018.

[14] T.-E. Stamati and P. Bauer, "On-road charging of electric vehicles," in *2013 IEEE transportation electrification conference and expo (ITEC)*, 2013: IEEE, pp. 1-8.

[15] K. A. Cheow. "Charging Electric Vehicle." https://medium.com/@ackhor/charging-electric-vehicle-bc16883051dc (accessed Jul 1,2020).

[16] B. Esteban, M. Sid-Ahmed, and N. C. Kar, "A comparative study of power supply architectures in wireless EV charging systems," *IEEE Transactions on Power Electronics*, vol. 30, no. 11, pp. 6408-6422, 2015.

[17] O. C. Onar, J. M. Miller, S. L. Campbell, C. Coomer, C. P. White, and L. E. Seiber, "A novel wireless power transfer for in-motion EV/PHEV charging," in

2013 Twenty-Eighth Annual IEEE Applied Power Electronics Conference and Exposition (APEC), 2013: IEEE, pp. 3073-3080.

[18] M. K. M. Tirupati. "An Overview on Electric Vehicle Charging Infrastructure." https://www.tataelxsi.com/Perspectives/WhitePapers/TataElxsi_Whitepaper_An_Overview_on_Electric_Vehicle_Charging_Infrastructure. (accessed Feburary 1, 2021

[19] A. M. Andwari, A. Pesiridis, S. Rajoo, R. Martinez-Botas, and V. Esfahanian, "A review of Battery Electric Vehicle technology and readiness levels," *Renewable and Sustainable Energy Reviews,* vol. 78, pp. 414-430, 2017.

[20] M. Budhia, G. A. Covic, J. T. Boys, and C.-Y. Huang, "Development and evaluation of single sided flux couplers for contactless electric vehicle charging," in *2011 IEEE Energy Conversion Congress and Exposition*, 2011: IEEE, pp. 614-621.

[21] E. V. Visser *et al.*, "Green energy based inductive Self-Healing highways of the future," 2016.

[22] A. Brooker, M. Thornton, and J. Rugh, "Technology improvement pathways to cost-effective vehicle electrification," 2010.

[23] "IEC Standards development." https://www.iec.ch/about/?ref=menu. (accessed 2020 October 24.

[24] "IEC 61851: Electric vehicle conductive charging system - Part 23.2014." https://webstore.iec.ch/publication/6032. (accessed 2020 October 30.

[25] H. S. Das, M. M. Rahman, S. Li, and C. Tan, "Electric vehicles standards, charging infrastructure, and impact on grid integration: A technological review," *Renewable and Sustainable Energy Reviews,* vol. 120, p. 109618, 2020.

[26] M. Yilmaz and P. T. Krein, "Review of battery charger topologies, charging power levels, and infrastructure for plug-in electric and hybrid vehicles," *IEEE transactions on Power Electronics,* vol. 28, no. 5, pp. 2151-2169, 2012.

[27] "SAE Standards." https://www.sae.org/works/customer.do (accessed 2020 October 24.

[28] "SAE J1772: SAE surface vehicle recommended practice J1772." https://www.sae.org/standards/content/j1772_201710/ (accessed 2020 October 28.

[29] "Electric vehicle charging station , technical installation guide " https://www.hydroquebec.com/data/electrification-transport/pdf/technical-guide.pdf 2015. (accessed 2020 October 28.

[30] "SAE J1773: SAE electric vehicle inductively coupled charging." https://www.sae.org/standards/content/j1773_201406 (accessed 2020 October 15.

[31] "Sae J1772: SAE surface vehicle recommended practice J1772, SAE electric vehicle conductive charge coupler." https://www.sae.org/standards/content/j1772_201710/ (accessed 2020 october 20).

[32] "Communication Between Plug-In Vehicles and Off-Board DC Chargers." https://www.sae.org/standards/content/j2847/2_201504/ (accessed 2020 October 25

[33] "Digital communications for plug-in electric vehicles j2931/1. 2012 " https://www.sae.org/standards/content/j2931/1/ (accessed 2020 October 24.

[34] "Wireless Power Transfer for Light-Duty Plug-in/Electric Vehicles and Alignment Methodology J2954_202010." https://www.sae.org/standards/content/j2954_202010/ (accessed 2020 October 31.

[35] D. Herron. "EV DC Fast Charging standards – CHAdeMO, CCS, SAE Combo, Tesla Supercharger." https://greentransportation.info/ev-charging/range-confidence/chap8-tech/ev-dc-fast-charging-standards-chademo-ccs-sae-combo-tesla-supercharger-etc.html. (accessed 2020 October 31.

[36] "CHAdeMO protocol development." https://www.chademo.com/activities/protocol-development/. (accessed.

[37] "GB/T 20234.1-2015:connection set for conductive charging of electric vehicles " https://www.chinesestandard.net/PDF/English.aspx/GBT20234.1-2015 (accessed.

[38] Y.-M. Chen, Y.-C. Liu, and S.-H. Lin, "Double-input PWM DC/DC converter for high-/low-voltage sources," *IEEE Transactions on Industrial Electronics*, vol. 53, no. 5, pp. 1538-1545, 2006.

[39] S. A. Gorji, H. G. Sahebi, M. Movahed, and M. Ektesabi, "Multi-Input Boost DC-DC Converter with Continuous Input-Output Current for Renewable Energy Systems," in *2019 IEEE 4th International Future Energy Electronics Conference (IFEEC)*, 2019: IEEE, pp. 1-5.

[40] M. Gavris, N. Muntean, and O. Cornea, "A new dual-input hybrid buck DC-DC converter," in *International Aegean Conference on Electrical Machines and Power Electronics and Electromotion, Joint Conference*, 2011: IEEE, pp. 109-114.

[41] S. Athikkal, K. Sundaramoorthy, and A. Sankar, "Development and performance analysis of dual-input DC–DC converters for DC microgrid application," *IEEJ Transactions on Electrical and Electronic Engineering*, vol. 13, no. 7, pp. 1034-1043, 2018.

[42] K. J. Reddy and S. Natarajan, "Energy sources and multi-input DC-DC converters used in hybrid electric vehicle applications–A review," *International journal of hydrogen energy*, vol. 43, no. 36, pp. 17387-17408, 2018.

[43] Y. Yuan-mao and K. W. E. Cheng, "Multi-input voltage-summation converter based on switched-capacitor," *IET Power Electronics*, vol. 6, no. 9, pp. 1909-1916, 2013.

[44] G. G. Kumar and S. Kumaravel, "Dual-Input Non-isolated DC-DC Converter with Vehicle to Grid Feature," *IEEE Journal of Emerging and Selected Topics in Power Electronics*, 2020.

[45] Z. Saadatizadeh, P. C. Heris, X. Liang, and E. Babaei, "Expandable Non-Isolated Multi-Input Single-Output DC-DC Converter With High Voltage Gain and Zero-Ripple Input Currents," *IEEE Access*, vol. 9, pp. 169193-169219, 2021.

[46] E. Meshkati, M. Packnezhad, and H. Farzanehfard, "Single Inductor Bidirectional Multi-Input Converter With Continuous Battery Current Based On Integration of Buck and Three Port Boost Topologies," in *2022 13th Power Electronics, Drive Systems, and Technologies Conference (PEDSTC)*, 2022: IEEE, pp. 362-367.

[47] Y. Song and B. Wang, "Survey on reliability of power electronic systems," *IEEE transactions on power electronics*, vol. 28, no. 1, pp. 591-604, 2012.

[48] J. Falck, C. Felgemacher, A. Rojko, M. Liserre, and P. Zacharias, "Reliability of power electronic systems: An industry perspective," *IEEE Industrial Electronics Magazine*, vol. 12, no. 2, pp. 24-35, 2018.

[49] D. Team. "Five Innovations Herald Easier and Faster EV Charging Future " https://driivz.com/blog/ev-charging-technology-innovations/ (accessed 2021 Feburary 1.

[50] E. A. M. Asciostioation. "A review of Battery technologies for automotive application."

https://scholar.uwindsor.ca/cgi/viewcontent.cgi?article=8885&context=etd (accessed Feb 16, 2021.
[51] C. Sen, "Performance analysis of batteries used in electric and hybrid electric vehicles," 2010.
[52] K. K. Gokul, B. P. Emmanuel, S. Ashok, and S. Kumaravel, "Design and control of non-isolated bidirectional DC-DC converter for energy storage application," in *2017 2nd IEEE International Conference on Recent Trends in Electronics, Information & Communication Technology (RTEICT)*, 2017: IEEE, pp. 289-293.
[53] "A review of Battery technologies for automotive application." https://www.acea.auto/publication/a-review-of-battery-technologies-for-automotive-applications/ (accessed 2021 Feb 16.
[54] S. M. Lukic, J. Cao, R. C. Bansal, F. Rodriguez, and A. Emadi, "Energy storage systems for automotive applications," *IEEE Transactions on industrial electronics*, vol. 55, no. 6, pp. 2258-2267, 2008.
[55] P. Svasta, R. Negroiu, and A. Vasile, "Supercapacitors—An alternative electrical energy storage device," in *2017 5th International Symposium on Electrical and Electronics Engineering (ISEEE)*, 2017: IEEE, pp. 1-5.
[56] M. K. Andreev, "An Overview of Supercapacitors as New Power Sources in Hybrid Energy Storage Systems for Electric Vehicles," in *2020 XI National Conference with International Participation (ELECTRONICA)*, 2020: IEEE, pp. 1-4.
[57] "Supercapacitor." https://eepower.com/capacitor-guide/types/supercapacitor/ (accessed 2021 December 12.
[58] "Mouser Electronics Inc. ." https://www.mouser.ca/ (accessed.
[59] T. Smith, J. Mars, and G. Turner, "Using supercapacitors to improve battery performance," in *2002 IEEE 33rd Annual IEEE Power Electronics Specialists Conference. Proceedings (Cat. No. 02CH37289)*, 2002, vol. 1: IEEE, pp. 124-128.
[60] "Time of Use " https://www.opuc.on.ca/time-of-use/ (accessed 2021-11-15.
[61] "Zero-emission vehicle registrations down slightly in 2020." https://www150.statcan.gc.ca/n1/daily-quotidien/210422/dq210422e-eng.htm (accessed 2021- 11-15.
[62] "Useable battery capacity of full electric vehicles." https://ev-database.org/cheatsheet/useable-battery-capacity-electric-car (accessed.
[63] T. Pamuła and W. Pamuła, "Estimation of the energy consumption of battery electric buses for public transport networks using real-world data and deep learning," *Energies*, vol. 13, no. 9, p. 2340, 2020.
[64] Z. Gao *et al.*, "Battery capacity and recharging needs for electric buses in city transit service," *Energy*, vol. 122, pp. 588-600, 2017.
[65] A. Hintz, U. R. Prasanna, and K. Rajashekara, "Novel modular multiple-input bidirectional DC–DC power converter (MIPC) for HEV/FCV application," *IEEE Transactions on Industrial Electronics*, vol. 62, no. 5, pp. 3163-3172, 2014.
[66] S. A. Lopa, S. Hossain, M. Hasan, and T. Chakraborty, "Design and simulation of DC-DC converters," *International Research Journal of Engineering and Technology (IRJET)*, vol. 3, no. 01, pp. 63-70, 2016.
[67] "SAE standards " https://www.sae.org/standards/content/j1772_201001/ (accessed 14th of November 2021.
[68] A. Lerma. "Lithium-Ion vs Lead Acid Battery Life." https://www.fluxpower.com/blog/lithium-ion-vs.-lead-acid-battery-life (accessed 15th of August 2022).